

# **Computation of hyperbolic structures on 3-dimensional orbifolds**

Damian Heard

Submitted in total fulfilment of the requirements  
of the degree of Doctor of Philosophy

---

December 2005

Department of Mathematics and Statistics  
The University of Melbourne

---



## Abstract

The computer programs `SnapPea` by Weeks and `Geo` by Casson have proven to be powerful tools in the study of hyperbolic 3-manifolds. Manifolds are special examples of spaces called orbifolds, which are modelled locally on  $\mathbb{R}^n$  modulo finite groups of symmetries. `SnapPea` can also be used to study orbifolds but it is restricted to those whose singular set is a link.

One goal of this thesis is to lay down the theory for a computer program that can work on a much larger class of 3-orbifolds. The work of Casson is generalized and implemented in a computer program `Orb` which should provide new insight into hyperbolic 3-orbifolds.

The other main focus of this work is the study of 2-handle additions. Given a compact 3-manifold  $M$  and an essential simple closed curve  $\alpha$  on  $\partial M$ , then we define  $M[\alpha]$  to be the manifold obtained by gluing a 2-handle to  $\partial M$  along  $\alpha$ . If  $\alpha$  lies on a torus boundary component, we cap off the spherical boundary component created and the result is just Dehn filling.

The case when  $\alpha$  lies on a boundary surface of genus  $\geq 2$  is examined and conditions on  $\alpha$  guaranteeing that  $M[\alpha]$  is hyperbolic are found. This uses a lemma of Scharlemann and Wu, an argument of Lackenby, and a theorem of Marshall and Martin on the density of strip packings. A method for performing 2-handle additions is then described and employed to study two examples in detail.

This thesis concludes by illustrating applications of `Orb` in studying orbifolds and in the classification of knotted graphs. Hyperbolic invariants are used to distinguish the graphs in Litherland's table of 90 prime  $\theta$ -curves and provide access to new topological information including symmetry groups. Then by prescribing cone angles along the edges of knotted graphs, tables of low volume orbifolds are produced.



## Declaration

This is to certify that

- (i) the thesis comprises only my original work towards the PhD except where indicated in the Preface,
- (ii) due acknowledgement has been made in the text to all other material used,
- (iii) the thesis is less than 100,000 words in length, exclusive of tables, maps, bibliographies and appendices.

Damian Heard



## Preface

Section 1.1 and 1.2 largely review known theory. Section 1.3 gives new results, building upon previous work of Thurston ([61]) and Ushijima ([66]).

Section 2.1 gives basic background on orbifolds. Section 2.2, 2.3 and 2.4 produce new results extending the work of Casson ([12]). In Section 2.5, the work of Frigerio and Petronio ([23]) is translated into the setting of Section 2.2.

Section 3.1 was inspired by the work of Scharlemann and Wu ([58]) and Lackenby ([41]) while Section 3.2 and 3.3 consist entirely of original work.

In Section 4.1 the knotted graphs in [43] and [47] are distinguished using hyperbolic invariants. Section 4.2 produces new tables of low volume hyperbolic 3-orbifolds.

The Appendix outlines an algorithm for triangulating 3-orbifolds based on the author's Honours project [30].



## Acknowledgements

I would like to express my gratitude to my supervisor Craig Hodgson. The last three and a half years have been a fantastic learning experience made possible by his patience and support.

I also thank the many other people who have helped me along the way: Oliver Goodman for insightful discussions on computer programming and hyperbolic geometry; Martin Scharlemann for informative correspondence on his paper [58]; Morwen Thistlethwaite who was only too willing to give advice and assistance regarding the development of `Orb`; and Jeff Weeks for the opportunity to use his ground-breaking computer program `SnapPea`.

Finally, I thank my girlfriend Alice. I have relied heavily on her continuous encouragement and support during this intense period.



## Contents

Abstract	i
Declaration	iii
Preface	v
Acknowledgements	vii
List of Figures	xi
List of Tables	xv
Notation	xvii
Introduction	1
Chapter 1. Generalized tetrahedra and their Gram matrices	5
1.1. Hyperbolic space	5
1.2. Generalized tetrahedra	9
1.3. Gram matrices	11
Chapter 2. Finding hyperbolic structures on 3-orbifolds	17
2.1. Orbifolds	17
2.2. The parameters and equations	21
2.3. Flat and negatively oriented tetrahedra	29
2.4. Pared manifolds	35
2.5. Canonical cell decompositions	37
2.6. Further extensions	45
Chapter 3. Attaching 2-handles	47
3.1. Bounds on exceptional curves	48
3.2. The algorithm	55
3.3. Two simple examples	58
3.4. Remarks on implementation	66
Chapter 4. Applications	69
4.1. Knotted $\theta$ -curves	69
4.2. Low volume hyperbolic 3-orbifolds	79

4.3. Future applications	81
Bibliography	87
Appendix A. Triangulating orbifolds of type $Q = (\mathbb{S}^3, \Gamma)$	A.91

## List of Figures

1.1	Lorentzian space $\mathbb{E}^{1,n}$ .	6
1.2	The signed distance from a hyperplane to a horosphere.	7
1.3	The picture in $\mathbb{P}_1^2$ .	9
1.4	Vertex truncation.	10
1.5	A length-0 edge.	11
1.6	A tetrahedron inscribed in a rectangular box.	15
2.1	A model from rotational symmetry.	18
2.2	A model from reflections.	18
2.3	The open sets $\mathcal{U}$ cover $X_Q$ .	19
2.4	The 2-orbifolds $\mathbb{T}(3)$ and $\mathbb{S}^2(2, 3, 4)$ .	19
2.5	The 2-orbifold $\mathbb{S}^2(2, 2, 2, 2)$ is Euclidean.	20
2.6	Graphs give orbifolds.	21
2.7	In the link of the cusp the preferred horospherical triangles match.	23
2.8	An example orbifold.	24
2.9	An example triangulation.	24
2.10	Non-uniqueness of solutions.	27
2.11	Some flat tetrahedra.	30
2.12	More flat tetrahedra.	30
2.13	Detecting negatively oriented tetrahedra.	32
2.14	The right hand rule.	33
2.15	The boundary of a pared manifold.	35
2.16	Labelling a trivalent graph $\infty$ produces a pared manifold.	36
2.17	Slicing off an edge.	37
2.18	The three to two move.	41
2.19	The positioning of $\Delta'$ .	43
3.1	A 2-handle addition.	47

3.2	Coplanar curves.	48
3.3	As $g \rightarrow \infty$ , $c(S_g) = O(\log(g))$ .	49
3.4	Pulling $P$ across the disc $D$ .	51
3.5	Boundary compression gives a new surface of lower complexity.	51
3.6	Two possible pictures when $\hat{P}$ is a torus.	52
3.7	Spinning the edges of $T$ around $\partial P$ .	53
3.8	The picture in the universal cover of $M$ .	53
3.9	A normal curve.	55
3.10	The subdivision of neighbouring tetrahedra.	56
3.11	After subdivision.	56
3.12	Ungluing faces.	57
3.13	A different view of the chasm.	57
3.14	Sliding tetrahedra down the chasm.	58
3.15	The knotted-Y $\mathcal{G}_1$ .	58
3.16	The gluing pattern for $\mathcal{M}_1$ .	60
3.17	A short meridian.	60
3.18	$\mathcal{M}_2$ is the complement of $\mathcal{G}_2$ in $\mathbb{S}^3$ .	61
3.19	The gluing pattern for $\mathcal{M}_2$ .	62
3.20	A short separating curve.	62
3.21	Estimating the distance between base points.	63
3.22	Calculating $m$ .	64
3.23	A piecewise geodesic path.	64
3.24	Expanding balls around the neighbours of $x$ .	65
4.1	Two composite graphs.	69
4.2	The smallest cusped orientable hyperbolic 3-orbifold and the smallest known orientable hyperbolic 3-orbifold.	79
4.3	The three smallest orientable hyperbolic 3-orbifolds with nonrigid cusps.	79
4.4	Enumerating knotted graphs	80
A.1	Truncating the vertices and then shrinking edges of $\Sigma(Q)$ .	A.91
A.2	$\Gamma$ is in $\mathbb{S}^3$ .	A.92
A.3	Cutting up $\mathbb{S}^2 \times I$ .	A.92

LIST OF FIGURES

xiii

A.4	One of the second types of pieces.	A.93
A.5	Cutting up $\mathbb{S}^2 \times I$ .	A.94



## List of Tables

3.1	The list of exceptional curves on $\partial\mathcal{M}_1$ (up to symmetry) of length $\leq c(S_2)$ .	59
3.2	The list of exceptional curves on $\partial\mathcal{M}_2$ (up to symmetry) of length $\leq c(S_2)$ and whose intersection with $\gamma$ is essential.	61
4.1	The orbifolds of the type $Q = (\mathbb{S}^3, \Gamma)$ found with $\text{vol}(Q) < 0.5$ , where $\Gamma$ is a connected, prime, trivalent two vertex graph with at most 7 crossings.	82
4.2	Some simple prime, trivalent two vertex graphs.	83
4.3	The orbifolds of the type $Q = (\mathbb{S}^3, \Gamma)$ found with $\text{vol}(Q) < 0.2$ , where $\Gamma$ is a connected, prime, trivalent four vertex graph with at most 7 crossings.	84
4.4	Some simple, prime, trivalent four vertex graphs.	85



## Notation

Symbol	Meaning
$\mathbb{E}^n$	Euclidean $n$ -space
$\mathbb{H}^n$	Hyperbolic $n$ -space
$\mathbb{S}^n$	Spherical $n$ -space
$\mathbb{E}^{1,n}$	Lorentzian $(n + 1)$ -space
$\langle \cdot, \cdot \rangle$	The Lorentzian inner product
$H_-$	The hyperboloid model of $\mathbb{H}^n$
$\mathbb{P}_1^n$	The plane $x_0 = 1$ in $\mathbb{E}^{1,n}$
$\mathcal{P}(\mathbf{x})$	The radial projection of $\mathbf{x} \in \mathbb{E}^{1,n}$ to $\mathbb{P}_1^n$
$\mathbb{B}^n$	The open unit ball in $\mathbb{P}_1^n$
$\Delta$	A tetrahedron
$\Delta'$	A generalized tetrahedron in $\mathbb{E}^{1,3}$
$\hat{\Delta}$	A generalized tetrahedron in $\mathbb{H}^3$
$\mathbf{v}_i$	The $i$ -th vertex of $\Delta'$ in $\mathbb{E}^{1,3}$
$v_{ij}$	$\langle \mathbf{v}_i, \mathbf{v}_j \rangle$
$V$	The matrix with the vertices $\mathbf{v}_i$ of $\Delta'$ as columns
$J$	The diagonal matrix diagonal $(-1, 1, 1, 1)$
$G$	The vertex Gram matrix of $\Delta' = V^t J V = (v_{ij})$
$\mathbf{w}_i$	A normal to the $i$ -th face of $\Delta'$ in $\mathbb{E}^{1,3}$
$w_{ij}$	$\langle \mathbf{w}_i, \mathbf{w}_j \rangle$
$W$	The matrix with the normals $\mathbf{w}_i$ of $\Delta'$ as columns
$G_*$	The normal Gram matrix of $\Delta' = W^t J W = (w_{ij})$
$G_{ij}$	The matrix obtained by deleting the $i$ -th row and $j$ -column from $G$
$c_{ij}$	The $(i, j)$ -th cofactor of $G = (-1)^{i+j} \det(G_{ij})$



## Introduction

The classification of 2-manifolds is something well understood. The classification of 3-manifolds is a much harder problem. We do not even have conjectural list of all 3-manifolds.

If Thurston’s Geometrization Conjecture is confirmed, which seems more and more likely due to the work of Perelman, then we would have a complete set of topological invariants. In particular, for irreducible atoroidal 3-manifolds, with the exception of lens spaces, the fundamental group would be a complete invariant. Unfortunately the fundamental group alone does not provide us a practical method of distinguishing 3-manifolds.

To this end, topologists have been relying heavily on geometry to distinguish between 3-manifolds. A geometric structure on a manifold is a complete, locally homogeneous Riemannian metric. In particular, a hyperbolic manifold is a Riemannian manifold with constant sectional curvature  $-1$ . Hyperbolic 3-manifolds are the most interesting, and most abundant, while non-hyperbolic 3-manifolds are largely understood.

In [61], Thurston introduced hyperbolic Dehn surgery, a method for continuously deforming the topology and geometry of a hyperbolic 3-manifold to a different 3-manifold. The computer program `SnapPea` ([69]), developed by Weeks, allows the user to explore this process. Manifolds are special examples of spaces called orbifolds, which are modelled locally on  $\mathbb{R}^n$  modulo finite groups of symmetries. One goal of this thesis is to extend the ideas used in `SnapPea` to the class of 3-orbifolds. These concepts are implemented in a computer program `Orb`. As with `SnapPea`, `Orb` should provide invaluable information on hyperbolic 3-orbifolds and aid future theoretical work.

The first chapter is a review of some hyperbolic geometry and a discussion of “generalized tetrahedra”. Generalized tetrahedra arise when we allow tetrahedra that have vertices ‘at’ and ‘beyond’ the boundary of 3-dimensional hyperbolic space  $\mathbb{H}^3$ . Combinatorially, a generalized tetrahedron is just a tetrahedron with some of its vertices sliced off. Such a tetrahedron can be realized geometrically in  $\mathbb{H}^3$  by slicing any hyperinfinite vertices off along their corresponding dual hyperplanes. See Section 1.2 for more details. We can use the hyperboloid model of hyperbolic space to position any generalized tetrahedron  $\Delta'$  in Lorentzian space  $\mathbb{E}^{1,3}$ . If

$\mathbf{v}_1, \mathbf{v}_2, \mathbf{v}_3, \mathbf{v}_4 \in \mathbb{E}^{1,3}$  are the vertices of  $\Delta'$ , then the vertex Gram matrix of  $\Delta'$  is the symmetric  $4 \times 4$  matrix of Lorentzian inner products  $G = (\langle \mathbf{v}_i, \mathbf{v}_j \rangle)$ . The matrix  $G$  completely determines  $\Delta'$  up to isometry and so it can be used to recover its dihedral angles and edge lengths.

In [61], Thurston devised a way of subdividing the figure-eight knot complement into two regular ideal hyperbolic tetrahedra. Weeks has drawn upon this approach to develop the computer program **SnapPea** which can subdivide the complement of a link in  $\mathbb{S}^3$  into ideal tetrahedra. It can then search for tetrahedra so that the sum of the dihedral angles around each edge in the triangulation is  $2\pi$ . This determines a hyperbolic structure on the manifold, giving access to a vast array of geometric invariants. Casson has also developed a program **Geo** ([12]) that computes geometric structures on closed 3-manifolds by subdividing them into finite tetrahedra. Although both these programs have proven invaluable in studying 3-manifolds, they are limited by the kind of tetrahedra they use.

Thurston also suggested that this method could be extended to work on graph complements. He showed in [62] that the complement of the *knotted*  $Y$  could be subdivided into two regular generalized tetrahedra. Frigerio and Petronio proposed one way of implementing this approach in [23] using the dihedral angles of the generalized tetrahedra as parameters. This has been implemented with Martelli in the computer program **oggraphs** ([21]).

The second chapter develops an alternative method for parametrizing generalized triangulations, using vertex Gram matrices of the generalized tetrahedra as parameters in an approach similar to that of Casson in **Geo**. The shapes of the generalized tetrahedra in a triangulation  $T$  can be completely determined by  $|T^0| + |T^1|$  parameters, where  $|T^i|$  is the number of  $i$ -cells in  $T$ , significantly fewer parameters than required by the approach in [23].

This technique for finding hyperbolic structures can also be used on closed and cusped 3-manifolds and on 3-manifolds with geodesic boundary. It can also be used to find structures on a very large class of 3-orbifolds. We can do this by relaxing the edge condition by allowing the cone angle around each edge to be  $\frac{2\pi}{n}$ , for some  $n \geq 1$ . Since orientable 3-orbifolds ‘look like’ orientable 3-manifolds with embedded trivalent graphs as singular loci, a very large class of orbifolds can be dealt with in this way.

**Orb** is a computer program which implements this method for parametrizing triangulations. It can start with a projection of a graph embedded in  $\mathbb{S}^3$ , and produce and simplify a triangulation with some prescribed subgraph as part of the 1-skeleton and the remainder of the graph drilled out. (This is described

in the Appendix.) `Orb` then uses the vertex Gram matrices to parametrize the triangulation and solve for a hyperbolic structure using Newton's method.

Given a compact 3-manifold  $M$  and an essential simple closed curve  $\alpha$  on  $\partial M$ , we define  $M[\alpha]$  to be the manifold obtained by gluing a 2-handle to  $\partial M$  along  $\alpha$ . If  $\alpha$  lies on a torus boundary component, we cap off the spherical boundary component created and the result is just Dehn filling.

Suppose  $T$  is a torus boundary component of  $\partial M$ ,  $\alpha \subset T$ , and suppose  $M$  is hyperbolic. By Thurston's Hyperbolic Dehn Surgery Theorem ([62]), there are only a finite number of slopes  $\alpha$  with non-hyperbolic  $M[\alpha]$ . Thurston and Gromov ([28],[6]) also showed that if the length of  $\alpha$ , as measured in the Euclidean metric on the boundary of a horoball neighbourhood of the cusp, is at least  $2\pi$  then  $M[\alpha]$  is negatively curved. Agol ([3]) and Lackenby ([42]) have independently shown that if the length of  $\alpha$  (measured as above) is at least 6 then  $M[\alpha]$  is irreducible, atoroidal and not Seifert fibered, and has an infinite, word hyperbolic fundamental group. Hodgson and Kerckhoff ([32]) have shown that the number of non-hyperbolic fillings is bounded by a number independent of  $M$ .

The third chapter examines the case when  $\alpha$  lies on a boundary surface of genus  $\geq 2$ . Using a lemma of Scharlemann and Wu ([58]), an argument of Lackenby ([41]) and a theorem on the density of strip packings, due to Marshall and Martin ([44]), the following result is proven.

**Theorem 3.1** *Let  $M$  be an orientable compact finite volume hyperbolic 3-manifold with non-empty geodesic boundary. Suppose  $\alpha$  is a simple closed geodesic on a boundary component  $S$ , with genus greater than one. Let*

$$c(S) = 6 \operatorname{ArcCosh} \left( 1 + \frac{2\sqrt{1 - 4/\chi(S)}}{\left(\sqrt{1 - 4/\chi(S)} - 1\right)^2} \right).$$

*Then  $M[\alpha]$  is hyperbolic provided that, if  $\alpha$  is separating then*

$$\operatorname{Length}(\alpha) > c(S),$$

*and if  $\alpha$  is non-separating, then all curves  $\alpha'$  coplanar to  $\alpha$  have*

$$\operatorname{Length}(\alpha') > c(S).$$

Two curves  $\alpha$  and  $\beta$  on surface  $S$  are *coplanar* if some component of  $S - (\alpha \cup \beta)$  is an annulus or a 3-punctured sphere. If  $M$  is hyperbolic and  $M[\alpha]$  is not then  $\alpha$  is called an *exceptional* curve.

The study of 2-handle additions concludes by enumerating exceptional curves on the boundary of two of the eight lowest volume hyperbolic 3-manifolds with geodesic boundary determined by Fujii in [24]. This is done by producing an algorithm which starts with a triangulated 3-manifold  $M$  with a curve  $\alpha \subset \partial M$

and creates a triangulation for  $M[\alpha]$ . These examples turn out to be very different, one having a finite list and the other an infinite list of exceptional curves.

The enumeration and classification of knots and links has benefited greatly from the information that hyperbolic structures provide. Mostow-Prasad rigidity implies that a complete hyperbolic structure is a complete invariant of a finite volume hyperbolic 3-manifold ([48],[52]). This result means that knots and links with hyperbolic complements can be distinguished by their geometric structures. Hyperbolic structures can be used in a similar fashion to distinguish between knotted graphs in  $\mathbb{S}^3$ .

A  $\theta$ -curve is a spatial graph in  $\mathbb{S}^3$  consisting of two vertices and three edges, where each edge joins the two vertices. Litherland ([43]) and later Moriuchi ([47]) enumerated all prime  $\theta$ -curves with up to seven crossings. The same spatial graph can be embedded in many different ways, so invariants are needed to build up a complete list of graphs without repetition. Litherland used the Alexander polynomial to distinguish between spatial graphs while Moriuchi employed the Yamada polynomial.

The final chapter shows how the prime  $\theta$ -curves with up to seven crossings can be completely distinguished by using hyperbolic structures alone. This is done by considering natural geometric structures associated with each graph, including the unique hyperbolic structure of the manifold with geodesic boundary produced by making the meridians of the edges of the graph parabolic. The same ideas have recently been used by Chiodo, Heard, Hodgson, Saunderson and Sheridan in [15] to extend the work of Litherland and Moriuchi and enumerate all prime two and four vertex trivalent spatial graphs with up to seven crossings.

Spatial graphs also give us access to a huge range of 3-orbifolds. By starting with a trivalent spatial graph, and varying the cone angles along the edges, we can produce an infinite family of orbifolds. This study concludes by compiling two large tables of low volume hyperbolic 3-orbifolds using the spatial graphs from [15]. The first fourteen low volume orbifolds were already known and appear in a paper of Zimmerman ([73]). After that, new low volume orbifolds begin to appear. These tables should provide useful in guiding future theoretical work on hyperbolic 3-orbifolds.

## CHAPTER 1

### Generalized tetrahedra and their Gram matrices

In [61] Thurston devised a method for placing hyperbolic structures on cusped hyperbolic 3-manifolds by subdividing them into ideal tetrahedra. The computer program `SnapPea` ([69]) has had great success implementing this approach on knot and link complements in  $\mathbb{S}^3$  and on closed 3-manifolds obtained from these by Dehn filling. `SnapPea` has proven to be invaluable in the enumeration and study of cusped and closed hyperbolic 3-manifolds ([31], [33]), enumeration of knots and links ([2], [35]) and the study of hyperbolic Dehn surgery (e.g. [34]).

In the case of 3-manifolds with higher genus boundary components, Thurston suggested that partially truncated tetrahedra could be used to find a hyperbolic structure with (totally) geodesic boundary. Later, Kojima ([39], [40]) showed that Epstein and Penner’s canonical cell decomposition ([19]) of cusped hyperbolic 3-manifolds could be naturally extended to this case. Capitalizing on this, Frigerio and Petronio ([23]) have constructed a census of hyperbolic 3-manifolds with geodesic boundary. Parametrizing their “generalized triangulations” using dihedral angles they have implemented many of these ideas in a computer program `oggraphs` [21] by Frigerio, Martelli and Petronio.

In this chapter we examine generalized tetrahedra and show they are completely determined (up to isometry) by their vertex Gram matrices. These tetrahedra are the building blocks of our generalized triangulations in Chapter 2.

#### 1.1. Hyperbolic space

This section gives a brief introduction to hyperbolic space. The reader is referred to [62], [54] or [5] for a more thorough account.

The  $(n + 1)$ -dimensional Lorentzian space  $\mathbb{E}^{1,n}$  is the real vector space  $\mathbb{R}^{n+1}$  of dimension  $n + 1$  equipped with the Lorentzian inner product

$$(1.1) \quad \langle \mathbf{x}, \mathbf{y} \rangle := -x_0y_0 + x_1y_1 + \dots + x_ny_n,$$

where  $\mathbf{x} = (x_0, x_1, \dots, x_n)$  and  $\mathbf{y} = (y_0, y_1, \dots, y_n)$ . Let

$$H_- := \{ \mathbf{x} \in \mathbb{E}^{1,n} \mid \langle \mathbf{x}, \mathbf{x} \rangle = -1, x_0 > 0 \}$$

be the upper half sheet of the two sheeted hyperboloid. The restriction of the quadratic form induced by  $\langle \cdot, \cdot \rangle$  on  $\mathbb{E}^{1,n}$  to the tangent space of  $H_-$  is positive definite and so it gives a Riemannian metric on  $H_-$  producing the *hyperboloid*

*model* of  $n$ -dimensional hyperbolic space  $\mathbb{H}^n$ . (See Figure 1.1.) Under this metric the hyperbolic distance  $d$  between two points  $\mathbf{x}, \mathbf{y} \in H_- \subset \mathbb{E}^{1,n}$  can be calculated by the following formula:

$$(1.2) \quad \langle \mathbf{x}, \mathbf{y} \rangle = -\cosh d.$$

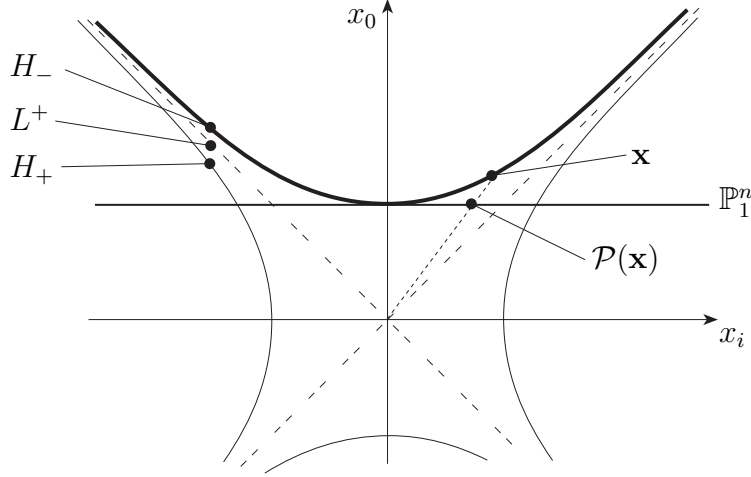


FIGURE 1.1. The real vector space  $\mathbb{R}^{n+1}$  equipped with the Lorentzian inner product is  $(n + 1)$ -dimensional Lorentzian space  $\mathbb{E}^{1,n}$ . Taking the upper sheet of the standard two sheeted hyperboloid with the induced metric gives  $n$ -dimensional hyperbolic space.

Let

$$L := \{\mathbf{x} \in \mathbb{E}^{1,n} \mid \langle \mathbf{x}, \mathbf{x} \rangle = 0\}$$

be the “light cone” and let

$$L^+ := \{\mathbf{x} \in \mathbb{E}^{1,n} \mid \langle \mathbf{x}, \mathbf{x} \rangle = 0, x_0 > 0\}$$

be its upper half. Then a ray in  $L^+$  starting at the origin corresponds to a point on boundary of  $\mathbb{H}^n$ . The set of such rays form the sphere at infinity  $\mathbb{S}_\infty^{n-1} = \partial\mathbb{H}^n$ . An arbitrary point  $\mathbf{u}$  in  $L^+$ , defines a *horosphere*

$$h_{\mathbf{u}} := \{\mathbf{x} \in \mathbb{H}^n \mid \langle \mathbf{x}, \mathbf{u} \rangle = -1\},$$

which inherits a Euclidean structure.

Let us denote by  $\mathcal{P}$  the radial projection from  $\{\mathbf{x} \in \mathbb{E}^{1,n} \mid x_0 \neq 0\}$  to the affine hyperplane

$$\mathbb{P}_1^n := \{\mathbf{x} \in \mathbb{E}^{1,n} \mid x_0 = 1\}$$

along the rays through the origin. The projection  $\mathcal{P}$  is a homeomorphism from  $H_-$  onto the  $n$ -dimensional open unit ball  $\mathbb{B}^n$  in  $\mathbb{P}_1^n$  centered at the origin  $(1, 0, 0, \dots, 0)$  of  $\mathbb{P}_1^n$ , which gives the *projective model* of  $\mathbb{H}^n$ . The affine hyperplane  $\mathbb{P}_1^n$  contains

$\mathbb{B}^n$  and its set theoretic boundary  $\partial\mathbb{B}^n$  in  $\mathbb{P}_1^n$ , which is identified with  $\mathbb{S}_\infty^{n-1}$ . Define  $\overline{\mathbb{B}^n} = \mathbb{B}^n \cup \partial\mathbb{B}^n$ .

The *one sheeted hyperboloid*  $H_+$  is defined to be

$$H_+ := \{\mathbf{x} \in \mathbb{E}^{1,n} \mid \langle \mathbf{x}, \mathbf{x} \rangle = 1\}.$$

For an arbitrary point  $\mathbf{u}$  in  $H_+$  define the geodesic hyperplane  $\mathbf{u}^\perp$  as

$$\mathbf{u}^\perp := \{\mathbf{x} \in \mathbb{H}^n \mid \langle \mathbf{x}, \mathbf{u} \rangle = 0\}.$$

A point  $\mathbf{u}$  in  $H_+$  also defines a half-space in  $\mathbb{H}^n$  given by

$$\Pi_{\mathbf{u}} = \{\mathbf{x} \in \mathbb{H}^n \mid \langle \mathbf{x}, \mathbf{u} \rangle \leq 0\}.$$

**Definition 1.1.** *The signed distance  $d$  between a horosphere and a hyperplane (resp. point, horosphere) is the distance by which the horosphere extends past the hyperplane (resp. point, horosphere). The distance  $d$  may be positive, negative or zero, as shown in Figure 1.2.*

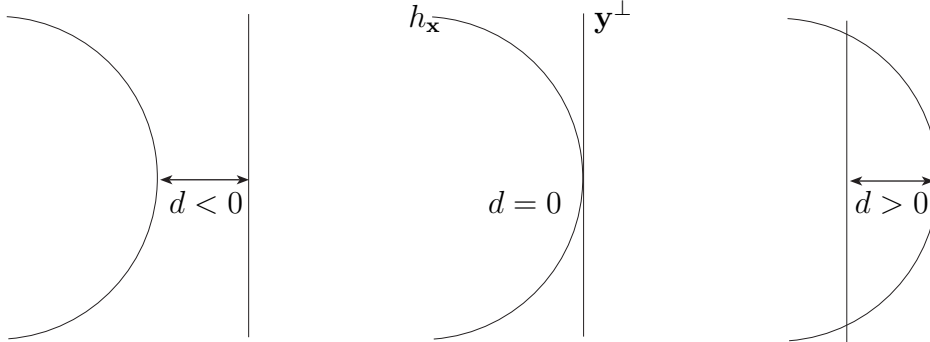


FIGURE 1.2. The signed distance from a hyperplane to a horosphere is the distance  $d$  by which the horosphere extends past the hyperplane.

The following theorem describes the relationship between the Lorentzian inner product and the geometry of points, hyperplanes and horospheres in  $\mathbb{H}^n$ . It is an extension of Propositions 2.1, 2.2 and 2.3 in [66] and Proposition 2.45 in [62].

**Theorem 1.2.** *The inner product of two points  $\mathbf{x}, \mathbf{y} \in H_- \cup L^+ \cup H_+$  can be interpreted as follows:*

- (1) *If  $\mathbf{x}, \mathbf{y} \in H_-$  then the hyperbolic distance  $d$  between them is given by*

$$\langle \mathbf{x}, \mathbf{y} \rangle = -\cosh d.$$

- (2) *If  $\mathbf{x}, \mathbf{y} \in H_+$  then one of the following holds:*

- (a) *The two geodesic hyperplanes  $\mathbf{x}^\perp$  and  $\mathbf{y}^\perp$  intersect in  $\mathbb{H}^n$  if and only if  $|\langle \mathbf{x}, \mathbf{y} \rangle| < 1$ . In this case the hyperbolic angle  $\theta$  between them, measured in  $\Pi_x$  and  $\Pi_y$ , is given by*

$$(1.3) \quad \langle \mathbf{x}, \mathbf{y} \rangle = -\cos \theta.$$

- (b) *The two geodesic hyperplanes  $\mathbf{x}^\perp$  and  $\mathbf{y}^\perp$  do not intersect in  $\overline{\mathbb{H}^n} = \mathbb{H}^n \cup \partial\mathbb{H}^n$  if and only if  $|\langle \mathbf{x}, \mathbf{y} \rangle| > 1$ . In this case the hyperbolic distance  $d$  between them is given by*

$$(1.4) \quad |\langle \mathbf{x}, \mathbf{y} \rangle| = \cosh d.$$

- (c) *Two geodesic hyperplanes  $\mathbf{x}^\perp$  and  $\mathbf{y}^\perp$  do not intersect in  $\mathbb{H}^n$  but intersect in  $\partial\mathbb{H}^n$  if and only if  $|\langle \mathbf{x}, \mathbf{y} \rangle| = 1$ . In this case the hyperbolic distance and angle between them are both 0.*

- (3) *Let  $\mathbf{x} \in H_-$  and  $\mathbf{y} \in H_+$ . Then the hyperbolic distance  $d$  between  $\mathbf{x}$  and  $\mathbf{y}^\perp$  is given by*

$$(1.5) \quad |\langle \mathbf{x}, \mathbf{y} \rangle| = \sinh d.$$

- (4) *Let  $\mathbf{x} \in H_+$  and  $\mathbf{y} \in L^+$ . Then the signed distance  $d$  between  $\mathbf{x}^\perp$  and  $h_{\mathbf{y}}$  is given by*

$$(1.6) \quad |\langle \mathbf{x}, \mathbf{y} \rangle| = e^{-d}.$$

- (5) *Let  $\mathbf{x} \in H_-$  and  $\mathbf{y} \in L^+$ . Then the signed distance  $d$  between  $\mathbf{x}$  and  $h_{\mathbf{y}}$  is given by*

$$(1.7) \quad \langle \mathbf{x}, \mathbf{y} \rangle = -e^{-d}.$$

- (6) *Let  $\mathbf{x}, \mathbf{y} \in L^+$ . Then the signed distance  $d$  between  $h_{\mathbf{x}}$  and  $h_{\mathbf{y}}$  is given by*

$$(1.8) \quad \langle \mathbf{x}, \mathbf{y} \rangle = -2e^{-d}.$$

PROOF. Note that the first equation is precisely (1.2). Here we prove equations (1.6), (1.7) and (1.8). The reader should refer to [62] for the remainder of the proof.

It is enough to prove equation (1.6) in  $\mathbb{H}^2$ . By an isometry of  $\mathbb{E}^{1,2}$  we can arrange that  $\mathbf{x}^\perp$  is contained in the  $x_0x_2$ -plane and the closest point on  $\mathbf{x}^\perp$  to  $h_{\mathbf{y}}$  is the origin. Then the unique geodesic that minimizes the distance between  $\mathbf{x}^\perp$  and  $h_{\mathbf{y}}$  must be contained in the  $x_0x_1$ -plane. (Refer to Figure 1.3.) So we can assume that  $\mathbf{y} = (s, s, 0) \in L^+$ , for some  $s > 0$ , and that  $\mathbf{x} = (0, \pm 1, 0) \in H_+$  (where the sign is determined by the sign of  $\langle \mathbf{x}, \mathbf{y} \rangle$ ). Then the point on  $h_{\mathbf{y}}$  that realizes the distance from  $\mathbf{x}^\perp$  to  $h_{\mathbf{y}}$  is  $(\cosh(-d), \sinh(-d), 0)$ . Since  $(\cosh(-d), \sinh(-d), 0) \in h_{\mathbf{y}}$ ,

$$\langle (\cosh(-d), \sinh(-d), 0), (s, s, 0) \rangle = -1,$$

giving  $s = e^{-d}$ . Hence,

$$\langle \mathbf{x}, \mathbf{y} \rangle = \langle (0, \pm 1, 0), (e^{-d}, e^{-d}, 0) \rangle = \pm e^{-d},$$

as required.

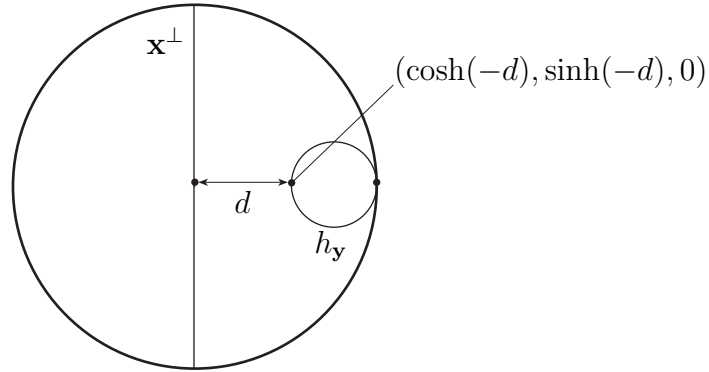


FIGURE 1.3. The picture in  $\mathbb{P}_1^2$ .

The proof of equation (1.7) is similar. It can be assumed that  $\mathbf{x}$  is positioned at  $(1, 0, 0)$  and  $\mathbf{y}$  is at  $(e^{-d}, e^{-d}, 0)$ . The result immediately follows.

For equation (1.8) it can be assumed that  $\mathbf{x} = (t, -t, 0) \in L^+$ , for some  $t > 0$ , and that the closest point on  $h_{\mathbf{x}}$  to  $h_{\mathbf{y}}$  is  $(1, 0, 0)$ . With this positioning  $\mathbf{y} = (s, s, 0) \in L^+$ , for some  $s > 0$ , and the point  $(\cosh(-d), \sinh(-d), 0)$  must be the closest point on  $h_{\mathbf{y}}$  to  $h_{\mathbf{x}}$ . Since  $(1, 0, 0) \in h_{\mathbf{x}}$ ,

$$\langle (1, 0, 0), (t, -t, 0) \rangle = -1$$

and so  $t = 1$ . On the other hand, because

$$\langle (s, s, 0), (\cosh(-d), \sinh(-d), 0) \rangle = -1,$$

it follows that  $s = e^{-d}$ . Therefore,

$$\langle \mathbf{x}, \mathbf{y} \rangle = \langle (1, -1, 0), (e^{-d}, e^{-d}, 0) \rangle = -2e^{-d},$$

as required.  $\square$

## 1.2. Generalized tetrahedra

Hyperbolic space is unique because unlike in spherical and Euclidean space, in hyperbolic space a tetrahedron can have vertices ‘at’ and ‘beyond’ the sphere at infinity. This is easiest to see in the projective model by moving the vertices from  $\mathbb{B}^3$  to  $\partial\mathbb{B}^3$ , and then outside  $\partial\mathbb{B}^3$ . This section defines a generalized tetrahedron and gives other related definitions. In the next chapter these will be the geometric building blocks used to find hyperbolic structures.

**Definition 1.3.** If  $\mathbf{v} \in \mathbb{E}^{1,n}$  then we define the normalized vector in the direction of  $\mathbf{v}$  as

$$\hat{\mathbf{v}} = \begin{cases} \frac{\mathbf{v}}{\sqrt{|\langle \mathbf{v}, \mathbf{v} \rangle|}}, & \text{if } \langle \mathbf{v}, \mathbf{v} \rangle \neq 0; \\ \mathbf{v}, & \text{otherwise.} \end{cases}$$

**Definition 1.4.** ([66]) Let  $\Delta$  be a simplex in  $\mathbb{P}_1^n$ . Suppose each codimension 2 face of  $\Delta$  intersects  $\overline{\mathbb{B}^n}$ .

- (1) Let  $\mathbf{v}$  be a vertex of  $\Delta$  outside  $\overline{\mathbb{B}^n}$ . The truncation at vertex  $\mathbf{v}$  is the operation of deleting the open neighbourhood of  $\mathbf{v}$  bounded by  $\mathcal{P}(\mathbf{v}^\perp)$ . The new face created  $\mathcal{P}(\mathbf{v}^\perp) \cap \Delta$  is called a truncation face.
- (2) The truncated simplex say,  $\Delta'$ , is the polyhedron in  $\mathbb{B}^n$  obtained by truncating  $\Delta$  at all its vertices lying outside  $\overline{\mathbb{B}^n}$  and omitting any vertices in  $\partial\mathbb{B}^n$ .
- (3) A generalized hyperbolic simplex in  $\mathbb{B}^n$  is a polyhedron which is either a simplex in the ordinary sense or a truncated simplex as described above. By a face of  $\Delta'$  we mean a face of the polyhedron which is not a truncation face.

By  $\hat{\Delta}$  we denote the projection of  $\Delta'$  to  $H_-$ . When  $n = 3$  this defines a generalized hyperbolic tetrahedron. Refer to Figure 1.4 for more detail.

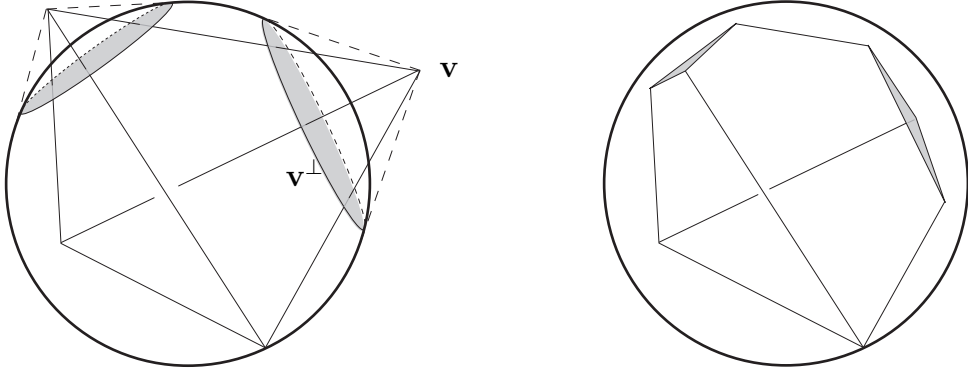


FIGURE 1.4. A tetrahedron in  $\mathbb{P}_1^3$  with one vertex in  $\mathbb{B}^3$ , one vertex in  $\partial\mathbb{B}^3$  and two vertices outside  $\overline{\mathbb{B}^3}$ . Truncation produces a generalized tetrahedron with one finite vertex, one ideal vertex and two truncation faces corresponding to hyperinfinite vertices.

By a *generalized tetrahedron* we will mean a generalized hyperbolic tetrahedron unless otherwise stated.

As in [66], we regard the vertices of  $\Delta'$  as those of  $\Delta$ . Any vertex of  $\Delta'$  lying outside  $\overline{\mathbb{B}^3}$  is no longer a vertex in the ordinary sense, but we will call it a

*hyperinfinite vertex* of  $\Delta'$ . Any vertex of  $\Delta'$  lying in  $\mathbb{B}^3$  (resp.  $\partial\mathbb{B}^3$ ) is also a vertex of  $\Delta'$  in the ordinary sense and we will call it a *finite* (resp. *ideal*) *vertex* of  $\Delta'$ .

Let  $\Delta'$  be a generalized tetrahedron in  $\mathbb{P}_1^3$  with vertices  $\mathbf{v}_1, \mathbf{v}_2, \mathbf{v}_3, \mathbf{v}_4$  in  $\mathbb{P}_1^3$ . Then we also regard  $\mathbf{u}_1, \mathbf{u}_2, \mathbf{u}_3, \mathbf{u}_4 \in \mathbb{E}^{1,3}$  as a set of vertices for  $\Delta'$  if  $\mathcal{P}(\mathbf{u}_i) = \mathbf{v}_i$  for  $i = 1, 2, 3, 4$ . The  $i$ -th *face* of  $\Delta'$  is the face opposite  $\mathbf{v}_i$ .

Denote the truncation triangle in  $\mathbb{H}^3$  at each hyperinfinite vertex  $\mathbf{v}_i \in \mathbb{E}^{1,3}$  by  $\Delta^{\mathbf{v}_i} = \hat{\Delta} \cap \mathbf{v}_i^\perp$ . Also denote by  $\Delta^{\mathbf{v}_i} = \hat{\Delta} \cap h_{\mathbf{v}_i}$  the horospherical Euclidean triangle in  $H_-$  at each ideal vertex of  $\mathbf{v}_i \in \mathbb{E}^{1,3}$ . Note that the definition of  $\Delta^{\mathbf{v}_i}$ , for an ideal vertex  $\mathbf{v}_i$ , is affected by the rescaling of  $\mathbf{v}_i$ .

A *length-0* edge is an edge of  $\Delta'$  that meets  $\overline{\mathbb{B}^3}$  only at  $\partial\mathbb{B}^3$ . The dihedral angle formed between the faces at such an edge is 0. See Figure 1.5 and refer to [23] for more detail.

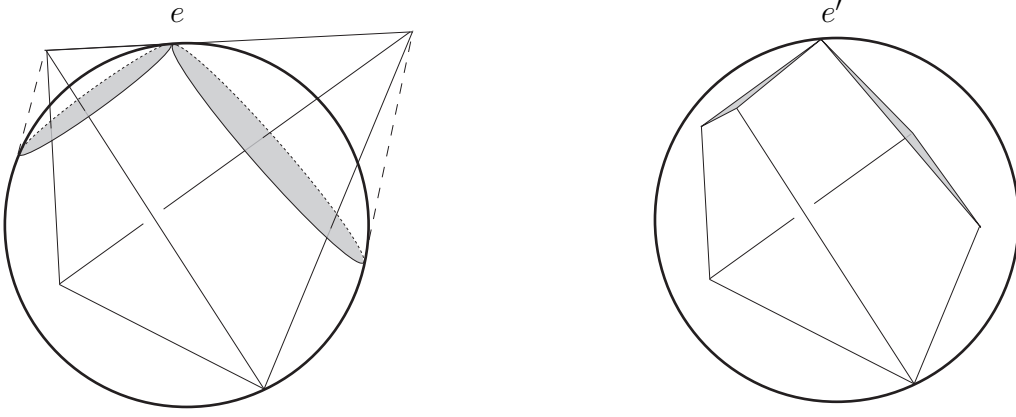


FIGURE 1.5. The edge  $e$  of  $\Delta$  meets  $\overline{\mathbb{B}^3}$  only at  $\partial\mathbb{B}^3$ . After truncation  $e$  becomes a length-0 edge  $e'$ .

### 1.3. Gram matrices

Let  $\Delta'$  be a generalized tetrahedron with vertices  $\mathbf{v}_1, \mathbf{v}_2, \mathbf{v}_3, \mathbf{v}_4$  in  $\mathbb{E}^{1,3}$ . Let  $V$  be the matrix with the  $\mathbf{v}_i$  as columns and denote by  $J$  the  $4 \times 4$  matrix

$$J = \begin{pmatrix} -1 & 0 & 0 & 0 \\ 0 & 1 & 0 & 0 \\ 0 & 0 & 1 & 0 \\ 0 & 0 & 0 & 1 \end{pmatrix}.$$

Then we define the *vertex Gram matrix* of  $\Delta'$  to be the symmetric  $4 \times 4$  matrix

$$(1.9) \quad G = V^t J V = \begin{pmatrix} v_{11} & v_{12} & v_{13} & v_{14} \\ v_{12} & v_{22} & v_{23} & v_{24} \\ v_{13} & v_{23} & v_{33} & v_{34} \\ v_{14} & v_{24} & v_{34} & v_{44} \end{pmatrix},$$

where  $v_{ij} = \langle \mathbf{v}_i, \mathbf{v}_j \rangle$ . It will be shown in Theorem 1.5 that  $G$  completely determines  $\Delta'$  up to hyperbolic isometry. Moreover, it also specifies a horospherical triangle  $\Delta^{\mathbf{v}_i} = \{\mathbf{x} \in \mathbb{H}^3 \mid \langle \mathbf{v}_i, \mathbf{x} \rangle = -1\} \cap \Delta'$  in the link of every ideal vertex  $\mathbf{v}_i$  of  $\Delta'$ .

Given  $\Delta'$  and some choice of vertices, we can define a unique choice of normals to faces  $\mathbf{w}_1, \mathbf{w}_2, \mathbf{w}_3, \mathbf{w}_4$  by the equation

$$(1.10) \quad V^t J W = \sqrt{-\det(G)} I,$$

where the  $\mathbf{w}_i$  make up the columns of  $W$ . (Note that  $\det(G) < 0$ .) Thus, given  $\Delta'$  and its vertices, we can define the *normal Gram matrix* of  $\Delta'$

$$G_* = W^t J W = \begin{pmatrix} w_{11} & w_{12} & w_{13} & w_{14} \\ w_{12} & w_{22} & w_{23} & w_{24} \\ w_{13} & w_{23} & w_{33} & w_{34} \\ w_{14} & w_{24} & w_{34} & w_{44} \end{pmatrix},$$

where  $w_{ij} = \langle \mathbf{w}_i, \mathbf{w}_j \rangle$ . According to Theorem 1.2 the dihedral angle  $\theta_{ij}$  between the  $i$ -th and  $j$ -th faces of  $\Delta'$  is given by

$$\cos \theta_{ij} = \frac{-w_{ij}}{\sqrt{w_{ii} w_{jj}}}.$$

Since

$$\begin{aligned} G G_* &= V^t J V W^t J W \\ &= V^t (W^t)^{-1} (W^t J V) W^t J W \\ &= \sqrt{-\det(G)} V^t J W \\ &= -\det(G) I, \end{aligned}$$

we have,

$$(1.11) \quad G_* = -\det(G) G^{-1}.$$

So the dihedral angles between the faces of  $\Delta'$  can be computed from the entries of  $G$  alone. Let  $G_{ij}$  be the matrix obtained by deleting the  $i$ -th row and  $j$ -th column of  $G$ . Then denote by  $c_{ij}$  the  $(i, j)$ -th cofactor of  $G$ ,

$$c_{ij} = (-1)^{i+j} \det(G_{ij}).$$

Equation (1.11) asserts that

$$(1.12) \quad c_{ij} = -w_{ij},$$

so

$$(1.13) \quad \cos \theta_{ij} = \frac{c_{ij}}{\sqrt{c_{ii} c_{jj}}}.$$

**Remark:** Thurston used similar calculations to express the angles between faces of generalized triangles in terms their edge lengths. Using this, he derived versions of the hyperbolic sine and cosine laws. See [61] or [62] for more details.

The following theorem determines the set of all vertex Gram matrices:

**Theorem 1.5.** *Let  $G$  be a real symmetric  $4 \times 4$  matrix. Then  $G = (v_{ij})$  is a vertex Gram matrix for some generalized hyperbolic tetrahedron  $\Delta'$  if and only if*

- (1)  $G$  has one negative and three positive eigenvalues,
- (2)  $c_{ii} < 0$  for all  $i$ ,
- (3)  $c_{ij}^2 \leq c_{ii}c_{jj}$  for all  $i$  and  $j$ ,

where the  $(i, j)$ -th cofactor of  $G$  is  $c_{ij}$ .

Furthermore, every such  $G$  represents a unique  $\Delta'$  in  $\mathbb{E}^{1,3}$  up to isometry.

In a sense this result is ‘dual’ to Theorem 3.2 in [66]. Recognizing the significance of the eigenvalues of the vertex Gram matrix provides a cleaner proof.

**PROOF.** Let  $G$  be a real symmetric  $4 \times 4$  matrix satisfying the above conditions. Then  $G$  has eigenvalues  $\lambda_0, \lambda_1, \lambda_2, \lambda_3$  where  $\lambda_0 < 0 < \lambda_1 \leq \lambda_2 \leq \lambda_3$ . There exists an orthogonal matrix  $U$  (whose columns are eigenvectors) such that

$$G = U\Lambda U^t,$$

where  $\Lambda = \text{diagonal}(\lambda_0, \lambda_1, \lambda_2, \lambda_3)$  is the diagonal matrix with diagonal entries  $\lambda_0, \lambda_1, \lambda_2$  and  $\lambda_3$ . Now define “ $\sqrt{\Lambda}$ ” to be the matrix

$$\sqrt{\Lambda} = \begin{pmatrix} \sqrt{-\lambda_0} & 0 & 0 & 0 \\ 0 & \sqrt{\lambda_1} & 0 & 0 \\ 0 & 0 & \sqrt{\lambda_2} & 0 \\ 0 & 0 & 0 & \sqrt{\lambda_3} \end{pmatrix}.$$

Then if  $V = \sqrt{\Lambda}U^t$  we see that

$$G = V^t J V.$$

The goal is to show that the columns of  $V$ , say  $\mathbf{v}_i$ , are the vertices of some generalized tetrahedron  $\Delta'$ . Since (1) holds,  $\det(V) \neq 0$ . So  $\{\mathbf{v}_1, \mathbf{v}_2, \mathbf{v}_3, \mathbf{v}_4\}$  is linearly independent and thus gives a basis for  $\mathbb{E}^{1,3}$ . Moreover, the convex hull  $C$  of the  $\mathbf{v}_i$  is a tetrahedron. All that remains to show is that each edge  $e_{ij}$ , between vertices  $\mathbf{v}_i$  and  $\mathbf{v}_j$ , passes through  $\mathbb{H}^3 \cup \partial\mathbb{H}^3$ .

Let  $W$  be the matrix such that

$$V^t J W = \sqrt{-\det(G)} I;$$

then the columns of  $W$  are normal to the faces of  $C$ . It follows from equation (1.12) that

$$G_* = W^t J W = (-c_{ij}),$$

and since  $c_{ii} < 0$  we have  $w_{ii} > 0$ , and so each face of  $C$  intersects  $\mathbb{H}^3$ . Furthermore, because  $c_{ij}^2 \leq c_{ii}c_{jj}$ ,  $|\langle \hat{\mathbf{w}}_i, \hat{\mathbf{w}}_j \rangle| \leq 1$ , for all  $i, j$ . Therefore Theorem 1.2 shows that each edge  $e_{ij}$  passes through  $\mathbb{H}^3 \cup \partial\mathbb{H}^3$ .

Conversely, let  $\Delta'$  be a generalized tetrahedron with vertex Gram matrix  $G$ . Then since the  $\mathbf{v}_i$  form a basis for  $\mathbb{E}^{1,3}$ ,  $\det(V) \neq 0$ . By applying Sylvester's inertia law to equation (1.9), it is apparent that  $G$  has one negative and three positive eigenvalues [29]. The second and third conditions follow from Theorem 1.2 and equation (1.12).

For the last part of the theorem, assume that the vertex Gram matrices of two generalized tetrahedra  $\Delta'_1, \Delta'_2 \subset \mathbb{E}^{1,3}$  are equal. Let  $V_i$  be the matrix with the vertices of  $\Delta'_i$  as columns. Then we have

$$(1.14) \quad V_1^t J V_1 = V_2^t J V_2.$$

We wish to find a hyperbolic isometry which extends to  $\mathbb{E}^{1,3}$  and maps the vertices of  $\Delta'_1$  to the vertices of  $\Delta'_2$ . Since  $V_1$  is invertible, it is enough to show that  $g = V_2 V_1^{-1}$  is the extension of a hyperbolic isometry. Equivalently, we must show that  $g \in O(1, 3)$  and  $g$  sends the upper half of  $\mathbb{E}^{1,3}$  to itself.

It follows immediately from equation (1.14), that

$$g^t J g = (V_2 V_1^{-1})^t J (V_2 V_1^{-1}) = J,$$

hence  $g$  is in  $O(1, 3)$ . To show  $g$  sends the upper half space of  $\mathbb{E}^{1,3}$  to itself, note that by multiplying the vertices of  $\Delta'_1$  and  $\Delta'_2$  by  $-1$  we can assume that the  $x_0$  coordinate of each of the vertices is positive. Let  $\mathbf{v}_i^1$  be the first vertex of  $\Delta'_i$ . Then since  $\mathbf{v}_1^1$  is mapped to  $\mathbf{v}_1^2$  the entire upper half of  $\mathbb{E}^{1,3}$  must be mapped to itself by  $g$ .  $\square$

The proof of Theorem 1.5 provides a method for realizing a tetrahedron from its vertex Gram matrix.

**Example 1.6.** Consider the vertex Gram matrix of the form

$$G = \begin{pmatrix} t & a & b & c \\ a & t & c & b \\ b & c & t & a \\ c & b & a & t \end{pmatrix}$$

with  $a, b, c < 0$ . Then  $G$  has eigenvalues

$$\lambda_0 = a + b + c + t, \lambda_1 = a - b - c + t, \lambda_2 = -a + b - c + t \text{ and } \lambda_3 = -a - b + c + t,$$

with corresponding orthonormal eigenvectors (with respect to the Euclidean inner product),

$$\mathbf{u}_0 = \frac{1}{2} \begin{pmatrix} 1 \\ 1 \\ 1 \\ 1 \end{pmatrix}, \mathbf{u}_1 = \frac{1}{2} \begin{pmatrix} 1 \\ 1 \\ -1 \\ -1 \end{pmatrix}, \mathbf{u}_2 = \frac{1}{2} \begin{pmatrix} 1 \\ -1 \\ 1 \\ -1 \end{pmatrix} \text{ and } \mathbf{u}_3 = \frac{1}{2} \begin{pmatrix} 1 \\ -1 \\ -1 \\ 1 \end{pmatrix}.$$

According to condition (1) of Theorem 1.5 in order for  $G$  to be the vertex Gram matrix of some generalized tetrahedron the eigenvalues must satisfy the inequalities

$$\lambda_0 < 0 \text{ and } \lambda_i > 0,$$

for  $i = 1, 2, 3$ . Given  $a, b, c < 0$ , this can only happen when  $t$  satisfies

$$(1.15) \quad \max(b + c - a, a + c - b, a + b - c) < t < -a - b - c.$$

As in the proof, the columns of the matrix

$$V = \frac{1}{2} \begin{pmatrix} \sqrt{-\lambda_0} & \sqrt{-\lambda_0} & \sqrt{-\lambda_0} & \sqrt{-\lambda_0} \\ \sqrt{\lambda_1} & \sqrt{\lambda_1} & -\sqrt{\lambda_1} & -\sqrt{\lambda_1} \\ \sqrt{\lambda_2} & -\sqrt{\lambda_2} & \sqrt{\lambda_2} & -\sqrt{\lambda_2} \\ \sqrt{\lambda_3} & -\sqrt{\lambda_3} & -\sqrt{\lambda_3} & \sqrt{\lambda_3} \end{pmatrix}$$

give the vertices of a tetrahedron, say  $\Delta$ . Notice that by realizing the tetrahedron

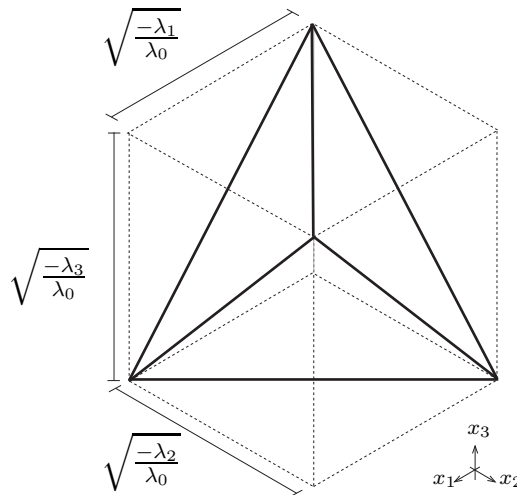


FIGURE 1.6.  $\Delta$  inscribed in a rectangular box centered at the origin with sides of length  $\sqrt{\frac{-\lambda_1}{\lambda_0}}$ ,  $\sqrt{\frac{-\lambda_2}{\lambda_0}}$ ,  $\sqrt{\frac{-\lambda_3}{\lambda_0}}$  parallel to the  $x_1$ ,  $x_2$ ,  $x_3$  axes.

through this method,  $\Delta$  is inscribed in a rectangular box centered at the origin as shown in Figure 1.6. Conditions (2) and (3) of Theorem 1.5 require that the edges of  $\Delta$  meet the closed unit ball. Using Figure 1.6 this can be ensured more directly.

With this description it is clear that the midpoints of the edges of  $\Delta$  must intersect the closed unit ball, which can only happen if

$$(1.16) \quad -\frac{\lambda_i}{\lambda_0} \leq 4$$

for  $i = 1, 2, 3$ . Combining equations (1.15) and (1.16) gives a non-empty convex set of  $(a, b, c, t)$  parametrizing generalized tetrahedra.

In Figure 1.6 it is also easy to see that as  $\lambda_i \rightarrow 0$  for some  $i > 0$ ,  $\Delta$  flattens into the plane defined by two coordinate axes, and its vertices become linearly dependent. Section 2.3 will establish a method of dealing with this issue and also allow tetrahedra to turn inside out — becoming *negatively oriented*. Until then assume all the tetrahedra are *positively oriented*, with dihedral angles lying in the interval  $(0, \pi)$ .

**Question:** In [66], Ushijima gives a formula for computing the volume of a generalized tetrahedron  $\Delta'$  in terms of dihedral angles. Is there a formula for computing the volume of  $\Delta'$  in terms of its vertex Gram matrix  $G$ ?

This question has been resolved in the case of a finite hyperbolic tetrahedron by Murakami and Ushijima in [49].

## CHAPTER 2

### Finding hyperbolic structures on 3-orbifolds

The collection of all manifolds is a subset of the collection of all orbifolds. Roughly speaking, an orbifold is modelled on Euclidean space modulo a finite group of symmetries. Orbifolds were first introduced by Thurston, and his lecture notes ([61]) still provide one of the best resources on the topic.

The section that follows is a brief introduction to orbifolds. For more detail the reader should refer to [8], [9], [10] or [61]. The definitions are as in [16] which provides an excellent reference. In practice the precise definition of an orbifold is not used, instead Theorem 2.1 is employed which asserts that a 3-orbifold looks like a 3-manifold containing a singular graph.

The remainder of the chapter outlines a new method for computing hyperbolic structures on 3-orbifolds. In general this process is too difficult to do by hand, so topologists rely heavily on computer programs such as SnapPea ([69]). SnapPea allows the user to perform orbifold surgeries on knot and links in  $\mathbb{S}^3$ . If the singular set of a 3-orbifold is more complicated than a link, then there has been no general tool available — until now. Orb is a computer program that implements this new method, allowing easy computation of many geometric and topological invariants on a large class of 3-orbifolds. Chapter 4 illustrates the application of this new tool.

#### 2.1. Orbifolds

The precise definition of a (smooth) orbifold is quite complicated. It looks similar to the definition of a (smooth) manifold except that each point in an orbifold has a neighbourhood that looks like Euclidean space divided out by a finite group of diffeomorphisms.

A *local model* is a pair  $(\tilde{U}, G)$ , where  $\tilde{U}$  is an open subset of  $\mathbb{R}^n$  and  $G$  is a finite group of diffeomorphisms of  $\tilde{U}$ . It is often convenient to abuse notation and refer to the quotient space  $U = \tilde{U}/G$  as the local model. An *orbifold map* between local models is a pair  $(\tilde{\psi}, \gamma)$  where  $\tilde{\psi} : \tilde{U} \rightarrow \tilde{U}'$  is smooth and,  $\gamma : G \rightarrow G'$  is a homomorphism such that  $\tilde{\psi}(g\tilde{x}) = \gamma(g)\tilde{\psi}(\tilde{x})$  for all  $g \in G$  and  $x \in \tilde{U}$ . Such a map  $\tilde{\psi}$  induces a map  $\psi : \tilde{U}/G \rightarrow \tilde{U}'/G'$  and if  $\gamma$  is a monomorphism and  $\psi, \tilde{\psi}$  are injective we say that  $\psi$  is an *orbifold isomorphism*. These local models are the

building blocks for an orbifold whilst the orbifold maps indicate how the pieces fit together. (Refer to Figures 2.1 and 2.2.)

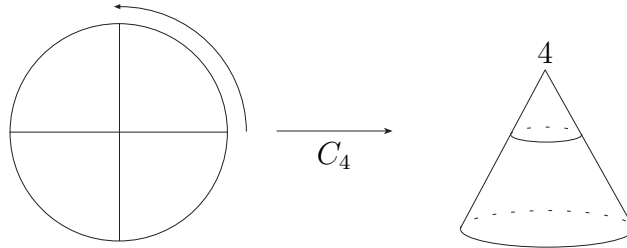


FIGURE 2.1. One possible model is given by dividing an open disc by a rotational symmetry. The result is a cone whose tip is called a *cone point*. If the cone is the quotient by a cyclic group of order  $n$  then the cone point is labelled  $n$  and the cone angle is  $\frac{2\pi}{n}$ .

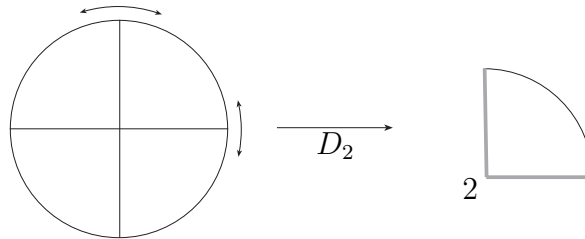


FIGURE 2.2. Another possible local model is given by dividing an open disc out by the dihedral group  $D_n$  of order  $2n$ . The result is a sector of a disc with a *corner point* with angle  $\frac{\pi}{n}$ . *Mirrors* are shaded in the picture while the corner point is labelled  $n$ .

An  $n$ -dimensional orbifold  $Q$  consists of a pair  $(X_Q, \mathcal{U})$  where  $X_Q$  is the *underlying space* which is a Hausdorff, paracompact, topological space and  $\mathcal{U}$  is an orbifold atlas. The atlas consists of a collection of *coordinate charts*  $(U_i, \phi_i)$  where the sets  $U_i$  form an open cover for  $X_Q$  such that every non-empty intersection of any pair of sets is also in the cover. For each chart there is a local model  $\tilde{U}_i/G_i$  and a homeomorphism  $\phi_i : U_i \rightarrow \tilde{U}_i/G_i$ . These charts must satisfy the *compatibility conditions* that whenever  $U_i \subset U_j$  the inclusion map is an orbifold local isomorphism. (See Figure 2.3.)

The *local group*  $G_x$  at a point  $x$  in a local model  $\tilde{U}/G$  is the stabilizer of any point  $\tilde{x} \in \tilde{U}$  projecting to  $x$ . The *singular locus*  $\Sigma(Q)$  of  $Q$  is defined to be  $\{x \in X_Q : G_x \neq \{1\}\}$ . Thus an orbifold is a *manifold* precisely when  $\Sigma(Q) = \emptyset$ .

An orbifold is *locally orientable* if it has an atlas  $\{(U_i, \phi_i)\}$  where each local model is given by a quotient  $U_i = \tilde{U}_i/G_i$  where  $G_i$  is an orientation preserving group. It is *orientable* if in addition the inclusion maps  $U_i \subset U_j$  are induced by orientation preserving maps  $\tilde{U}_i \rightarrow \tilde{U}_j$ .

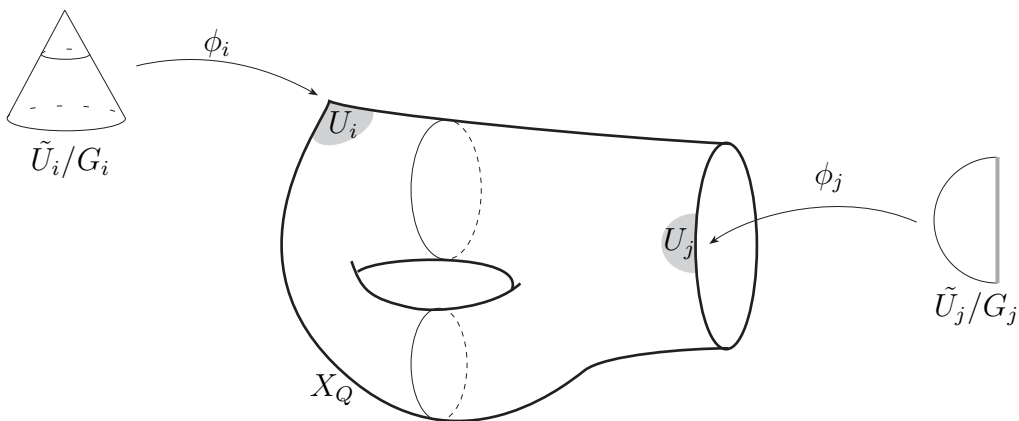


FIGURE 2.3. The open sets  $\mathcal{U}$  cover  $X_Q$ . Each set  $U_i \in \mathcal{U}$  has a chart  $\phi_i$  and a local model  $\tilde{U}_i/G_i$ . The compatibility conditions imply that two overlapping sets  $U_i$  and  $U_j$  have local models that agree.

It is often easiest to describe low dimensional orbifolds pictorially. On the left of Figure 2.4 is a torus with one cone point labelled 3. The torus is the underlying space of the orbifold and the 3 indicates that the local group at the cone point is  $C_3$ ; the cyclic group of order 3. The notation we use to denote such an orbifold is  $\mathbb{T}(3)$ . More generally, we denote an orientable 2-orbifold  $Q$  by  $X_Q(c_1, \dots, c_n)$  where  $X_Q$  is the underlying space and  $c_1, \dots, c_n$  indicate the cyclic groups at the cone points.

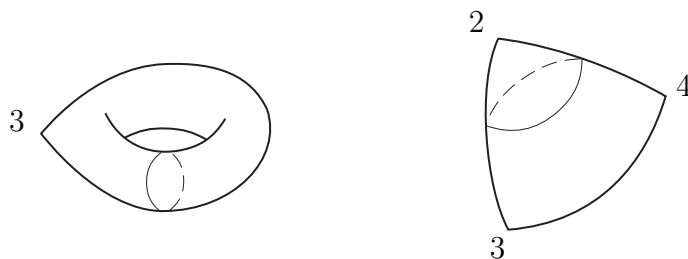


FIGURE 2.4. The 2-orbifolds  $\mathbb{T}(3)$  and  $\mathbb{S}^2(2, 3, 4)$ .

An *orbifold with boundary*  $Q$  is defined similarly by replacing  $\mathbb{R}^n$  by the closed half space  $\mathbb{R}_+^n$ . The *orbifold boundary*  $\partial_{orb}Q$  of  $Q$  corresponds to the points in the boundary of  $\mathbb{R}_+^n$  in the local models. Thus a point  $x$  is in  $\partial_{orb}Q$  if there is a coordinate chart  $\phi : U \rightarrow \tilde{U}/G$  with  $x \in U$  such that  $\phi(x) \in (\tilde{U} \cap \partial\mathbb{R}_+^n)/G$ . An orbifold is *closed* if it is compact and the orbifold boundary is empty.

Note that the orbifold boundary is generally not the same as the boundary of the underlying space. The set of points in the singular locus of an orbifold  $Q$  which are locally modelled on the quotient of  $\mathbb{R}^n$  by reflection, is called the *mirror singular locus*  $\Sigma_{mirror}(Q)$ . The boundary of the underlying space is  $\partial_{top}X_Q = \partial_{orb}Q \cup \Sigma_{mirror}(Q)$ .

Let  $X$  be a Riemannian manifold and  $G$  a group acting transitively on  $X$ . Then a  $(G, X)$ -orbifold is locally modelled on  $X$  modulo finite subgroups of  $G$ . In particular an orbifold is *hyperbolic* if  $X = \mathbb{H}^n$  and  $G = \text{Isom}(X)$ . Similarly, if  $X = \mathbb{E}^n$  or  $\mathbb{S}^n$  and  $G = \text{Isom}(X)$  then the orbifold is *Euclidean* or *spherical*. Such orbifolds have more structure as they inherit metrics from  $X$ . We say an orbifold is *complete* if it is complete as a metric space.

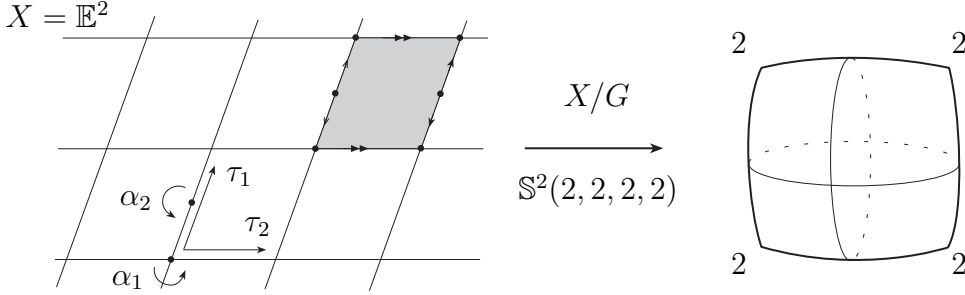


FIGURE 2.5. The 2-orbifold  $\mathbb{S}^2(2, 2, 2, 2)$  is Euclidean. It can be created by dividing  $\mathbb{E}^2$  by the group generated by the two rotations  $\alpha_1, \alpha_2$  and the two translations  $\tau_1, \tau_2$  of the Euclidean plane.

It turns out that if a given orbifold  $Q$  is 2-dimensional there is an easy way to determine if it has a hyperbolic, Euclidean or spherical structure. This identification relies on the *orbifold Euler characteristic*  $\chi(Q)$ . To evaluate  $\chi(Q)$ , first  $Q$  must be decomposed into open cells so the local group associated to the interior points of any cell is constant. Then  $\chi(Q)$  is defined by the formula

$$\chi(Q) = \sum_{c_i} (-1)^{\dim(c_i)} \frac{1}{|G_{c_i}|}$$

where  $c_i$  ranges over the cells and  $|G_{c_i}|$  is the order of the group  $G_{c_i}$  associated to the cell.

Apart from orbifolds of the type  $\mathbb{S}^2(n)$  and  $\mathbb{S}^2(n, m)$  ( $n > m \geq 2$ ) every closed orientable 2-orbifold  $Q$  has a spherical, Euclidean or hyperbolic structure determined by the sign of  $\chi(Q)$ :

- $Q$  is spherical if and only if  $\chi(Q) > 0$ ;
- $Q$  is Euclidean if and only if  $\chi(Q) = 0$ ;
- $Q$  is hyperbolic if and only if  $\chi(Q) < 0$ ;

It is then easy to show that the only closed orientable Euclidean 2-orbifolds are the torus,  $\mathbb{S}^2(2, 2, 2, 2)$ ,  $\mathbb{S}^2(2, 3, 6)$ ,  $\mathbb{S}^2(2, 4, 4)$  and  $\mathbb{S}^2(3, 3, 3)$ . The only closed orientable spherical 2-orbifolds are  $\mathbb{S}^2$ ,  $\mathbb{S}^2(2, 3, 3)$ ,  $\mathbb{S}^2(2, 3, 4)$ ,  $\mathbb{S}^2(2, 3, 5)$ ,  $\mathbb{S}^2(n, n)$  and  $\mathbb{S}^2(2, 2, n)$ , for  $n \geq 2$ .

Let  $Q_1 = \mathbb{H}^n/G_1$  and  $Q_2 = \mathbb{H}^n/G_2$  be two complete hyperbolic  $n$ -orbifolds of finite volume ( $n \geq 3$ ). Then Mostow-Prasad rigidity says that  $Q_1$  and  $Q_2$  are

isomorphic orbifolds if and only if the groups  $G_1$  and  $G_2$  are conjugate in  $\text{Isom}(\mathbb{H}^n)$ . Hence, geometric invariants of complete hyperbolic 3-orbifolds are also topological invariants. See [48] or [52] for more detail.

Let  $Q$  be an  $n$ -orbifold and let  $x \in Q$ . Since  $n$ -orbifolds are locally modelled on  $\mathbb{R}^n$  modulo finite subgroups of  $O(n)$ ,  $x$  has a neighbourhood which is a cone on a spherical  $(n - 1)$ -orbifold  $\mathbb{S}^{n-1}/G$ . This gives us an extremely convenient way of describing 3-orbifolds:

**Theorem 2.1.** [61] *Let  $Q$  be an orientable 3-orbifold. Then the underlying space  $X_Q$  is an orientable 3-manifold and the singular set consists of edges of order  $k \geq 2$  and vertices where 3 edges meet. At a vertex the three edges have orders corresponding to the cone points on a compact orientable spherical 2-orbifold. Conversely, every such labelled graph in an orientable 3-manifold describes an orientable 3-orbifold.*

The remainder of this chapter will avoid local models, charts and atlases by using this result. We will regard an orientable 3-orbifold as a 3-manifold containing a labelled singular graph that satisfies the conditions of Theorem 2.1. (See Figure 2.6.)

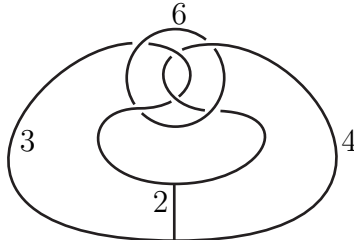


FIGURE 2.6. Consider this labelled knotted graph  $\Gamma$  as the singular set of a 3-orbifold with underlying space  $\mathbb{S}^3$ . By relabelling the edges in a manner that agrees with Theorem 2.1, a family of 3-orbifolds can be created. The numbers along the edges of  $\Gamma$  describe the local groups.

## 2.2. The parameters and equations

Let  $M$  be a closed 3-manifold and  $\Gamma \subset M$  a labelled graph satisfying the conditions of Theorem 2.1. Then we can define a 3-orbifold  $Q$  by the pair  $(M, \Gamma)$ .

For orientable hyperbolic 3-orbifolds with finite volume the scope of the labelling on  $\Gamma$  can be increased to allow for vertices coned on closed orientable Euclidean 2-orbifolds. A hyperbolic structure can be placed on  $Q$  by removing any such vertex from  $M$ , creating a cusp. We can also allow vertices coned on closed orientable

hyperbolic 2-orbifolds. In this case we can slice a neighbourhood of the vertex off, creating a 3-orbifold with (totally) geodesic boundary. (See [23], [24], [61].)

Let  $\Gamma$  be a graph in a closed 3-manifold  $M$  with vertices of degree 3 and edges labelled by integers  $\geq 2$ . A *triangulation*  $T$  of  $Q = (M, \Gamma)$  is a decomposition of  $M$  into “topological generalized tetrahedra” with

- $\Sigma(Q)$  contained in the 1-skeleton of  $T$ , and
- one vertex for each vertex of  $\Gamma$ .

An algorithm for finding such a triangulation when  $M = \mathbb{S}^3$  and  $\Gamma$  is represented by a projection is described in the Appendix.

The labelling on the edges  $\Sigma(Q)$  induces a labelling on the edges of  $T$ . Let  $n_e$  denote the labelling on an edge  $e$  of  $T$ , taking  $n_e$  to be 1 if  $e$  does not contain an edge of  $\Sigma(Q)$ . Denote the orbifold in the link of vertex  $v$  by  $S_v$ .

Then to place a complete hyperbolic structure with geodesic boundary on  $Q$  we need to replace this topological triangulation by a triangulation realized by generalized hyperbolic tetrahedra so that:

- (1) The gluing maps are hyperbolic isometries.
- (2) The sum of the dihedral angles of the tetrahedra incident to each edge  $e$  in  $T$  is  $\frac{2\pi}{n_e}$ .
- (3) For each vertex  $v$  of  $T$  with  $\chi(S_v) \leq 0$  we have:
  - (a) If  $v$  is ideal then the cusp produced by omitting  $v$  has a horospherical cross-section.
  - (b) If  $v$  is hyperinfinite then the boundary component of  $\partial Q$  produced by removing a neighbourhood is (totally) geodesic.

Condition (2) is known as the *edge condition*. Conditions (1) and (2) are enough to give a hyperbolic structure. Conditions (3a) and (3b) guarantee completeness and geodesic boundary.

We now examine what happens if we replace condition (1) above by the condition:

- (1') We can realize the tetrahedra of  $T$  in Lorentzian space so that the gluing maps are Lorentzian isometries.

With this stronger hypothesis consider the link of a cusp  $C$  of  $Q$ . Choose a generalized tetrahedron  $\Delta'_1 \subset \mathbb{E}^{1,3}$  whose vertex  $\mathbf{v}_1$  maps into  $C$ . Since  $\mathbf{v}_1$  lies on the light cone it specifies a *preferred* horospherical triangle in  $\mathbb{H}^3$  given by  $\Delta^{\mathbf{v}_1} = \{\mathbf{x} \in \mathbb{H}^3 \mid \langle \mathbf{x}, \mathbf{v}_1 \rangle = -1\} \cap \Delta'_1$ . Let  $\Delta'_{f_1} \subset \mathbb{E}^{1,3}$  denote one of the faces of  $\Delta'_1$  incident to  $\mathbf{v}_1$ . Then

$$\Delta^{\mathbf{v}_1}_{f_1} = \{\mathbf{x} \in \mathbb{H}^3 \mid \langle \mathbf{x}, \mathbf{v}_1 \rangle = -1\} \cap \Delta'_{f_1} = \Delta^{\mathbf{v}_1} \cap \Delta'_{f_1}$$

is a *preferred* horocycle for  $\Delta'_{f_1}$ . Note that this is just the restriction of  $\Delta^{\mathbf{v}_1}$  to  $\Delta'_{f_1}$ .

Let  $\Delta'_2 \subset \mathbb{E}^{1,3}$  be a generalized tetrahedron neighbouring  $\Delta'_1$  in  $T$  whose vertex  $\mathbf{v}_2$  maps into cusp  $C$ . Let  $\Delta'_{f_2}$  denote the face of  $\Delta'_2$  that is glued to  $\Delta'_{f_1}$ . Then by the same argument as above, the restriction of the preferred horospherical triangle  $\Delta^{\mathbf{v}_2}$  to  $\Delta'_{f_2}$  gives the preferred horocycle  $\Delta^{\mathbf{v}_2}_{f_2}$  of  $\Delta'_{f_2}$  at  $\mathbf{v}_2$  (Figure 2.7).

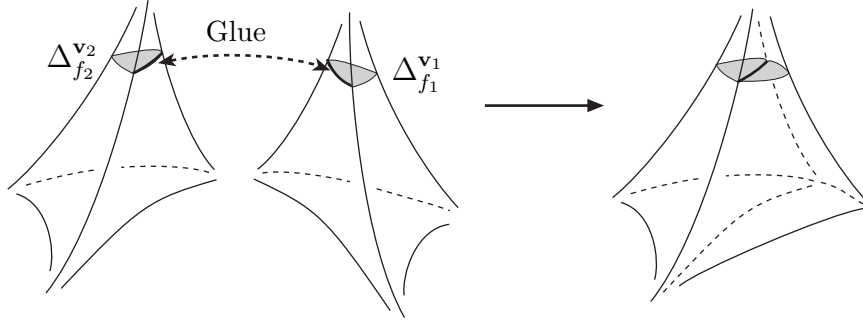


FIGURE 2.7. In the link of the cusp the preferred horospherical triangles match up at the same height.

But since (1') holds the horocycles  $\Delta^{\mathbf{v}_1}_{f_1}$  and  $\Delta^{\mathbf{v}_2}_{f_2}$  are identified under the gluing map. So in  $Q$  the horospherical triangles  $\Delta^{\mathbf{v}_1}$  and  $\Delta^{\mathbf{v}_2}$  match up at precisely the same height. Applying the same argument to the neighbouring tetrahedra we see that the cusp  $C$  has a horospherical cross-section. That is, if condition (1) is replaced by (1') then condition (3a) is automatic. A similar argument also shows that if condition (1) is replaced by (1') then condition (3b) is automatic. This gives the result:

**Lemma 2.2.** *Let  $Q$  be triangulated 3-orbifold such that:*

- (1') *We can realize the tetrahedra of  $T$  by generalized hyperbolic tetrahedra in Lorentzian space so that the gluing maps are Lorentzian isometries.*
- (2) *The sum of the dihedral angles of the tetrahedra incident to each edge  $e$  in  $T$  is  $\frac{2\pi}{n_e}$ .*

*Then  $Q$  admits a complete hyperbolic structure (with totally geodesic boundary).*

From Section 1.3 we know that a generalized hyperbolic tetrahedron is completely determined (up to Lorentzian isometry) by the 10 entries in its vertex Gram matrix. So, a triangulation can be completely parametrized by entries of the vertex Gram matrices. At first glance this might seem like a large number of parameters (10 per tetrahedron) however condition (1') creates considerable redundancy amongst these parameters. Using a 2-dimensional version of Theorem 1.5, we can force faces paired by gluing maps to be Lorentzian isometric by requiring their vertex Gram matrices to match. This leaves one parameter per vertex and one parameter per edge of  $T$  that completely determine the shapes of the tetrahedra of  $T$ .

We define a parameter  $\alpha_v$  associated to each vertex  $v$  of  $T$ , and a parameter  $\beta_e$  associated to each edge  $e$  as follows. Let  $\Delta'_n \subset \mathbb{E}^{1,3}$  represent the  $n$ -th tetrahedron of  $T$ . Denote the  $i$ -th vertex of  $\Delta'_n$  by  $\mathbf{v}_i^n$ , and let  $f_i^n$  be the face opposite  $\mathbf{v}_i^n$ ,  $e_{ij}^n$  the edge running between  $\mathbf{v}_i^n$  and  $\mathbf{v}_j^n$ , and  $G^n = (v_{ij}^n)$  the vertex Gram matrix of  $\Delta'_n$ . If the  $i$ -th vertex of  $\Delta'_n$  projects to a vertex  $v$  of triangulation  $T$ , then  $v_{ii}^n = \alpha_v$ . If the edge  $(i, j)$  of  $\Delta'_n$  projects to an edge  $e$  of  $T$ , then  $v_{ij}^n = \beta_e$ . We illustrate these parameters with an example.

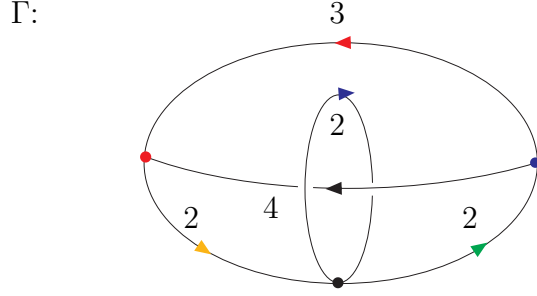


FIGURE 2.8. This 3-orbifold  $Q = (\mathbb{S}^3, \Gamma)$  can be triangulated by two tetrahedra.

**Example 2.3.** Consider the orbifold  $Q = (\mathbb{S}^3, \Gamma)$ , where  $\Gamma$  is depicted in Figure 2.8. We can produce a triangulation  $T$  for  $Q$  with three vertices, five edges and two tetrahedra (see Figure 2.9.)

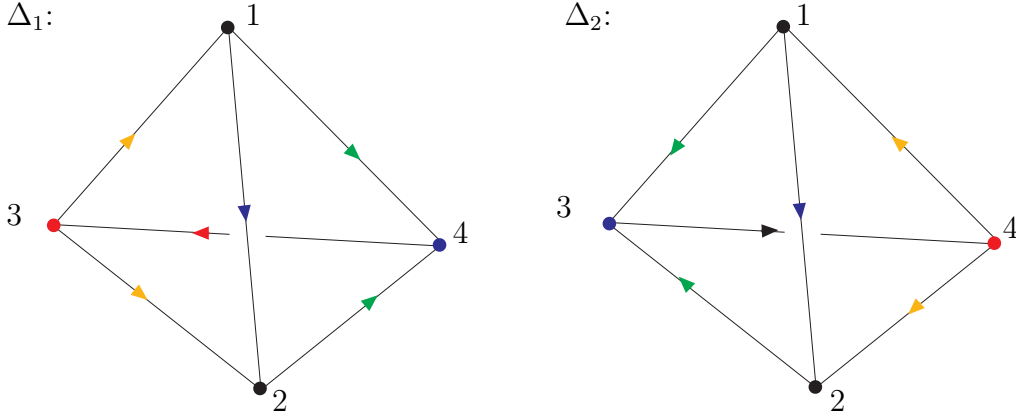


FIGURE 2.9. These two tetrahedra identified via the gluing patterns give a triangulation for the 3-orbifold in Figure 2.8.

Then since  $f_3^1$  is glued to  $f_4^2$  in  $T$ , condition (1') requires that these faces are isometric under the gluing map

$$\mathbf{v}_1^1 \leftrightarrow \mathbf{v}_1^2, \quad \mathbf{v}_2^1 \leftrightarrow \mathbf{v}_2^2, \quad \mathbf{v}_4^1 \leftrightarrow \mathbf{v}_3^2.$$

Let  $G_i^n$  denote the vertex Gram matrices of the generalized (hyperbolic) triangles  $f_i^n$ . Note that  $G_i^n$  can be obtained deleting the  $i$ -th row and column of  $G^n$ .

So

$$G_3^1 = \begin{pmatrix} v_{11}^1 & v_{12}^1 & v_{14}^1 \\ v_{12}^1 & v_{22}^1 & v_{24}^1 \\ v_{14}^1 & v_{24}^1 & v_{44}^1 \end{pmatrix} \quad G_4^2 = \begin{pmatrix} v_{11}^2 & v_{12}^2 & v_{13}^2 \\ v_{12}^2 & v_{22}^2 & v_{23}^2 \\ v_{13}^2 & v_{23}^2 & v_{33}^2 \end{pmatrix}$$

Since generalized triangles, like generalized tetrahedra, are completely determined (up to Lorentzian isometry) by their vertex Gram matrices, we can fix  $f_3^1$  and  $f_4^2$  to be Lorentzian isometric by setting  $G_3^1 = G_4^2$ . We can make this identification of  $G_3^1$  and  $G_4^2$  because the entry  $(i, j)$  in  $G_3^1$  represents the same edge or vertex as entry  $(i, j)$  in  $G_4^2$ . In general some relabelling of vertices may be required to ensure this.

Repeating this process for all the faces identified in  $T$ , the vertex Gram matrices  $G^1$  and  $G^2$  can be rewritten as

$$G^1 = \begin{pmatrix} \alpha_1 & \beta_1 & \beta_2 & \beta_3 \\ \beta_1 & \alpha_1 & \beta_2 & \beta_3 \\ \beta_2 & \beta_2 & \alpha_2 & \beta_4 \\ \beta_3 & \beta_3 & \beta_4 & \alpha_3 \end{pmatrix} \quad \text{and} \quad G^2 = \begin{pmatrix} \alpha_1 & \beta_1 & \beta_3 & \beta_2 \\ \beta_1 & \alpha_1 & \beta_3 & \beta_2 \\ \beta_3 & \beta_3 & \alpha_2 & \beta_5 \\ \beta_2 & \beta_2 & \beta_5 & \alpha_3 \end{pmatrix},$$

where the variables  $\alpha_1, \alpha_2, \alpha_3, \beta_1, \beta_2, \beta_3, \beta_4$  and  $\beta_5$  parametrize  $T$ . We are left with one parameter per vertex ( $\alpha_1, \alpha_2$  and  $\alpha_3$ ) and one parameter for each edge of  $T$  ( $\beta_1, \beta_2, \beta_3, \beta_4$  and  $\beta_5$ ).

If we know that  $Q$  is a closed orbifold then we can do away with the  $\alpha_v$  by setting them all equal to  $-1$ . This equivalent to fixing all the vertices of  $T$  to lie on  $H_-$ . This leaves us with one parameter for every edge in  $T$ . This closely resembles the approach used by Casson in **Geo** ([12]) to calculate hyperbolic structures on closed 3-manifolds. Casson used the internal edge lengths in the triangulation as parameters.

Similarly, if every vertex of  $\Gamma$  produces geodesic boundary we can fix the  $\alpha_v$  equal to 1. The significance of the  $\alpha_v$  is they allow for transitions between finite, ideal and hyperinfinite vertices. This allows for computation of hyperbolic structures on

- closed hyperbolic 3-orbifolds;
- cusped hyperbolic 3-orbifolds;
- hyperbolic 3-orbifolds with geodesic boundary

and continuous deformation between them.

Combining lemma 2.2 with our choice of parameters gives the following result:

**Lemma 2.4.** *Let  $Q$  be a 3-orbifold. Assume that we can find vertex and edge parameters for the triangulation  $T$  of  $Q$  such that:*

- (i) The vertex Gram matrix for each tetrahedron defines a generalized hyperbolic tetrahedron.
- (ii) The sum of the dihedral angles of the tetrahedra incident to each edge  $e$  in  $T$  is  $\frac{2\pi}{n_e}$ .

Then this defines a complete hyperbolic structure on  $Q$  (with totally geodesic boundary).

**Remark:** It also follows from the assumptions of the lemma that for each vertex  $v$  of  $T$ :

- If  $\chi(S_v) > 0$  then  $v$  is finite.
- If  $\chi(S_v) = 0$  then  $v$  is ideal.
- If  $\chi(S_v) < 0$  then  $v$  is hyperinfinite.

This is a consequence of the Gauss-Bonnet theorem and the fact that a finite (resp. ideal, hyperinfinite) vertex produces a surface  $S_v$  with a spherical (resp. Euclidean, hyperbolic) structure.

`Orb` uses Newton's method to solve for hyperbolic structures. Weeks implemented Newton's method to find hyperbolic structures in `SnapPea` ([69]). Casson ([12]) and Frigerio, Martelli, Petronio ([21]) also used this method with great success.

**Technical remark:** We use Newton's method with an initial guess of regular truncated tetrahedra with vertex Gram matrices

$$(2.1) \quad \begin{pmatrix} 0.5 & -1 & -1 & -1 \\ -1 & 0.5 & -1 & -1 \\ -1 & -1 & 0.5 & -1 \\ -1 & -1 & -1 & 0.5 \end{pmatrix}.$$

This choice is somewhat arbitrary. Generalized tetrahedra with all length-0 edges would seem to be a more obvious choice since these attain the maximum volume, but as discussed in Section 2.4 this case presents difficulties.

As in `SnapPea`, we trust the direction of the gradient in Newton's method but not the magnitude ([72]). On each step of Newton's method we renormalize the gradient vector to ensure that the tetrahedra can always be realized.

`Orb` solves the edge condition numerically ensuring that at each stage the vertex Gram matrices represent generalized hyperbolic tetrahedra. Let  $|T^i|$  denote the number of  $i$ -cells in  $T$ . Since the edge condition gives  $|T^1|$  equations and there are  $|T^0| + |T^1|$  parameters, the solution space (if any) will have dimension greater than or equal to  $|T^0|$ . The size of this solution space is not surprising as our discussion prior to lemma 2.4 indicated that we have the freedom to renormalize

the parameters  $\alpha_v$ . When calculating a structure on a closed manifold, the solution space is even larger, see Figure 2.10.

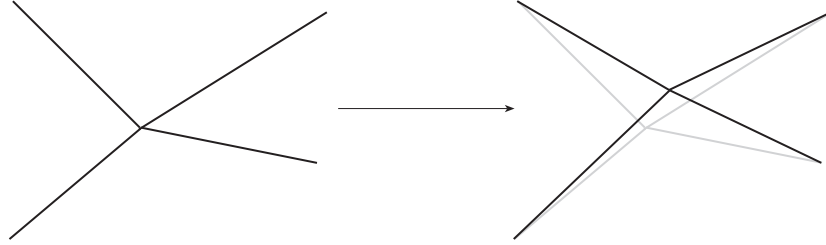


FIGURE 2.10. Given a triangulation that realizes a hyperbolic structure on a closed 3-manifold, perturbing any vertex in the triangulation will result in a 3-parameter family of different solutions.

Newton's method can still be used provided it is modified so on each iteration a unique gradient direction can be selected. Let  $D$  denote the subset of  $\mathbb{R}^{|T^0|+|T^1|}$  in which the tetrahedra of  $T$  can be realized as generalized hyperbolic tetrahedra. Let the map

$$\mathbf{e} : D \rightarrow \mathbb{R}^{|T^1|},$$

describe the error in the cone angle around each edge of  $T$  for any  $\mathbf{x} \in D$ . So if  $e_i$  denotes the  $i$ -th edge of  $T$  then the  $i$ -th component of  $\mathbf{e}$  is

$$\mathbf{e}^i = \frac{2\pi}{n_{e_i}} - \theta_{e_i},$$

where  $n_{e_i}$  is the label on  $e_i$  and  $\theta_{e_i}$  is the sum of the dihedral angles around it. Then in Newton's method we want to solve  $\mathbf{e}(\mathbf{x}) = \mathbf{0}$ , with  $\mathbf{x} \in D$ .

Let  $\mathbf{x}_n$  be the current position in Newton's method and  $M$  be the Jacobi matrix

$$M = \left( \frac{\partial \mathbf{e}^j}{\partial \mathbf{x}^i} \right)_{i,j} \Big|_{\mathbf{x}=\mathbf{x}_n}.$$

Then normally the next position in Newton's method would be

$$\mathbf{x}_{n+1} = \mathbf{x}_n - \delta,$$

where  $\delta$  is the solution to the equation

$$(2.2) \quad M\delta = \mathbf{e}(\mathbf{x}_n).$$

The problem is that there are an infinite number of  $\delta$  to choose from. Newton's method requires a unique choice of  $\delta$  on each iteration.

When  $M$  has full rank, the matrix  $MM^t$  is invertible. We can find a unique solution for equation (2.2) by first solving

$$MM^t \mathbf{z} = \mathbf{e}(\mathbf{x}_n)$$

for  $\mathbf{z}$  and then setting

$$\delta = M^t \mathbf{z}.$$

Geometrically, we are moving orthogonal to the solution set of the linearized equations. When  $M$  has less than full rank, we compute  $\delta$  in the same way, except we first select a set of linearly independent equations from the system of equations (2.2). This approach overcomes any ambiguity in the choice of direction of Newton's method and in practice gives excellent convergence, even on closed manifolds.

The following lemma tells us how to calculate the entries of the Jacobi matrix in Newton's method:

**Lemma 2.5.** *Let  $\Delta'$  be a generalized tetrahedron with vertex Gram matrix  $G$ . Then if  $G_{ij}$  is the matrix obtained from  $G$  by deleting the  $i$ -th row and  $j$ -th column then the  $(i, j)$ -th cofactor of  $G$  can be written as*

$$c_{ij} = (-1)^{i+j} \det(G_{ij}).$$

Let  $\theta_{ij}$  be the dihedral angle between the faces opposite vertices  $\mathbf{v}_i$  and  $\mathbf{v}_j$  of  $\Delta'$ . Then:

$$\begin{aligned} C_{ij} \frac{\partial \theta_{ij}}{\partial v_{ij}} &= 2c_{ii}c_{ij}c_{jj}(v_{mm}v_{nn} - v_{mn}^2), \\ C_{ij} \frac{\partial \theta_{ij}}{\partial v_{ii}} &= c_{ii}c_{ij}^2(v_{mm}v_{nn} - v_{mn}^2), \\ C_{ij} \frac{\partial \theta_{ij}}{\partial v_{in}} &= 2c_{ii}c_{ij}^2(v_{im}v_{mn} - v_{in}v_{mm}) \\ &\quad + 2c_{ii}c_{ij}c_{jj}(v_{jm}v_{mn} - v_{jn}v_{mm}), \\ C_{ij} \frac{\partial \theta_{ij}}{\partial v_{nn}} &= c_{ii}c_{ij}^2(v_{ii}v_{mm} - v_{im}^2) \\ &\quad + 2c_{ii}c_{ij}c_{jj}(v_{ij}v_{mm} - v_{im}v_{jm}) \\ &\quad + c_{ij}^2c_{jj}(v_{jj}v_{mm} - v_{jm}^2), \\ C_{ij} \frac{\partial \theta_{ij}}{\partial v_{mn}} &= 2c_{ii}c_{ij}^2(v_{im}v_{in} - v_{ii}v_{mn}) \\ &\quad + 2c_{ii}c_{ij}c_{jj}(v_{im}v_{jn} - 2v_{ij}v_{mn} + v_{in}v_{jm}) \\ &\quad + 2c_{ij}^2c_{jj}(v_{jm}v_{jn} - v_{jj}v_{mn}), \end{aligned}$$

where  $i, j, m$  and  $n$  are distinct and

$$C_{ij} = \sin(2\theta_{ij})c_{ii}^2c_{jj}^2.$$

PROOF. First note that it is enough to calculate the partial derivatives  $\frac{\partial\theta_{12}}{\partial v_{12}}, \frac{\partial\theta_{12}}{\partial v_{14}}, \frac{\partial\theta_{12}}{\partial v_{34}}, \frac{\partial\theta_{12}}{\partial v_{44}}$  and  $\frac{\partial\theta_{12}}{\partial v_{11}}$ , and deduce the result. We start by taking the square of equation (1.13)

$$\cos^2(\theta_{12}) = \frac{c_{12}^2}{c_{11}c_{22}}$$

then implicitly differentiating we get

$$(2.3) \quad \sin(2\theta_{12})c_{11}^2c_{22}^2\frac{\partial\theta_{12}}{\partial v_{mn}} = c_{12}^2\left(c_{11}\frac{\partial c_{22}}{\partial v_{mn}} + c_{22}\frac{\partial c_{11}}{\partial v_{mn}}\right) - 2c_{11}c_{22}c_{12}\frac{\partial c_{12}}{\partial v_{mn}},$$

where  $m \neq n$ . More easy, but tedious, calculations give:

$$\begin{aligned} c_{11} = \det \begin{pmatrix} v_{22} & v_{23} & v_{24} \\ v_{23} & v_{33} & v_{34} \\ v_{24} & v_{34} & v_{44} \end{pmatrix} &\Rightarrow \begin{aligned} \frac{\partial c_{11}}{\partial v_{11}} &= 0 \\ \frac{\partial c_{11}}{\partial v_{44}} &= v_{22}v_{33} - v_{23}^2 \\ \frac{\partial c_{11}}{\partial v_{12}} &= 0 \\ \frac{\partial c_{11}}{\partial v_{14}} &= 0 \\ \frac{\partial c_{11}}{\partial v_{34}} &= -2(v_{22}v_{34} - v_{23}v_{24}); \end{aligned} \\ \\ c_{22} = \det \begin{pmatrix} v_{11} & v_{13} & v_{14} \\ v_{13} & v_{33} & v_{34} \\ v_{14} & v_{34} & v_{44} \end{pmatrix} &\Rightarrow \begin{aligned} \frac{\partial c_{22}}{\partial v_{11}} &= v_{33}v_{44} - v_{34}^2 \\ \frac{\partial c_{22}}{\partial v_{44}} &= v_{11}v_{33} - v_{13}^2 \\ \frac{\partial c_{22}}{\partial v_{12}} &= 0 \\ \frac{\partial c_{22}}{\partial v_{14}} &= 2(v_{13}v_{34} - v_{14}v_{33}) \\ \frac{\partial c_{22}}{\partial v_{34}} &= -2(v_{11}v_{34} - v_{13}v_{14}); \end{aligned} \\ \\ c_{12} = -\det \begin{pmatrix} v_{12} & v_{23} & v_{24} \\ v_{13} & v_{33} & v_{34} \\ v_{14} & v_{34} & v_{44} \end{pmatrix} &\Rightarrow \begin{aligned} \frac{\partial c_{12}}{\partial v_{11}} &= 0 \\ \frac{\partial c_{12}}{\partial v_{44}} &= -(v_{12}v_{33} - v_{13}v_{23}) \\ \frac{\partial c_{12}}{\partial v_{12}} &= -(v_{33}v_{44} - v_{34}^2) \\ \frac{\partial c_{12}}{\partial v_{14}} &= -(v_{23}v_{34} - v_{24}v_{33}) \\ \frac{\partial c_{12}}{\partial v_{34}} &= 2v_{12}v_{34} - v_{14}v_{23} - v_{13}v_{24}. \end{aligned} \end{aligned}$$

Substituting these calculations into equation (2.3) gives the required derivatives.  $\square$

**Technical remark:** Although we only dealt explicitly with orbifolds in this section, the same method can be used to place hyperbolic structures with cusps and geodesic boundary on link and graph complements. In this case there is no singular locus and the surfaces in the links of the vertices are tori and higher genus surfaces. These differences have no impact on the algorithm.

### 2.3. Flat and negatively oriented tetrahedra

Recall the generalized tetrahedron inscribed in a rectangular box from example 1.6 in Section 1.3. As an eigenvalue  $\lambda_i$  (for  $i > 0$ ) approaches 0 the box collapses into

a coordinate plane and the vertices of the tetrahedra become linearly dependent. So equation (1.10) is

$$V^t J W = 0,$$

and  $V$  is no longer an invertible matrix, so the previous method for calculating the matrix of normals  $W$  is no longer valid.

Let  $\Delta'$  be a generalized tetrahedron in  $\mathbb{H}^3$  with vertex Gram matrix  $G$  and some choice of vertices  $V$  in  $\mathbb{E}^{1,3}$ . Then there are a variety of ways that the vertices of  $\Delta'$  can become coplanar. The flat tetrahedra in Figure 2.11 are much nicer than those in Figure 2.12 because the directions of the normals to faces are clearly defined.

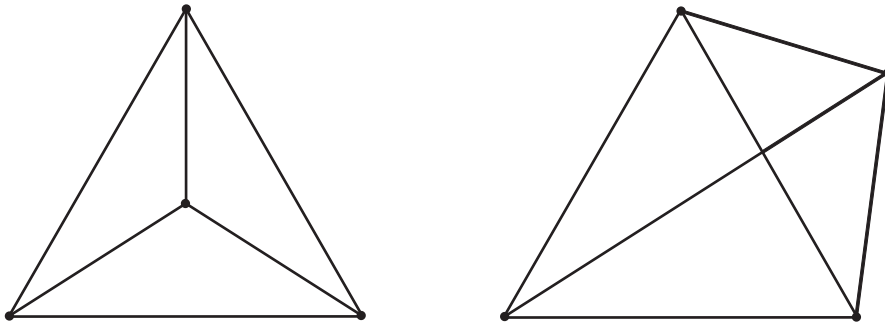


FIGURE 2.11. Two flat tetrahedra drawn in the projective model. Unlike the configurations of vertices in Figure 2.12 the normals to faces are clearly defined.

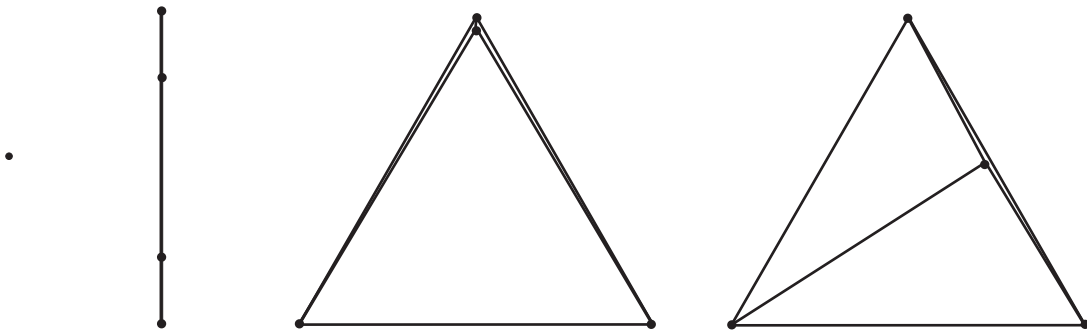


FIGURE 2.12. Other ways a tetrahedron can be flattened.

**Definition 2.6.** Let  $\{\mathbf{u}_1, \mathbf{u}_2, \mathbf{u}_3, \mathbf{u}_4\}$  be a linearly dependent set in  $\mathbb{P}_1^3$  such that any three of the points define a triangle. Then  $\{\mathbf{u}_1, \mathbf{u}_2, \mathbf{u}_3, \mathbf{u}_4\}$  defines a flat tetrahedron in  $\mathbb{P}_1^3$ .

A flat generalized (hyperbolic) tetrahedron is a generalized tetrahedron in every sense except that the tetrahedron it was created from in  $\mathbb{P}_1^3$  is flat.

**Definition 2.7.** Let  $\Delta$  be a flat tetrahedron in  $\mathbb{P}_1^3$ . Suppose each edge of  $\Delta$  intersects  $\overline{\mathbb{B}^n}$ .

- (1) The truncated flat hyperbolic tetrahedron say  $\Delta'$ , is the polyhedron in  $\mathbb{B}^n$  obtained by truncating  $\Delta$  at all its vertices lying outside  $\overline{\mathbb{B}^n}$  and omitting any vertices in  $\partial\mathbb{B}^n$ .
- (2) A flat generalized hyperbolic tetrahedron in  $\mathbb{B}^n$  is either a flat tetrahedron in the ordinary sense or a truncated flat tetrahedron described above.

By  $\hat{\Delta}$  we denote the projection of  $\Delta'$  to  $H_-$ .

We then have the following result on the vertex Gram matrices of flat generalized tetrahedra:

**Lemma 2.8.** Let  $\Delta'$  be a flat generalized hyperbolic tetrahedron with vertex Gram matrix  $G = (v_{ij})$ . Then

- (1)  $G$  has one negative, one zero and two positive eigenvalues,
- (2)  $c_{ii} < 0$ , for all  $i$ ,
- (3)  $c_{ij}^2 = c_{ii}c_{jj}$ , for all  $i$  and  $j$ ,

where  $c_{ij}$  is the  $(i, j)$ -th cofactor of  $G$ .

PROOF. Let  $\Delta'$  be a flat generalized tetrahedron with vertex matrix  $V$  and vertex Gram matrix  $G$ . According to definition 2.7, the nullspace of  $G$  is one dimensional and so  $G$  has one zero eigenvalue. Moreover, any three vertices of  $\Delta'$  define a generalized hyperbolic triangle so Sylvester's inertia law implies that there is one negative and two positive eigenvalues.

Setting  $A = G$  and taking  $p = 2$  in Jacobi's theorem (Theorem 2.9, stated below) we get

$$(2.4) \quad c_{ii}c_{jj} - c_{ij}^2 = \det(G)(v_{mm}v_{nn} - v_{mn}^2),$$

where  $i, j, m, n$  are distinct and  $c_{ij}$  is the  $(i, j)$ -th cofactor of  $G$ . Since  $\det(G) = 0$  it is clear that  $c_{ii}c_{jj} = c_{ij}^2$ . To show that  $c_{ii} < 0$  first note that  $c_{ii} = \det(G_{ii})$ . Since  $G_{ii}$  is the vertex Gram matrix for a generalized hyperbolic triangle it follows it has one negative, and two positive eigenvalues and so  $c_{ii} = \det(G_{ii}) < 0$ .  $\square$

**Theorem 2.9. [Jacobi's theorem ([53])]** Let  $A = (a_{ij})$  be a square matrix of order  $n$ ,  $(\text{adj}(A))^t = (A_{ij})$ ,  $1 \leq p < n$ ,  $\sigma = \begin{pmatrix} i_1 & \cdots & i_n \\ j_1 & \cdots & j_n \end{pmatrix}$  an arbitrary permutation. Then

$$\det \begin{pmatrix} A_{i_1 j_1} & \cdots & A_{i_1 j_p} \\ \vdots & \ddots & \vdots \\ A_{i_p j_1} & \cdots & A_{i_p j_p} \end{pmatrix} = (-1)^\sigma \det \begin{pmatrix} a_{i_{p+1} j_{p+1}} & \cdots & a_{i_{p+1} j_n} \\ \vdots & \ddots & \vdots \\ a_{i_n j_{p+1}} & \cdots & a_{i_n j_n} \end{pmatrix} \det(A)^{p-1}.$$

Here  $\text{adj}(A)$  denotes the adjoint of  $A$ , given by

$$A \cdot \text{adj}(A) = \det(A)I.$$

**Remark:** There is a similar result to Lemma 2.8 for each of the degenerate tetrahedra in Figure 2.12. The number of zero eigenvalues of their vertex Gram matrices will be  $4 - d$  where  $d$  is the dimension of the span of the vertices. For every face that has collapsed to a point or a line, the corresponding  $c_{ii}$  will be 0. This follows from the fact that  $c_{ii} = \det(G_{ii})$ , and  $\det(G_{ii}) = 0$  because the vertices of the corresponding faces are linearly dependent.

Henceforth a flat generalized hyperbolic tetrahedron is considered as a generalized hyperbolic tetrahedron. Call a generalized triangulation consisting of positively oriented (and possibly some flat) generalized tetrahedra a *geometric* triangulation. A geometric triangulation truly represents the hyperbolic structure of a 3-orbifold because any flat tetrahedra can be removed by a natural subdivision of the surrounding tetrahedra, into polyhedra. There is one exceptional case: when the singular locus bumps into itself as a result of a tetrahedron flattening out. In this instance the result is not a geometric triangulation of the orbifold.

A tetrahedron that has continued past flat, and turned inside out is *negatively oriented*. (See Figure 2.13.) Although it is useful at times to allow negatively oriented tetrahedra in a triangulation, there is no guarantee that this represents a hyperbolic structure (Petronio, Weeks [51]).

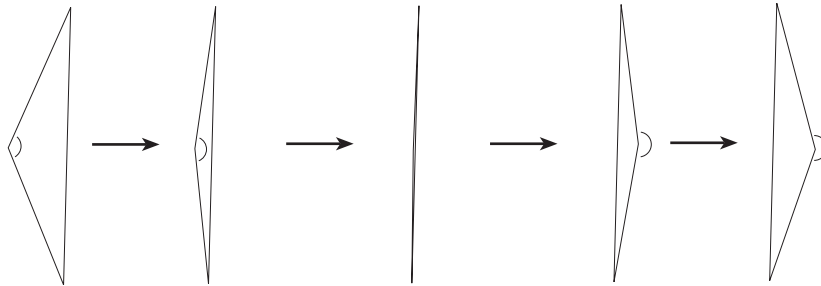


FIGURE 2.13. In order to detect a tetrahedron turning inside out we must keep track of the branches of  $\arccos(x)$  giving the dihedral angles.

**Definition 2.10.** Let  $\Delta'$  be a generalized hyperbolic tetrahedron in  $\mathbb{E}^{1,3}$  with (ordered) vertices  $\mathbf{v}_1, \mathbf{v}_2, \mathbf{v}_3, \mathbf{v}_4$  and corresponding vertex matrix  $V = (\mathbf{v}_1, \mathbf{v}_2, \mathbf{v}_3, \mathbf{v}_4)$ . Then the orientation parameter of  $\Delta'$  is  $\tau = \det(V)$ .

**Remark:** If the vertices of  $\Delta'$  are labelled according to the right hand rule (Figure 2.14), then  $\tau > 0$  and the tetrahedron is “positively oriented”. If the vertices are

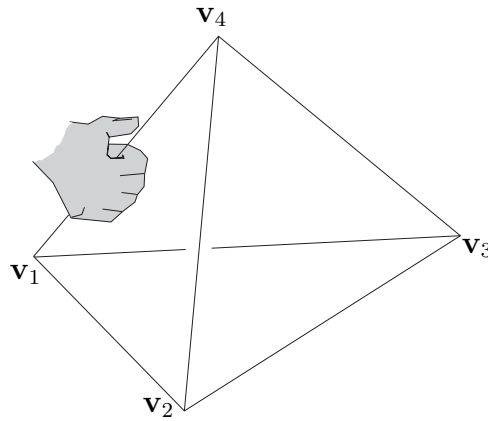


FIGURE 2.14. A tetrahedron labelled according to the right hand rule. If you place your right hand on the edge  $e_{14}$ , with your thumb pointing towards  $\mathbf{v}_4$ , then your fingers should point in the direction from  $\mathbf{v}_2$  towards  $\mathbf{v}_3$ .

labelled according to the left hand rule then  $\tau < 0$  and  $\Delta'$  is “negatively oriented”. Also, it follows immediately from equation (1.9) that

$$(2.5) \quad \det(G) = \det(V^t J V) = -\tau^2.$$

So equation (1.10) becomes

$$(2.6) \quad V^t J W = \tau I.$$

When tetrahedra flatten out there is a problem in using equation (1.13) to calculate the dihedral angles of  $\Delta'$ , since this requires calculation of  $\arccos(x)$  as  $x$  approaches 1 or  $-1$ . Remember also that  $G$  only parameterizes  $\Delta'$  up to isometry, so it is not enough to distinguish between positively and negatively oriented tetrahedra. But, by introducing the orientation parameter  $\tau$  these tetrahedra can be distinguished. Furthermore,  $\theta_{ij}$  can be written in terms of  $\arcsin(x)$  using the following corollary to Jacobi’s theorem.

**Corollary 2.11.** *If  $\Delta'$  is a generalized hyperbolic tetrahedron then*

$$(2.7) \quad \sin(\theta_{ij}) = \tau \sqrt{\frac{v_{mn}^2 - v_{mm}v_{nn}}{c_{ii}c_{jj}}},$$

where  $i, j, m, n$  are distinct.

PROOF. Recall equation (2.4):

$$c_{ii}c_{jj} - c_{ij}^2 = \det(G)(v_{mm}v_{nn} - v_{mn}^2),$$

where  $i, j, m, n$ .

Using equations (1.13), (2.4) and (2.5) gives:

$$(2.8) \quad \sin^2(\theta_{ij}) = \tau^2 \frac{v_{mn}^2 - v_{mm}v_{nn}}{c_{ii}c_{jj}}.$$

The choice of sign follows from the fact that  $\theta_{ij} \in (0, \pi)$  for a positively oriented tetrahedron. Note that  $\frac{v_{mn}^2 - v_{mm}v_{nn}}{c_{ii}c_{jj}} \geq 0$ .  $\square$

In Newton's method, if an angle  $\theta_{ij}$  approaches 0 or  $\pi$ , we introduce an orientation parameter and add equation (2.5) to the set of equations to solve. Limiting the amount each dihedral angle can change in an iteration of Newton's method ensures that the branch of  $\arccos(x)$  or  $\arcsin(x)$  on which  $\theta_{ij}$  lies is always clear. In fact, by ensuring no angle changes by more than  $\frac{\pi}{4}$ , and making the convention to calculate angle  $\theta_{ij}$  with equation (2.7) if  $|\sin(\theta_{ij})| < \frac{1}{\sqrt{2}}$  and equation (1.13) if  $|\cos(\theta_{ij})| \leq \frac{1}{\sqrt{2}}$ , the branch of  $\theta_{ij}$  can always be varied continuously. As in the previous section, the implementation of Newton's method requires understanding how the  $\theta_{ij}$  are affected by small changes in our parameters when using equation (2.7):

**Lemma 2.12.** *Let  $\Delta'$  be a generalized tetrahedron with vertex Gram matrix  $G$  and orientation parameter  $\tau$ . Let  $\theta_{ij}$  denote the dihedral angle of  $\Delta'$  between faces  $i$  and  $j$ , and let  $c_{ij}$  be the  $(i, j)$ -th cofactor of  $G$ . Then*

$$\begin{aligned} C_{ij} \frac{\partial \theta_{ij}}{\partial \tau} &= 2\tau c_{ii} c_{jj} (v_{mn}^2 - v_{mm}v_{nn}), \\ C_{ij} \frac{\partial \theta_{ij}}{\partial v_{ij}} &= 0, \\ C_{ij} \frac{\partial \theta_{ij}}{\partial v_{in}} &= 2\tau^2 c_{ii} (v_{mm}v_{nn} - v_{mn}^2) (v_{im}v_{mn} - v_{in}v_{mm}), \\ C_{ij} \frac{\partial \theta_{ij}}{\partial v_{ii}} &= \tau^2 c_{ii} (v_{mm}v_{nn} - v_{mn}^2)^2, \\ C_{ij} \frac{\partial \theta_{ij}}{\partial v_{nn}} &= \tau^2 ((v_{mm}v_{nn} - v_{mn}^2) (c_{ii} (v_{ii}v_{mm} - v_{im}v_{im}) \\ &\quad + c_{jj} (v_{jj}v_{mm} - v_{jm}^2)) - c_{ii} c_{jj} v_{mm}), \\ C_{ij} \frac{\partial \theta_{ij}}{\partial v_{mn}} &= 2\tau^2 ((v_{mn}^2 - v_{mm}v_{nn}) (c_{ii} (v_{ii}v_{mn} - v_{im}v_{in}) \\ &\quad + c_{jj} (v_{jj}v_{mn} - v_{jm}v_{jn})) + c_{ii} c_{jj} v_{mn}), \end{aligned}$$

where  $i, j, m$  and  $n$  are distinct and

$$C_{ij} = \sin(2\theta_{ij}) c_{ii}^2 c_{jj}^2.$$

PROOF. As in lemma 2.5 it is enough to compute the derivatives when  $i = 1$  and  $j = 2$ . The partial derivative  $\frac{\partial \theta_{12}}{\partial \tau}$  follows immediately from equation (2.8).

For the remainder, implicitly differentiating equation (2.8) gives

$$\sin(2\theta_{12})c_{11}^2c_{22}^2\frac{\partial\theta_{12}}{\partial v_{mn}} = \tau^2(c_{11}c_{22}\frac{\partial}{\partial v_{mn}}(v_{34}^2 - v_{33}v_{44}) - (\frac{\partial c_{11}}{\partial v_{mn}}c_{22} + \frac{\partial c_{22}}{\partial v_{mn}}c_{11})(v_{34}^2 - v_{33}v_{44})),$$

and then we reuse the calculations in the proof of lemma 2.5.  $\square$

## 2.4. Pared manifolds

As in the beginning of Section 2.2, let  $\Gamma$  be a graph in a closed 3-manifold  $M$ , with vertices of degree 3 and edges labelled by integers  $\geq 2$ . We now examine what happens to the hyperbolic 3-orbifold  $Q = (M, \Gamma)$  as the labels on the edges of  $\Gamma$  approach infinity. For simplicity we will assume that each of the edges of  $\Gamma$  is labelled  $n \geq 2$ .

Let  $T$  be a triangulation of  $Q$  as described in Section 2.2 and let  $S_v$  denote the orbifold in the link of vertex  $v$  of  $T$ . Then at each vertex  $v$ ,  $S_v$  is a  $\mathbb{S}^2(n, n, n)$  orbifold. As  $n$  approaches  $+\infty$  the cone angle  $\frac{2\pi}{n}$  around each of the cone points on  $S_v$  approaches 0. This arises in the proof of the orbifold theorem ([16], [7]). In the limit  $\partial Q$  consists of geodesic 3-punctured spheres. This produces a so-called *pared hyperbolic manifold* (Flapan [20], Kapovich [36], Morgan [46]), which is the complement of a neighbourhood of  $\Gamma$  in  $M$  with its meridian curves parabolic.

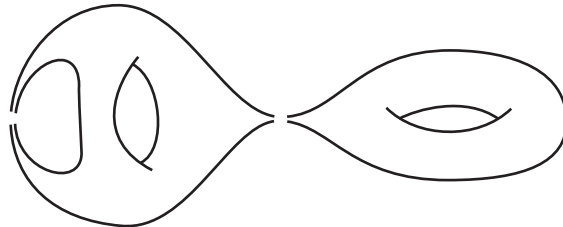


FIGURE 2.15. The boundary of a pared manifold with two annulus cusps and two punctured geodesic boundary components.

**Definition 2.13.** *A pared 3-manifold  $(N, P)$  is an orientable compact 3-manifold  $N$  together with a family  $P$  of disjoint incompressible annuli and tori in  $\partial N$ .*

As noted in [20], a pared manifold is a special case of a manifold with boundary patterns in the sense of Johannson [38] or a 3-manifold pair in the sense of Jaco-Shalen [37]. The following definition agrees with [38] and [37].

**Definition 2.14.** *The pared manifold  $(N, P)$  is simple if the following conditions hold:*

- (1)  $N$  is irreducible and  $\partial N - P$  is incompressible
- (2)  $N$  is atoroidal

- (3) Any annulus  $A$  in  $N$  with  $\partial A \subset \partial N - P$  is either compressible or parallel to an annulus  $A'$  in  $\partial N$  with  $\partial A' = \partial A$  and such that  $A' \cap P$  consists of zero or one annular component of  $P$ .

**Definition 2.15.** A pared manifold  $(N, P)$  is said to be Seifert fibered if there is a Seifert fibration of  $N$  for which  $P$  is a union of fibers. A pared manifold  $(N, P)$  is said to be  $I$ -fibered if there is an  $I$ -bundle map of  $N$  over a surface  $B$  such that  $P$  is in the preimage of  $\partial B$ .

The following is an existence theorem for hyperbolic structures on pared manifold:

**Thurston's Hyperbolization Theorem for Pared Manifolds** ([36], [47], [63]). *If  $(N, P)$  is simple,  $N$  is connected, and  $\partial N$  is non-empty, then either  $(N, P)$  admits a finite volume complete hyperbolic metric with geodesic boundary and parabolic cusps along  $P$ , or  $(N, P)$  is Seifert fibered or  $I$ -fibered.*

Given  $Q = (M, \Gamma)$  as above, we can calculate hyperbolic structures on pared manifolds using `Orb` by fixing the cone angle around each edge of  $\Gamma$  to be 0. We represent this on  $\Gamma$  by labelling each of its edges  $\infty$ . (See Figure 2.16.)

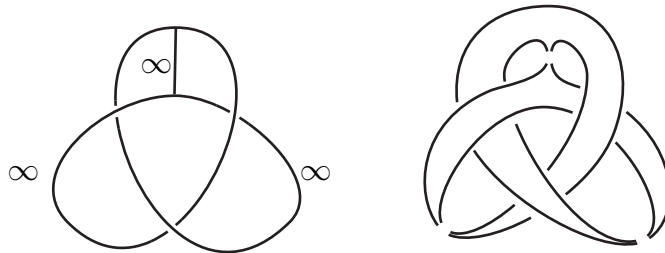


FIGURE 2.16. Labelling a trivalent graph  $\infty$  produces a pared manifold whose boundary consists of geodesic 3-punctured spheres.

Let  $e$  be an edge in  $T$  labelled  $\infty$  and let  $\Delta'$  be a generalized tetrahedron incident to  $e$ . Let  $v_1$  and  $v_2$  denote the vertices of  $T$  at either end of  $e$ . Then  $S_{v_1}$  and  $S_{v_2}$  are 3-punctured spheres.

It follows from Theorem 1.2 that fixing the cone angle around  $e$  to be 0 is equivalent to forcing the equation

$$(2.9) \quad \beta_e^2 = \alpha_{v_1} \alpha_{v_2}$$

to hold. So  $e$  is a length-0 edge.

Although the dihedral angle of  $\Delta'$  at  $e$  is 0, the determinant of its vertex Gram matrix can still be non-zero. So the orientation parameter  $\tau$  of  $\Delta'$  can be non-zero. Consequently, the method for handling dihedral angles near zero, outlined

in Section 2.3, does not apply. Since  $e$  meets  $\overline{\mathbb{B}^3}$  only at  $\partial\mathbb{B}^3$ ,  $\Delta'$  is at the boundary of the space of all generalized tetrahedra. If  $e$  moves beyond  $\partial\mathbb{B}^3$  it will be truncated entirely. (Refer to Figures 1.5 and 2.17.) In practice this issue can be avoided by using equation (2.9) to eliminate the parameter  $\beta_e$  entirely. Then by applying Newton's method in the new parameter system we can stay in the space of generalized tetrahedra.

**Question:** Is there a more natural method of dealing with length-0 edges? That is, is there another set of parameters that will allow us to continuously deform to the length-0 edge case and back?

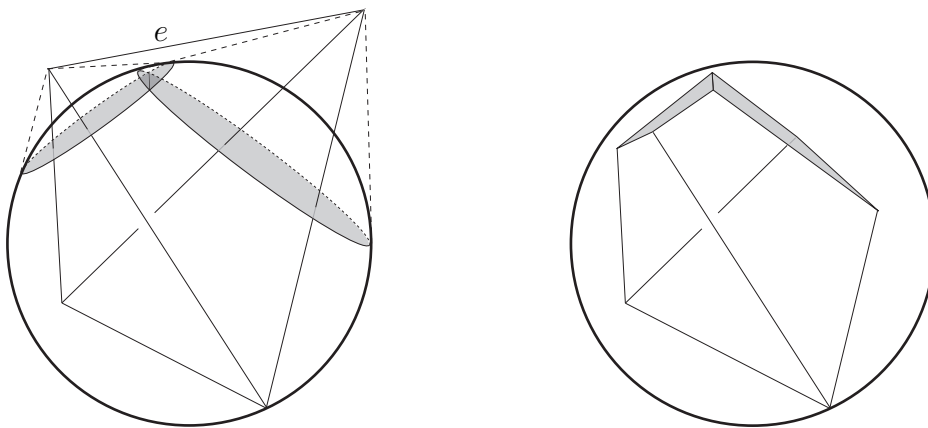


FIGURE 2.17. The edge  $e$  of  $\Delta$  does not meet  $\overline{\mathbb{B}^3}$ , so after truncation  $e$  is sliced completely off  $\Delta$ .

## 2.5. Canonical cell decompositions

In [19], Epstein and Penner showed that a convex hull construction in Lorentzian space determines a canonical cell decomposition of a cusped hyperbolic 3-manifold. Using this approach, Weeks ([70]) outlined an algorithm for computing a canonical cell decomposition for a cusped hyperbolic 3-manifold. This algorithm is implemented in SnapPea ([69]) and the applications to hyperbolic manifolds have been abundant (e.g. [31], [2], [33], [34], [57]).

Kojima extended the work of Epstein and Penner in [39] and [40], which allowed Frigerio and Petronio to develop an equally useful algorithm ([23]) for the computation of a canonical triangulation for a hyperbolic 3-manifold with geodesic boundary. This procedure has proved to be invaluable in the computation of symmetry groups and the construction of a census of these objects ([22]).

The canonical cell decomposition is constructed by creating an equivariant tessellation of the universal cover. Working in Lorentzian space, geodesic boundary components are represented by points on the one sheeted hyperboloid  $H_+$ . The

orbits of these points turn out to be discrete and by truncating their convex hull along their dual hyperplanes a truncated polyhedron is created in  $\mathbb{H}^3$ . The faces of this truncated polyhedron give rise to the pieces of the tessellation. By projecting these faces down to the manifold, it is decomposed into its canonical cell decomposition. For more details see [39], [40] or [23].

The following section examines how this construction is affected by our new choice of parameters. One of the biggest obstacles is checking the convexity of the truncated polyhedron in  $\mathbb{H}^3$ . This hinges on the so-called *tilt formula* and we begin our discussion there. (Refer to [67], [70], [55] or [23]).

For a generalized tetrahedron  $\Delta' \subset \mathbb{E}^{1,3}$ , with vertices  $\mathbf{v}_1, \mathbf{v}_2, \mathbf{v}_3, \mathbf{v}_4$ , define a *normal vector*  $\mathbf{p}$  to  $\Delta'$  by the condition  $\langle \mathbf{p}, \hat{\mathbf{v}}_i \rangle = -1$  for all  $i$  where according to definition 1.3

$$\hat{\mathbf{v}}_i = \begin{cases} \frac{\mathbf{v}_i}{\sqrt{|\langle \mathbf{v}_i, \mathbf{v}_i \rangle|}}, & \text{if } \langle \mathbf{v}_i, \mathbf{v}_i \rangle \neq 0; \\ \mathbf{v}_i, & \text{otherwise.} \end{cases}$$

Let  $F_i$  denote the face opposite vertex  $\mathbf{v}_i$ . Then the *tilt*  $t_k$  of  $\Delta'$  relative to  $F_k$  is the inner product

$$(2.10) \quad t_k = \langle \hat{\mathbf{w}}_k, \mathbf{p} \rangle,$$

where  $\mathbf{w}_i$  is the normal to face  $F_i$  satisfying equation (1.10) and  $\hat{\mathbf{w}}_i$  is the unit normal in the direction of  $\mathbf{w}_i$ . The following result of Ushijima indicates how the tilts are used to measure the convexity of the angle between two neighbouring tetrahedra in  $\mathbb{E}^{1,3}$ .

**Lemma 2.16.** (Tilt Proposition [67]) *Let  $\Delta'_1$  and  $\Delta'_2$  be two neighbouring generalized hyperbolic tetrahedra in  $\mathbb{E}^{1,3}$ . We denote by  $t_1$  (resp.  $t_2$ ) the tilt of  $\Delta'_1$  (resp.  $\Delta'_2$ ) with respect to their joint face. Then the dihedral angle formed between  $\Delta'_1$  and  $\Delta'_2$  is convex (resp. flat, concave) if and only if  $t_1 + t_2 < 0$  (resp.  $= 0, > 0$ ).*

The following result shows that the tilts can be computed easily with our choice of parameters:

**Theorem 2.17.** *Let  $\Delta'$  be a geometric generalized tetrahedron. Then the tilts  $t_k$  of  $\Delta'$  are given by:*

$$t_k = \langle \mathbf{p}, \hat{\mathbf{w}}_k \rangle = \frac{1}{\tau} \sum_{i=1}^4 \sqrt{\left| \frac{l_i}{c_{kk}} \right|} c_{ik},$$

where

$$l_i = \begin{cases} 1 & , \text{if } v_{ii} = 0, \\ v_{ii} & , \text{otherwise.} \end{cases}$$

PROOF. First we prove that

$$(2.11) \quad \mathbf{p} = -\frac{1}{\tau} \sum_{i=1}^4 \sqrt{|l_i|} \mathbf{w}_i.$$

Then the result follows.

Let  $V$  be the matrix with the  $\mathbf{v}_i$  as columns and  $W$  be the matrix with the  $\mathbf{w}_i$  as columns satisfying equation (2.6)

$$V^t J W = \tau I.$$

Then by Theorem 1.5,  $\det(V) \neq 0$  which implies  $\det(W) \neq 0$ . So the  $\mathbf{w}_i$  are linearly independent and therefore form a basis for  $\mathbb{E}^{1,3}$ . Hence we can write

$$(2.12) \quad \mathbf{p} = \sum_{i=1}^4 \alpha_i \hat{\mathbf{w}}_i,$$

for some unique  $\alpha_i \in \mathbb{R}$ . Denote by  $\hat{W}$  and  $\hat{V}$  the matrices of “unit” normals and vertices of  $\Delta'$ . Then since  $V^t J W = \tau I$ , the matrix  $\hat{V}^t J \hat{W} = (\langle \hat{\mathbf{v}}_i, \hat{\mathbf{w}}_j \rangle)$  is diagonal. Applying the function  $\langle \cdot, \hat{\mathbf{v}}_i \rangle$  to both sides of equation (2.12) gives

$$\alpha_i = \frac{\langle \mathbf{p}, \hat{\mathbf{v}}_i \rangle}{\langle \hat{\mathbf{w}}_i, \hat{\mathbf{v}}_i \rangle}.$$

Since  $\langle \mathbf{p}, \hat{\mathbf{v}}_i \rangle = -1$  and  $\langle \mathbf{v}_i, \mathbf{w}_i \rangle = \tau$ ,

$$\mathbf{p} = -\sum_{i=1}^4 \frac{\hat{\mathbf{w}}_i}{\langle \hat{\mathbf{v}}_i, \hat{\mathbf{w}}_i \rangle} = -\sum_{i=1}^4 \frac{\mathbf{w}_i}{\langle \hat{\mathbf{v}}_i, \mathbf{w}_i \rangle} = -\sum_{i=1}^4 \sqrt{|l_i|} \frac{\mathbf{w}_i}{\langle \mathbf{v}_i, \mathbf{w}_i \rangle} = -\sum_{i=1}^4 \frac{\sqrt{|l_i|}}{\tau} \mathbf{w}_i,$$

as required.

We can then use equation (1.12) which says

$$\langle \mathbf{w}_i, \mathbf{w}_j \rangle = w_{ij} = -c_{ij},$$

and apply  $\langle \cdot, \hat{\mathbf{w}}_k \rangle$  to both sides of equation (2.11) to produce the result

$$t_k = \langle \mathbf{p}, \hat{\mathbf{w}}_k \rangle = -\frac{1}{\tau} \sum_{i=1}^4 \sqrt{|l_i|} \frac{w_{ik}}{\sqrt{w_{kk}}} = \frac{1}{\tau} \sum_{i=1}^4 \sqrt{\left| \frac{l_i}{c_{kk}} \right|} c_{ik}.$$

□

Although the algorithm in [23] is only defined for hyperbolic 3-manifolds with geodesic boundary, it is still extremely useful for distinguishing hyperbolic 3-orbifolds. Let  $Q$  be an orientable hyperbolic 3-orbifold and let  $l(e)$  denote the labelling on edge  $e$  of  $\Sigma(Q)$ .

There is a pared 3-manifold  $M_Q$  obtained from  $Q$  by setting the finite labels on  $\Sigma(Q)$  to  $\infty$  and creating one annulus cusp  $a_e$  for each singular edge  $e$  in  $\Sigma(Q)$ . Now if  $Q_1$  and  $Q_2$  are hyperbolic 3-orbifolds with geodesic boundary then they can be distinguished by computing the canonical cell decompositions of  $M_{Q_1}$  and

$M_{Q_2}$  and checking for isometries between them. Every isometry  $\gamma : M_{Q_1} \rightarrow M_{Q_2}$  induces a map  $\gamma_a$  between annulus cusps. If there exists an isometry  $\gamma$  between pared manifolds such that  $\gamma_a(a_e) = a_{e'}$  implies the labels  $l(e), l(e')$  are equal then  $\gamma$  can be extended to an isomorphism between  $Q_1$  and  $Q_2$ .

We now give an outline of the algorithm in [23] when cusps are not involved. The input for the algorithm is a geometric triangulation  $T$  of a hyperbolic 3-manifold  $M$  with geodesic boundary, such that  $T$  realizes the hyperbolic structure on  $M$ . The following is the algorithm restated:

- (1) Pick a face  $F$  of  $T$  such that the two incident tetrahedra are distinct. Use Theorem 2.17 and lemma 2.16 to determine if the angle at  $F$  is concave. If it is, move to step 2. If it is not, move to another face. If all the faces are visited and no concave angle is found then  $T$  is the canonical cell decomposition, or a subdivision of it.
- (2) If a *two-to-three* move can be performed at  $F$  without creating negatively oriented tetrahedra, do so and then go back to step 1. Otherwise, check if one of the non-length-0 edges of  $F$  can be removed by a *three-to-two* move, while still maintaining a geometric triangulation. If the aforementioned move can be completed, do so, then go back to step 1. If not, go back to step 1 and move to a new face. If all concave faces are visited and no move can be applied to any of them, we give up.

Frigerio and Petronio showed that if this process does not get stuck during step 2 then the canonical decomposition is output in a finite number of steps. We now describe the *three-to-two* and *two-to-three* moves used above.

The three-to-two move can be applied to a triangulation when there are three distinct tetrahedra incident to an edge of order three, say  $e$ . (See Figure 2.18.) If  $e$  is *not labelled*, the three tetrahedra can be replaced by two sharing a face.

The two-to-three move is essentially the inverse of the three-to-two move. Given two distinct tetrahedra sharing a face they are replaced by three tetrahedra sharing a common edge. This move can always be performed and introduces a new edge  $e$  into the triangulation. The following lemma shows how to calculate  $e$ 's edge parameter:

**Lemma 2.18.** *Let  $\Delta'_1$  and  $\Delta'_2$  be two generalized tetrahedra sharing a common face in a triangulation with vertices*

$$\mathbf{v}_1, \mathbf{v}_2, \mathbf{v}_3, \mathbf{v}_4 \text{ and } \mathbf{v}_5, \mathbf{v}_2, \mathbf{v}_3, \mathbf{v}_4,$$

*and vertex Gram matrices  $G_1$  and  $G_2$ . (See Figure 2.18.) Then*

$$\langle \mathbf{v}_1, \mathbf{v}_5 \rangle = \frac{-v_{12}c_{12} - v_{13}c_{13} - v_{14}c_{14} + \tau_1\tau_2}{c_{11}},$$

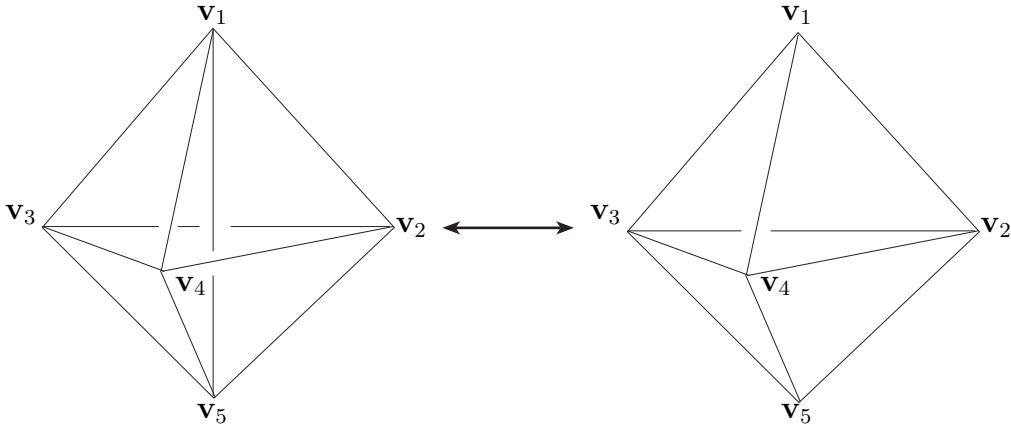


FIGURE 2.18. On the left are three distinct tetrahedra sharing an edge  $e$  of order 3. If  $e$  is not labelled then the tetrahedra can be replaced by two tetrahedra sharing a common face. This is known as the three-to-two move. Its inverse, the two-to-three move, creates a new edge of order 3 from two distinct tetrahedra sharing a face.

where  $\tau_1$  and  $\tau_2$  are the orientation parameters,  $v_{ij} = \langle \mathbf{v}_i, \mathbf{v}_j \rangle$  and  $c_{ij}$  is the  $(i, j)$ -th cofactor of  $G_2$ .

PROOF. Since  $\mathbf{v}_2, \mathbf{v}_3$  and  $\mathbf{v}_4$  are linearly independent and  $\mathbf{w}_1$  is normal to the plane containing them, the equation

$$\mathbf{v}_5 = \alpha_1 \mathbf{w}_1 + \alpha_2 \mathbf{v}_2 + \alpha_3 \mathbf{v}_3 + \alpha_4 \mathbf{v}_4$$

has a unique solution. Taking the inner product of both sides with  $\mathbf{v}_i$  for  $i = 2, 3, 4$  produces the following equations for  $\alpha_2, \alpha_3$  and  $\alpha_4$

$$\alpha_2 v_{22} + \alpha_3 v_{23} + \alpha_4 v_{24} = v_{25}$$

$$\alpha_2 v_{23} + \alpha_3 v_{33} + \alpha_4 v_{34} = v_{35}$$

$$\alpha_2 v_{24} + \alpha_3 v_{34} + \alpha_4 v_{44} = v_{45},$$

which can be solved by applying Cramer's rule

$$\begin{bmatrix} \alpha_2 \\ \alpha_3 \\ \alpha_4 \end{bmatrix} = \begin{bmatrix} v_{22} & v_{23} & v_{24} \\ v_{23} & v_{33} & v_{34} \\ v_{24} & v_{34} & v_{44} \end{bmatrix}^{-1} \begin{bmatrix} v_{25} \\ v_{35} \\ v_{45} \end{bmatrix} = \frac{-1}{c_{11}} \begin{bmatrix} c_{12} \\ c_{13} \\ c_{14} \end{bmatrix}.$$

Now since  $\mathbf{v}_2, \mathbf{v}_3$  and  $\mathbf{v}_4$  are contained in the plane  $\mathbf{w}_1^\perp = \mathbf{w}_5^\perp$  we have

$$\mathbf{w}_5 = \mp \sqrt{\frac{\langle \mathbf{w}_5, \mathbf{w}_5 \rangle}{\langle \mathbf{w}_1, \mathbf{w}_1 \rangle}} \mathbf{w}_1,$$

taking the minus sign when both  $\Delta'_1$  and  $\Delta'_2$  have the same orientation. However, by equation (1.12),  $\langle \mathbf{w}_5, \mathbf{w}_5 \rangle = \langle \mathbf{w}_1, \mathbf{w}_1 \rangle$ , so

$$\mathbf{w}_5 = \mp \mathbf{w}_1.$$

As the vector  $\alpha_1 \mathbf{w}_1$  is the orthogonal projection of  $\mathbf{v}_5$  onto the space spanned by  $\mathbf{w}_1$ ,

$$\alpha_1 = \frac{\langle \mathbf{v}_5, \mathbf{w}_1 \rangle}{\langle \mathbf{w}_1, \mathbf{w}_1 \rangle} = \mp \frac{\langle \mathbf{v}_5, \mathbf{w}_5 \rangle}{\langle \mathbf{w}_5, \mathbf{w}_5 \rangle} = \mp \frac{\sqrt{-\det(G_2)}}{\langle \mathbf{w}_5, \mathbf{w}_5 \rangle} = \pm \frac{\sqrt{-\det(G_2)}}{c_{11}},$$

taking the plus sign when the orientations of  $\Delta'_1$  and  $\Delta'_2$  agree. Since

$$\mathbf{v}_5 = \frac{1}{c_{11}}(-c_{12}\mathbf{v}_2 - c_{13}\mathbf{v}_3 - c_{14}\mathbf{v}_4 \pm \sqrt{-\det(G_2)}\mathbf{w}_1),$$

we conclude by taking the inner product of both sides with  $\mathbf{v}_1$  and then applying equations (2.5) and (2.6) to determine the choice of sign.  $\square$

The aforementioned algorithm is slightly more complicated when  $M$  has cusps. The issue arises because ideal vertices of  $T$  are lifted to  $L_+$  in  $\mathbb{E}^{1,3}$ . As a result there is ambiguity in the choice of lift. In [23], Frigerio and Petronio explain that by choosing lifts that correspond to sufficiently small horospheres, the above algorithm will still produce a canonical cell decomposition. In particular, a choice of horospheres  $\mathcal{O}$  on  $M$  satisfying the following will do:

- (1) Any distinct components  $\mathcal{O}_1$  and  $\mathcal{O}_2$  of  $\mathcal{O}$  are disjoint and

$$e^{-d(\mathcal{O}_1, \partial \tilde{M})} + e^{-d(\mathcal{O}_2, \partial \tilde{M})} < 2e^{-d(\mathcal{O}_1, \mathcal{O}_2)},$$

- (2) The toric cusps in  $M$  determined by  $\mathcal{O}$  do not contain vertices of  $\text{Cut}(M, \partial M)$ , and for any such vertex  $u$

$$\sinh d(u, \partial M) < e^{-d(u, \mathcal{O})},$$

where  $\tilde{M}$  is the universal cover of  $M$ . The *cut-locus*  $\text{Cut}(M, \partial M)$  of  $M$  relative to  $\partial M$  is defined to be the set of all points of  $M$  that admit at least two different shortest paths to  $\partial M$ . A point is a *vertex* of the cut-locus if it admits four different shortest paths to  $\partial M$ , whose initial tangent vectors span the tangent space to  $M$  at the point.

**Question:** Is there a universal bound on how small the cusp cross-sections have to be to satisfy these properties? In [70], Weeks has answered the question when the boundary of  $M$  consists of tori. In this case, shrinking the cross-sections to area  $\frac{3\sqrt{3}}{8}$  will do. If such a bound is found, then we could use Theorem 2.19 and corollary 2.20 (below) to renormalize the cusp areas.

Let  $\mathbf{v}_i$  be an ideal vertex of some generalized tetrahedron  $\Delta'$ . The following result explains how the Euclidean triangle  $\Delta^{\mathbf{v}_i} = \hat{\Delta} \cap h_{\mathbf{v}_i}$  is affected by the renormalization of  $\mathbf{v}_i$ :

**Theorem 2.19.** *Let  $\Delta'$  be a generalized tetrahedron with vertices  $\mathbf{v}_1, \mathbf{v}_2, \mathbf{v}_3, \mathbf{v}_4 \in \mathbb{E}^{1,3}$ . Then if  $\mathbf{v}_1$  is an ideal vertex, the area of  $\Delta^{\mathbf{v}_1}$  is given by*

$$(2.13) \quad \text{Area}(\Delta^{\mathbf{v}_1}) = \frac{-\det(G)^2}{2c_{22}c_{33}c_{44} \sin \theta_{24} \sin \theta_{23} \sin \theta_{34}}.$$

PROOF. By an isometry of  $\mathbb{E}^{1,3}$  we can assume  $\mathbf{v}_1 = (1, 0, 1, 0)$ ,  $\mathbf{v}_4 = (u, 0, v, 0)$  and  $\mathbf{w}_2 = (0, a, 0, 0)$ , where  $a, u, v \in \mathbb{R}$ . It follows from

$$\langle \mathbf{v}_1, \mathbf{w}_3 \rangle = \langle \mathbf{v}_4, \mathbf{w}_3 \rangle = 0 \text{ and } \langle \mathbf{w}_2, \mathbf{w}_3 \rangle = \|\mathbf{w}_2\| \|\mathbf{w}_3\| \cos \theta_{23}$$

that  $\mathbf{w}_3 = (0, b \cos \theta_{23}, 0, \pm b \sin \theta_{23})$ , where  $b \in \mathbb{R}$ . Since

$$\langle \mathbf{v}_1, \mathbf{w}_4 \rangle = 0 \text{ and } \langle \mathbf{w}_2, \mathbf{w}_4 \rangle = \|\mathbf{w}_2\| \|\mathbf{w}_4\| \cos \theta_{24}$$

we can conclude that  $\mathbf{w}_4 = (c_0, -c \cos \theta_{24}, c_0, \pm c \sin \theta_{24})$ , where  $c_0, c \in \mathbb{R}$ . If we assume the 3-rd and 4-th faces of  $\Delta'$  lie 'below' the 2-nd face we can resolve the ambiguity in sign. So

$$\mathbf{w}_3 = (0, b \cos \theta_{23}, 0, b \sin \theta_{23}) \text{ and } \mathbf{w}_4 = (c_0, -c \cos \theta_{24}, c_0, c \sin \theta_{24}).$$

Refer to Figure 2.19. Moreover, we can adjust the lengths of these normals so equation (1.10) is satisfied.

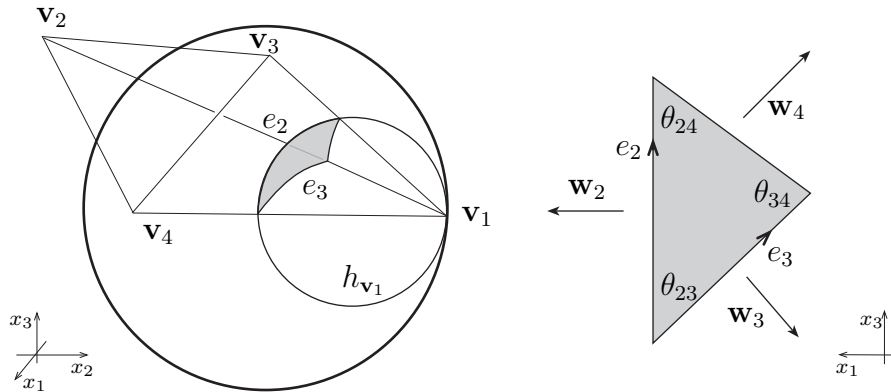


FIGURE 2.19. The positioning of  $\Delta'$  in  $\mathbb{H}^3$ , illustrated in the projective model.

Let  $\mathbf{x} = (x_0, x_1, x_2, x_3) \in H_-$  denote a point on  $h_{\mathbf{v}_1}$ . Then since  $\mathbf{x} \in h_{\mathbf{v}_1} \cap H_-$ ,  $\langle \mathbf{x}, \mathbf{v}_1 \rangle = -1$  and  $\langle \mathbf{x}, \mathbf{x} \rangle = -1$  we have  $x_0 = x_2 + 1$ . So the equation of the horosphere  $h_{\mathbf{v}_1}$  is

$$-1 = -(x_2 + 1)^2 + x_1^2 + x_2^2 + x_3^2,$$

and if  $\alpha = x_1$  and  $\beta = x_3$ ,  $h_{\mathbf{v}_1}$  can be parametrized by

$$h_{\mathbf{v}_1} = \{g(\alpha, \beta) | \alpha, \beta \in \mathbb{R}\},$$

where

$$g(\alpha, \beta) = \left( \frac{\alpha^2 + \beta^2}{2} + 1, \alpha, \frac{\alpha^2 + \beta^2}{2}, \beta \right).$$

Since

$$\frac{\partial g}{\partial \alpha} = (\alpha, 1, \alpha, 0) \text{ and } \frac{\partial g}{\partial \beta} = (\beta, 0, \beta, 1),$$

it follows that

$$\left\langle \frac{\partial g}{\partial \alpha}, \frac{\partial g}{\partial \alpha} \right\rangle = 1, \left\langle \frac{\partial g}{\partial \beta}, \frac{\partial g}{\partial \beta} \right\rangle = 1 \text{ and } \left\langle \frac{\partial g}{\partial \alpha}, \frac{\partial g}{\partial \beta} \right\rangle = 0$$

and so from this parametrization we can clearly see the Euclidean structure of  $h_{\mathbf{v}_1}$ .

Let

$$g_2(t) = g(0, t) = \left( \frac{t^2}{2} + 1, 0, \frac{t^2}{2}, t \right).$$

Then since  $\langle g_2(t), \mathbf{w}_2 \rangle = 0$  and  $\langle g_2(0), \mathbf{w}_3 \rangle = 0$ ,  $g_2$  parametrizes edge  $e_2 = \Delta^{\mathbf{v}_1} \cap \mathbf{w}_2^\perp$ . Moreover, because  $\langle \dot{g}_2, \dot{g}_2 \rangle = 1$ ,  $\text{Length}(e_2)$  is given by solving

$$0 = \langle g_2(t), \mathbf{w}_4 \rangle = -c_0 \left( \frac{t^2}{2} + 1 \right) + c_0 \frac{t^2}{2} + ct \sin \theta_{24}$$

for  $t$ . So

$$\text{Length}(e_2) = t = \frac{c_0}{c \sin \theta_{24}}.$$

Let

$$g_3(t) = g(-t \sin \theta_{23}, t \cos \theta_{23}) = \left( \frac{t^2}{2} + 1, -t \sin \theta_{23}, \frac{t^2}{2}, t \cos \theta_{23} \right).$$

Then since  $\langle g_3(0), \mathbf{w}_2 \rangle = 0$  and  $\langle g_3(t), \mathbf{w}_3 \rangle = 0$ ,  $g_3$  parametrizes edge  $e_3 = \Delta^{\mathbf{v}_1} \cap \mathbf{w}_2^\perp$ . It is easy to check  $\langle \dot{g}_3, \dot{g}_3 \rangle = 1$ , so solving  $\langle g_3(t), \mathbf{w}_4 \rangle = 0$ , and noting that

$$\theta_{34} = \pi - \theta_{23} - \theta_{24}$$

we get

$$\text{Length}(e_3) = \frac{c_0}{c(\sin \theta_{24} \cos \theta_{23} + \sin \theta_{23} \cos \theta_{24})} = \frac{c_0}{c \sin \theta_{34}}.$$

So the area of  $\Delta^{\mathbf{v}_1}$  is given by

$$\begin{aligned} \text{Area}(\Delta^{\mathbf{v}_1}) &= \frac{1}{2} \text{Length}(e_2) \text{Length}(e_3) \sin \theta_{23} \\ &= \frac{c_0^2 \sin \theta_{23}}{2c^2 \sin \theta_{24} \sin \theta_{34}} \\ &= \frac{\det(G) \sin \theta_{23}}{2v_{14}^2 c_{44} \sin \theta_{24} \sin \theta_{34}}, \end{aligned}$$

because equation (1.10) implies  $\sqrt{-\det(G)} = \langle \mathbf{v}_4, \mathbf{w}_4 \rangle = c_0(v - u) = c_0 v_{14}$  and  $w_{44} = c^2 = -c_{44}$ . To get this equation in a more symmetric form, apply equation

(2.7) giving

$$\begin{aligned}
\text{Area}(\Delta^{\mathbf{v}_1}) &= \frac{\sin^2 \theta_{23} \det(G)}{2v_{14}^2 c_{44} \sin \theta_{24} \sin \theta_{23} \sin \theta_{34}} \\
&= \frac{\det(G)^2 (v_{11} v_{44} - v_{14}^2)}{2v_{14}^2 c_{22} c_{33} c_{44} \sin \theta_{24} \sin \theta_{23} \sin \theta_{34}} \\
&= \frac{-\det(G)^2}{2c_{22} c_{33} c_{44} \sin \theta_{24} \sin \theta_{23} \sin \theta_{34}}
\end{aligned}$$

since  $v_{11} = 0$  as  $\mathbf{v}_1$  is ideal. □

**Corollary 2.20.** *Let  $\mathbf{v}_1$  be an ideal vertex of  $\Delta'$ , then*

$$\text{Area}(\Delta^{\alpha \mathbf{v}_1}) = \frac{1}{\alpha^2} \text{Area}(\Delta^{\mathbf{v}_1}),$$

where  $\alpha > 0$ .

**PROOF.** Let  $G'$  be the vertex Gram matrix of the generalized tetrahedron with vertices  $\alpha \mathbf{v}_1, \mathbf{v}_2, \mathbf{v}_3, \mathbf{v}_4$  and let  $c'_{ij}$  denote its cofactors. Then  $\det(G') = \alpha^2 \det(G)$  and  $c'_{ii} = \alpha^2 c_{ii}$ , for  $i > 1$ . Applying equation (2.13) gives the required result. □

## 2.6. Further extensions

By building upon the code from the `SnapPea` kernel we can use `Orb` to find a large number of geometric and topological invariants of hyperbolic 3-orbifolds including

- Fundamental groups,
- Covering spaces,
- Matrix generators,
- Length spectra,
- Canonical cell decompositions and
- Symmetry groups.

Matrix generators can be fed into `SnapPea` where Dirichlet domains can be viewed. We can also use `Snap` ([27]) by Goodman to find exact representations for these matrices giving us access to arithmetic invariants.

`Orb` also allows the user describe any orbifold whose singular set can be represented by a labelled graph  $\Gamma$  in  $\mathbb{S}^3$ . A projection for  $\Gamma$  can be drawn and, using the algorithm in the Appendix, the 3-orbifold  $Q = (\mathbb{S}^3, \Gamma)$  can be triangulated. In addition, graph complements can be triangulated and, using the same method as in Section 2.2, `Orb` can find complete hyperbolic structures with geodesic boundary.

`Orb` accepts 3-orbifolds in a variety of other formats including those used by `SnapPea` and `Geo`. A large number of knotted graphs is also available with `Orb`, and

these can be used to produce large numbers of orbifolds and graph complements. See Section 4.2 for details on how `Orb` was used in the enumeration of these knotted graphs and how these provide us with a huge class of 3-orbifolds.

There are several obvious extensions to the algorithm outlined in Section 2.2. Currently the algorithm only finds geometric structures on orbifolds with constant sectional curvature  $-1$ . One possible extension is to introduce a curvature parameter and allow for all geometric structures of constant sectional curvature; allowing for Euclidean and spherical orbifolds. This can be implemented with equations (10.91), (10.92) and (10.93) from [17] and should provide an even more robust algorithm. Casson's `Geo` works well on hyperbolic and spherical closed 3-manifolds by employing this approach.

Another possibility is to allow for generalized tetrahedra with completely truncated edges, as in Figure 2.17. Such tetrahedra could be used to find hyperbolic structures on hyperbolic 3-manifolds with geodesic boundary creased or bent along a collection of disjoint simple closed curves. One could prescribe an angle  $\theta$  at the crease by modifying equation (2.9) to

$$\beta_e^2 = \alpha_{v_1} \alpha_{v_2} \cos \theta,$$

with the special case of a length-0 edge occurring as a limiting case when  $\theta = 0$ .

## CHAPTER 3

### Attaching 2-handles

Throughout this chapter  $M$  will denote an orientable 3-manifold, and  $\alpha$  a simple closed curve on its boundary  $\partial M$ . Then by  $M[\alpha]$  we denote the 3-manifold obtained by gluing a 2-handle to  $\partial M$  along  $\alpha$ , and capping off any spherical boundary components created. That is, when  $\alpha$  lies on a torus component of  $\partial M$ ,  $M[\alpha]$  is exactly the manifold obtained by doing Dehn filling on the slope  $\alpha$ . Otherwise,  $M[\alpha]$  is simply the 3-manifold produced by gluing a thickened disc to  $M$  along  $\alpha$ . When  $\alpha$  does lie on a boundary component with genus  $g > 1$ , then we call this operation a *handle addition* along curve  $\alpha$ . Refer to Figure 3.1.

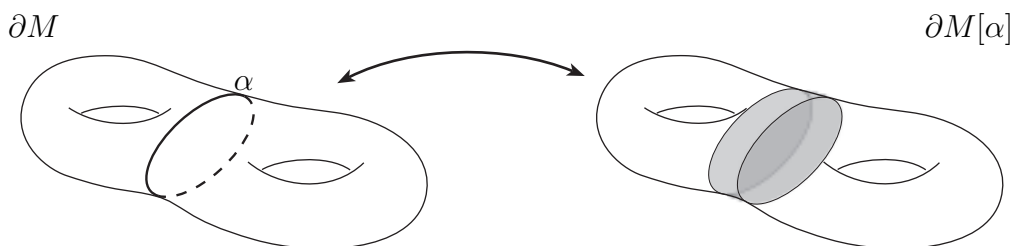


FIGURE 3.1. If  $\alpha$  is a simple closed curve on  $\partial M$ , then gluing a thickened disc along  $\alpha$  produces  $M[\alpha]$ .

According to Thurston's Hyperbolization Theorem, if  $M$  is Haken, then  $M$  is hyperbolic with geodesic boundary if and only if  $M$  is irreducible,  $\partial$ -reducible, atoroidal and anannular. If  $M$  is hyperbolic but  $M[\alpha]$  is not, then  $\alpha$  is an *exceptional curve*. Then there is a properly embedded surface  $S$  in  $M[\alpha]$ , which is either a reducing sphere, a  $\partial$ -reducing disc, an essential annulus or an essential torus. We call  $S$  a *degenerating surface*.

Finally, any two curves  $\alpha$  and  $\beta$  on a surface  $S$  are *coplanar* if some component of  $S - (\alpha \cup \beta)$  is an annulus or a once-punctured annulus. (See Figure 3.2.) If  $\alpha$  is non-separating and  $\beta$  is separating and coplanar to  $\alpha$ , then  $\alpha$  lies in a punctured torus in  $\partial M$  bounded by  $\beta$ , and it is clear that  $M[\alpha] = M[\beta][\alpha]$ .

The next section gives conditions on a curve  $\alpha$  on the boundary to ensure that  $M[\alpha]$  is hyperbolic. In the following section, an algorithm for attaching 2-handles to a triangulated 3-manifold is discussed. The chapter concludes by applying these results to study several examples.

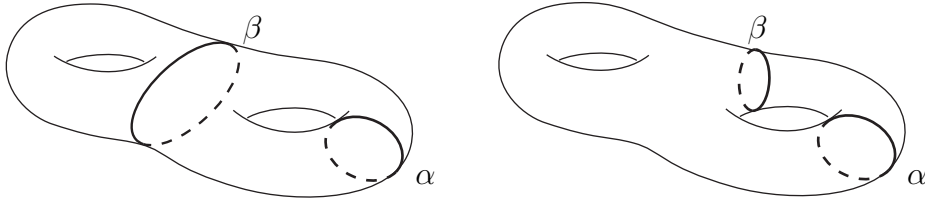


FIGURE 3.2. Two sets of coplanar curves.

### 3.1. Bounds on exceptional curves

Suppose  $T$  is a torus component of  $\partial M$ ,  $\alpha \subset T$ , and suppose  $M$  is hyperbolic. By Thurston's Hyperbolic Dehn Surgery Theorem ([61]), there are only finitely many  $\alpha$  (up to isotopy) with non-hyperbolic  $M[\alpha]$ . Thurston and Gromov ([28],[6]) also showed that if the length of  $\alpha$ , as measured in the Euclidean metric on the boundary of a horoball neighbourhood of the cusp, is at least  $2\pi$  then  $M[\alpha]$  is negatively curved. Agol ([3]) and Lackenby ([42]) have independently shown that if the length of  $\alpha$  is at least 6, then  $M[\alpha]$  is irreducible, atoroidal and not Seifert fibered, and has an infinite, word hyperbolic fundamental group. Hodgson and Kerckhoff ([32]) have shown that the number of non-hyperbolic fillings is bounded by a number independent of  $M$ . But do any of these results extend to the case where  $\alpha$  lies on a boundary component of higher genus?

That is, if  $S_g$  is a boundary component of  $M$  with genus  $g > 1$ , then are there only finitely many curves  $\alpha$  on  $S_g$  (up to isotopy) such that  $M[\alpha]$  is non-hyperbolic? In general this is not the case. In fact, it is easy to construct counterexamples, for instance see [58]. The problem is that if  $S_g$  contains an exceptional curve  $\beta$  bounding a punctured torus  $P$ , then any curve  $\alpha$  contained in  $P$  is also exceptional since  $M[\alpha] = M[\beta][\alpha]$  and  $M[\beta]$  is non-hyperbolic. With this in mind we can produce the following result:

**Theorem 3.1.** *Let  $M$  be an orientable compact finite volume hyperbolic 3-manifold with non-empty geodesic boundary. Suppose  $\alpha$  is a simple closed geodesic on a boundary component  $S_g$ , with genus  $g > 1$ . Let*

$$c(S_g) = 6\text{ArcCosh} \left( 1 + \frac{2\sqrt{1 - 4/\chi(S_g)}}{(\sqrt{1 - 4/\chi(S_g)} - 1)^2} \right).$$

*Then  $M[\alpha]$  is hyperbolic provided that, if  $\alpha$  is separating then*

$$\text{Length}(\alpha) > c(S_g),$$

*and if  $\alpha$  is non-separating, then all curves  $\alpha'$  coplanar to  $\alpha$  have*

$$\text{Length}(\alpha') > c(S_g).$$

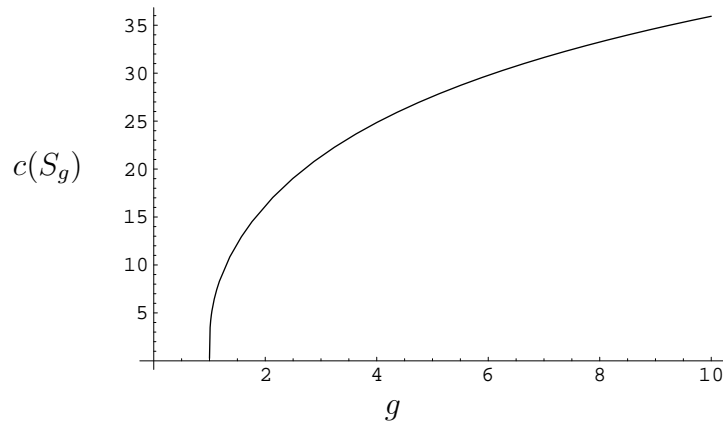


FIGURE 3.3. As  $g \rightarrow \infty$ ,  $c(S_g) = O(\log(g))$ .

The number  $c(S_g)$  only depends on the genus of  $S_g$ . If all the separating curves bounding once punctured tori are long enough then there are only finitely many exceptional curves.

**Corollary 3.2.** *If there is no exceptional simple closed geodesic of length less than or equal to  $c(S_g)$  that bounds a once punctured torus on  $S_g$ , then there are only a finite number of exceptional simple closed geodesics on  $S_g$ .*

**PROOF OF COROLLARY 3.2.** Let  $N$  denote the set of all exceptional simple closed geodesics that have length greater than  $c(S_g)$ . Since there are only a finite number of simple closed geodesics on  $S_g$  with length less than or equal to  $c(S_g)$  it is enough to show that  $N$  is a finite set. Note that it follows from the theorem that  $N$  consists entirely of non-separating curves.

Let  $L$  denote the set of simple closed geodesics on  $S_g$  that bound a once punctured torus in  $S_g$  and have length less than or equal to  $c(S_g)$ . Then by Theorem 3.1 any curve in  $N$  must be coplanar to at least one curve in  $L$ . For each curve  $\alpha \in L$  let  $C_\alpha$  denote the set of all curves in  $N$  coplanar to  $\alpha$ . Then it is clear that  $N = \cup_{\alpha \in L} C_\alpha$ .

Recall that for any curve  $\beta \in C_\alpha$  we have the equality

$$M[\alpha][\beta] = M[\beta].$$

Since  $M[\alpha]$  is hyperbolic by assumption, Thurston's Hyperbolic Dehn Surgery Theorem shows there can only be a finite number of curves in  $C_\alpha$ . Thus  $N$  can be written as a finite union of finite sets and so is also a finite set.  $\square$

Theorem 3.1 is closely related to one in [41] where Lackenby showed that if no short curves become trivial when a handlebody is glued to  $\partial M$ , then the resulting manifold is *hyperbolic*. This differs from the above result in the sense that multiple 2-handles are being glued to the boundary in one operation.

In [58], Scharlemann and Wu have found a bound on the number of *basic* curves with non-hyperbolic additions. An exceptional curve  $\alpha$  is basic if it is separating, or there are no exceptional separating curves coplanar to  $\alpha$ . It is interesting to note that the proof uses mainly combinatorial arguments and little of the geometry of the manifold. The proof of Theorem 3.1 uses the following extension of Lemma 3.3 from [58]:

**Lemma 3.3.** *Assume  $M$  and  $\alpha$  are as in Theorem 3.1. If  $\alpha$  is an exceptional curve on  $\partial M$  then there is a degenerating surface  $\hat{P}$  in  $M[\alpha]$  such that  $P = M \cap \hat{P}$  is essential in  $M$  and the components of  $\partial P$  not in  $\partial \hat{P}$  are coplanar to  $\alpha$ . Moreover, if  $\alpha$  is separating then  $P$  can be chosen so that all the components of  $\partial P$  not in  $\partial \hat{P}$  are parallel to  $\alpha$ .*

PROOF. The first sentence in the statement above can be extracted from the first paragraph of the proof of Lemma 3.3 in [58]. Here we follow Scharlemann and Wu's proof and establish that the statement can be strengthened when  $\alpha$  is separating.

Let  $\alpha$  be an exceptional separating curve on  $\partial M$ . Since  $\alpha$  is exceptional then we can find an essential sphere, disc, annulus or torus  $\hat{P}$  in  $M[\alpha]$ . Then after an isotopy we can arrange that the surface  $P = \hat{P} \cap M$  has boundary  $\partial P = \partial_1 \cup \partial \hat{P}$  where  $\partial_1$  consists of boundary components parallel to  $\alpha$  and  $\hat{P}$  is obtained from  $P$  by capping off the curves in  $\partial_1$  by disjoint discs in  $M[\alpha]$ . Define

$$b(\hat{P}) = \begin{cases} 0 & \text{if } \hat{P} \text{ is a sphere;} \\ 1 & \text{if } \hat{P} \text{ is a disc;} \\ 2 & \text{if } \hat{P} \text{ is an annulus;} \\ 3 & \text{if } \hat{P} \text{ is a torus.} \end{cases}$$

Define the complexity of  $P$  to be  $c(P) = (b(\hat{P}), |\partial P|)$  in lexicographic order. We select a degenerating surface  $\hat{P}$  with  $\partial P = \partial_1 \cup \partial \hat{P}$  as above so that the surface  $P$  has least complexity. We now show that this choice guarantees  $P$  is essential in  $M$ . Clearly  $P$  is incompressible in  $M$ , for a compression would produce a surface of lower complexity.

Suppose  $P$  is  $\partial$ -compressible, with  $D$  a  $\partial$ -compression disc in  $M$ . Write  $\partial D = u \cup v$ , where  $u$  is an arc in  $\partial M$ , and  $v$  is an arc in  $P$ . Since  $P$  is incompressible,  $u$  cannot be isotoped into  $\partial P$  relative to  $\partial u$ . There are three types of boundary compression to consider.

Case (1):  $u$  has endpoints on different components of  $\partial P$ .

Since  $\hat{P}$  is  $\partial$ -incompressible,  $u$  cannot have both ends on  $\partial \hat{P}$ . If  $u$  has ends on different components of  $\partial_1$  then since  $\alpha$  is separating, this boundary compression

produces a trivial boundary component on  $\partial M$ . Cap the new boundary component off and call the new surface  $P'$ . It is clear that  $\hat{P}' = \hat{P}$  and  $|\partial P'| < |\partial P|$  so  $P'$  is a surface of lower complexity. (Figure 3.4.)

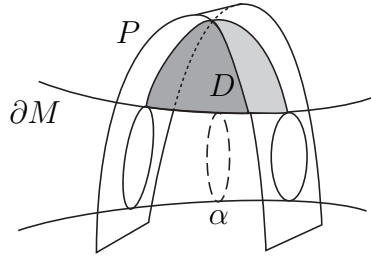


FIGURE 3.4. In this case we see that we can pull  $P$  across the disc  $D$  and then past  $\partial M$ , reducing the complexity.

If  $u$  has one end on  $\partial_1$  and one on  $\partial \hat{P}$  then this boundary compression merges a component of  $\partial_1$  with a component of  $\partial \hat{P}$  creating a new boundary component which is not homotopic to  $\alpha$ . Again we see that the new surface created  $P'$  has  $\hat{P}' = \hat{P}$  and  $|\partial P'| < |\partial P|$  so  $P'$  is a surface of lower complexity. (Figure 3.5.)

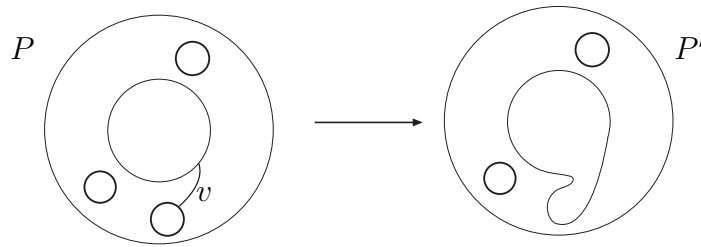


FIGURE 3.5. Here  $P$  is a punctured annulus. The boundary components in  $\partial_1$  are drawn with thicker lines. Boundary compression gives a new surface with  $\hat{P}' = \hat{P}$  but with fewer boundary components in  $\partial_1$ .

Case (2):  $u$  has both endpoints contained in one component of  $\partial \hat{P}$ . In this case boundary compression along  $D$  produces a new surface  $P'$  and since  $\hat{P}$  is  $\partial$ -incompressible,  $\hat{P}'$  must have a component isotopic to  $\hat{P}$ . The corresponding component of  $P'$  has lower complexity.

Case (3):  $u$  has both endpoints contained in one component of  $\partial_1$ . Boundary compress along  $D$  and call the new surface  $P'$ . Figure 3.6 illustrates the case when  $\hat{P}$  is a torus. In general we see that the two new boundary curves created are essential on  $\partial M[\alpha]$  and not parallel to  $\alpha$ , so  $|\partial \hat{P}'| = |\partial \hat{P}| + 2$ . Moreover, either a component of  $\hat{P}'$  is a boundary compression disc for  $M[\alpha]$ , or  $\hat{P}'$  is one or two annuli. In the former case, the compression disc is a surface of lower complexity. In

the latter case we see that  $\hat{P}'$  can be obtained from  $\hat{P}$  by 2-surgery along an annulus so that one of the components of  $\hat{P}'$  is essential. The corresponding component of  $P'$  is a surface of lower complexity. (Figure 3.6.)

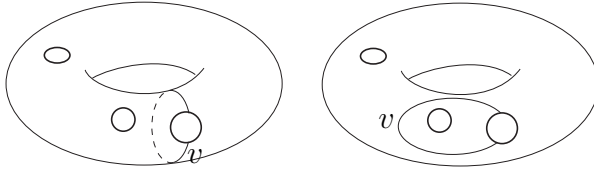


FIGURE 3.6. The boundary compression on the left produces a punctured annulus. The boundary compression on the right produces a disconnected surface consisting of a punctured disc and a punctured torus.

Note that the only new boundary components created by these three types of boundary compressions belong to  $\partial\hat{P}'$ . In the proof in [58] we see that there are actually five types of boundary compression to consider when we allow for the possibility that  $\alpha$  is a non-separating curve. In that case, it is possible that a boundary compression may introduce a new boundary curve, that is not contained in  $\partial\hat{P}'$ , and is coplanar but not parallel to  $\alpha$ .  $\square$

Scharlemann and Wu's combinatorial theorem contrasts with Lackenby's theorem which uses much of the manifold's structure. Theorem 3.1 combines both these approaches and calls upon a result on strip packing densities in [44].

**Theorem [44]:** *A strip of radius  $r$  in the hyperbolic plane is the set of points within distance  $r$  of a given geodesic. The density of a packing of strips of radius  $r$  in the plane can not exceed*

$$\frac{3}{\pi} \sinh r \operatorname{ArcCosh} \left( 1 + \frac{1}{2 \sinh^2 r} \right).$$

*This bound is sharp for every value of  $r$ .*

**Remark:** The same strip packing density arguments can also be used to sharpen Lackenby's result.

**PROOF OF THEOREM 3.1.** Suppose that  $M$  and  $\alpha$  satisfy the conditions of Theorem 3.1 and that  $M[\alpha]$  is not hyperbolic.

Lemma 3.3 says we can find a punctured sphere or punctured torus  $P$  and an essential map  $f : P \rightarrow M$  such that  $f(\partial P) = \partial_1 \cup \partial_2$ , where  $\partial_1$  consists of all the boundary components coplanar to  $\alpha$ . The lemma also says that  $|\partial_2| \leq 2$ , with  $|\partial_2| = 0$  if  $P$  is a punctured torus. Moreover, if  $\alpha$  is separating then we can choose  $P$  so that all the components in  $\partial_1$  are parallel to  $\alpha$ . We can assume that the components of  $\partial P$  map to geodesics on  $\partial M$ .

Next we replace  $f$  by a *pleated map*  $g : P \rightarrow M$  as described in Thurston [64] or Agol [3] (Lemma 4.1). Choose a topological ideal triangulation  $T$  for  $\text{int}P$  so that each edge  $e$  is essential in  $P$ . So when we lift  $f(e)$  to the universal cover  $\tilde{M}$  its end points lie on distinct geodesic boundary planes. Now spin the triangles of  $T$  around  $\partial P$  (Figures 3.7). Let  $E$  denote the edges of  $T$ . Lifting  $f(P)$  to  $\tilde{M}$ ,

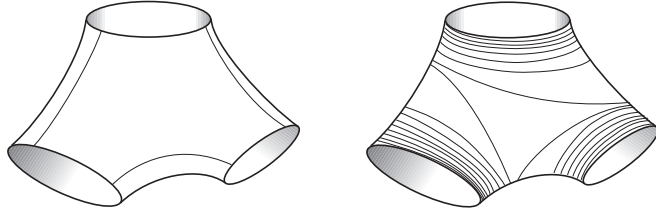


FIGURE 3.7. Spinning the edges of  $T$  around  $\partial P$ .

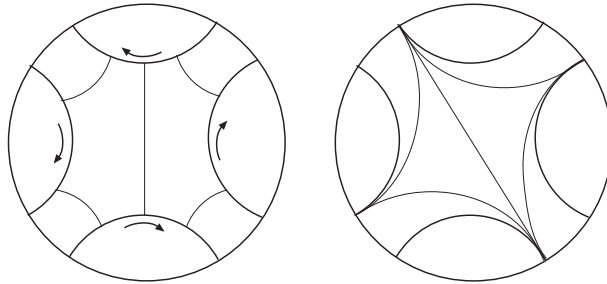


FIGURE 3.8. The picture in the universal cover of  $M$ .

this spinning corresponds to dragging the end points of the components of  $f(E)$  along the lifts of the components of  $f(\partial P)$  to  $\partial\mathbb{H}^3$  (Figure 3.8). Since the lift of each component of  $f(E)$  runs between distinct boundary planes we see that the end points of each component of  $f(E)$  are carried to distinct points on  $\partial\mathbb{H}^3$ . So we may homotope  $f$  so that each edge of  $T$  maps to a unique geodesic in  $M$ . Then we can homotope  $f$  so that each ideal triangle is totally geodesic by a homotopy extension giving a pleated map  $g : \text{int}P \rightarrow M$ . Since this new map is pleated there is an induced hyperbolic metric on  $\text{int}P$ .

Let  $\beta$  denote an edge in  $g(E)$  and let  $\beta'$  be the corresponding edge in  $f(E)$ . Then since the ends of each component in  $E$  are quasi-geodesic (after spinning), each end of  $\beta$  lies within a bounded neighbourhood of the corresponding end of  $\beta'$ . So the ends of  $\beta$  limit to the same closed geodesics on  $\partial M$  as the ends of  $\beta'$ . Furthermore, when an end of  $\beta'$  wraps closely once around a component of  $f(\partial P)$  the corresponding end of  $\beta$  wraps closely once around the same component of  $f(\partial P)$ . Thus, as in the proof of Lemma 4.1 of [3], we can complete the metric on  $\text{int}P$  by extending  $g$  to be an isometry on  $\partial P$ .

Let  $N(S)$  be the points in  $M$  at distance at most  $U$  from  $S = S_g$ . Using Basmajian's theorem ([4]), if

$$U = \text{ArcSinh} \left( \frac{(1 - 4/\chi(S))^{1/4} - (1 - 4/\chi(S))^{-1/4}}{2} \right),$$

then  $N(S)$  will be a collar on  $S$ .

Let  $N(\partial P)$  be the points of  $P$  at distance at most  $U$  from  $\partial P$ , using the induced metric. Then  $N(\partial P)$  is a collar on  $\partial P$ . To see this, increase  $U$  from zero to its final value. Near zero,  $N(\partial P)$  is clearly a collar. But suppose that as it expands, there is some point at which a self tangency is created. This point on  $P$  has property that it has two shortest geodesic arcs to the boundary,  $\gamma_1$  and  $\gamma_2$ . Since this is the first point the bumping occurs, these two arcs form a smooth geodesic  $\gamma = \gamma_1 \cup \gamma_2$  in  $P$ . Hence,  $\gamma$  is essential in  $P$ .

As pleated maps shrink distances we have  $g(N(\partial P)) \subseteq N(S)$ , and so  $g(\gamma)$  is contained entirely in  $N(S)$ , which is a collar. Hence,  $g(\gamma)$  can be homotoped to  $S$  keeping endpoints fixed. This contradicts  $P$  being essential and so  $N(\partial P)$  is a collar.

Since  $\text{Length}(\alpha) > c(S)$  and  $\partial_1$  consists of boundary components parallel to  $\alpha$  we have

$$\begin{aligned} \text{Area}(N(\partial P)) &= \sinh(U)\text{Length}(\partial P) \\ &\geq \sinh(U)\text{Length}(\partial_1) \\ &> \sinh(U)c(S)|\partial_1| \\ &= 6 \sinh(U)\text{ArcCosh} \left( 1 + \frac{1}{2 \sinh^2(U)} \right) |\partial_1|. \end{aligned}$$

Now using the theorem of Marshall and Martin,

$$\text{Area}(N(\partial P)) \leq \frac{3}{\pi} \sinh(U)\text{ArcCosh} \left( 1 + \frac{1}{2 \sinh^2(U)} \right) \text{Area}(P)$$

and so by combining the previous two inequalities with Gauss-Bonnet we get

$$2\pi\chi(P) = \int_P K dA \leq -\text{Area}(P) < -2\pi|\partial_1|.$$

There are two cases to consider. If  $P$  is a punctured torus its Euler characteristic is  $-|\partial_1|$  which gives

$$-2\pi|\partial_1| < -2\pi|\partial_1|,$$

which is an obvious contradiction. If  $P$  is a punctured sphere then we get

$$2\pi(2 - |\partial_1| - |\partial_2|) < -2\pi|\partial_1|,$$

which again is a contradiction since  $|\partial_2| \leq 2$ . Therefore the surface  $P$  cannot exist and  $M[\alpha]$  is hyperbolic. This completes the proof of the theorem.  $\square$

### 3.2. The algorithm

We now outline an algorithm for attaching a 2-handle to a manifold  $M$  triangulated by generalized tetrahedra. When  $M$  is a graph complement in  $\mathbb{S}^3$  such a triangulation can be found using `Orb`. (See Appendix.) This algorithm is applied in the section to two examples, and combined with Theorem 3.1 to describe the non-hyperbolic handle additions. The procedure works for attaching 2-handles to both torus and higher genus boundary components. No assumptions are made about geometric structures as the algorithm is completely topological.

Suppose we wish to produce a triangulation for  $M[\alpha]$ , where  $\alpha$  is an essential simple closed curve in  $\partial M$ . Since  $M$  is triangulated there is an induced triangulation on  $\partial M$  and we can draw  $\alpha$  as it passes through it. Denote by  $T_0$  the triangulation for  $M$  and note that  $T_0$  induces a triangulation  $T_0^1$  on  $\partial M$ . Homotope  $\alpha$  so that it is a *normal curve* with respect to  $T_0^1$ , and lies within an  $\epsilon$ -neighborhood of the dual 1-skeleton  $D$  of  $T_0^1$ . (See Figure 3.9.) It is clear that this can be achieved without making  $\alpha$  self-intersect. Let  $t(e)$  denote the number of arcs of  $\alpha$  running parallel to edge  $e$  of  $D$ .

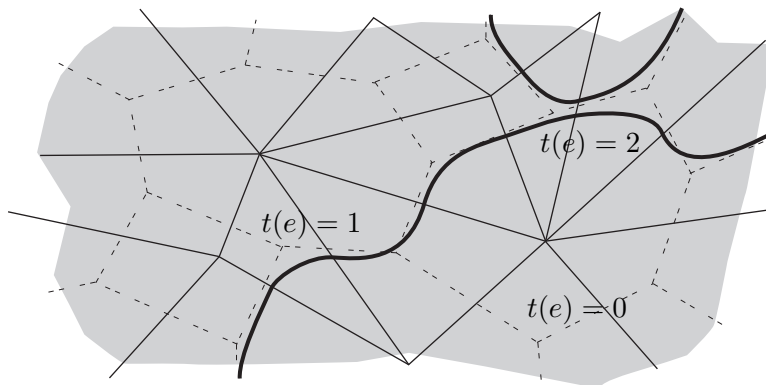


FIGURE 3.9. A normal curve  $\alpha$  on  $\partial M$ . A normal curve is made up of non-intersecting *normal arcs*. A normal arc enters and leaves a triangle through distinct faces. The dual spine  $D$  has one vertex in the middle of each triangle, and for every edge in  $T_0^1$ , an edge joining the vertices of the neighbouring triangles (represented by the dashed lines.) The map  $t(e)$  is the number of normal arcs of  $\alpha$  running parallel to edge  $e$  of  $D$ .

The remainder of the algorithm can be thought of as follows. Take a thickened disc, a 2-handle, and align its boundary with  $\alpha$  as it lies on  $\partial M$ . Pushing the boundary of the disc into  $\partial M$  along  $\alpha$  produces  $M[\alpha]$ .

The description sounds simple but in practice things are complicated by the need to maintain a triangulation. This means that not only must the thickened

disc be subdivided into tetrahedra, but after it is slid into  $\partial M$  what is left must be a triangulation. The problem is simplified by retriangulating  $T_0$ . This is done by:

- (1) Introducing a vertex in the middle of each tetrahedron and then coning its faces to the middle. This replaces each tetrahedron by four, meeting at a common vertex.
- (2) Performing two-to-three moves (as discussed in Section 2.5) on the faces that were not created by the previous step.

Call the new triangulation  $T$  and refer to Figure 3.10 for an illustration. As a result of the subdivision,  $D$  is contained in the 1-skeleton of  $T^1$ , so  $\alpha$  lies within an  $\epsilon$ -neighbourhood of the 1-skeleton of  $T^1$ . Here  $T^1$  is the triangulation of  $\partial M$  induced by  $T$ .

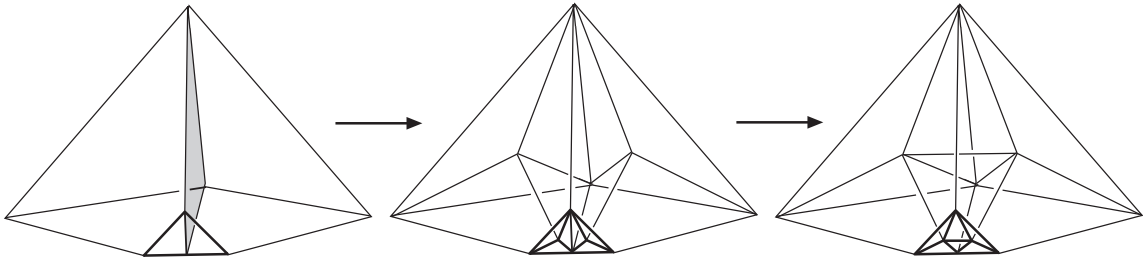


FIGURE 3.10. Start with two neighbouring tetrahedra (separated by the grey face) and then perform a one-to-four move followed by a two-to-four move. The retriangulation on the boundary is illustrated by slicing off the link of a vertex.

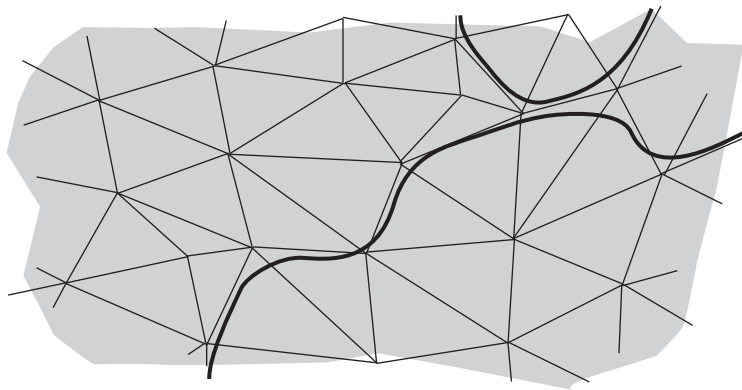


FIGURE 3.11. After subdivision  $\alpha$  now lies within an  $\epsilon$ -neighbourhood of the 1-skeleton of  $T^1$ .

For each edge  $e$  of  $D$  there is a unique face  $F_e$  in  $T$  lying in the interior of  $M$ . The face  $F_e$  is a quadrilateral with one edge being  $e$  and the remaining three belonging to  $T$ . Now for every edge  $e$  of  $D$  with  $t(e) > 0$ , unglue  $T$  along  $F_e$ . The

result is a cell decomposition with two unidentified faces for every face unglued. See Figure 3.12.

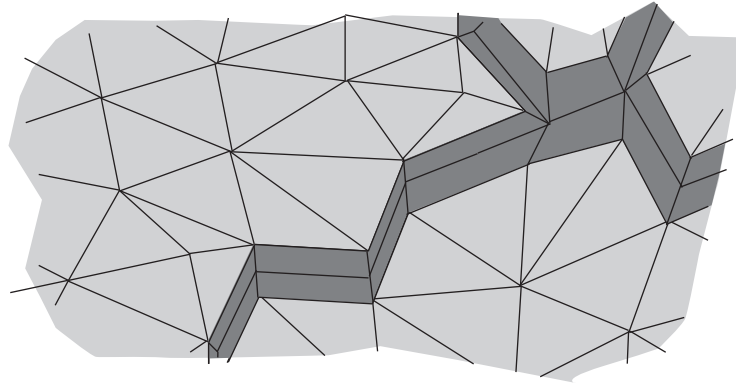


FIGURE 3.12. This is what  $\partial M$  looks like after we unglue the faces of  $T$  incident to  $\alpha$ . The boundary has new pairs of quadrilateral faces. These quadrilaterals come from the truncated triangles in the interior of  $T$  that were unglued. These new faces form a chasm that cuts into  $M$  where  $\alpha$  once ran.

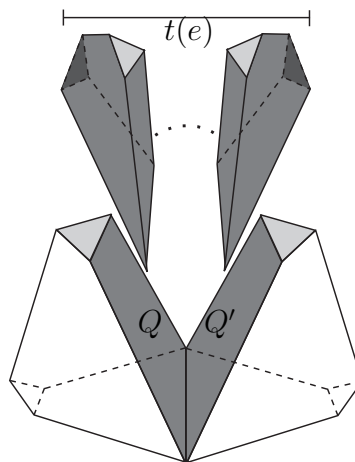


FIGURE 3.13. Here we see the chasm at  $(Q, Q')_e$ . We slide and glue  $t(e)$  truncated tetrahedra down the chasm.

For each unglued face  $F_e$ , denote by  $(Q, Q')_e$ , the pair of unidentified quadrilaterals on the boundary. At every pair  $(Q, Q')_e$  on the boundary, insert  $t(e)$  tetrahedra down the chasm. This is best explained pictorially so refer to Figures 3.13 and 3.14.

The algorithm is essentially complete. These newly positioned tetrahedra glue together to form the required 2-handle. To glue the tetrahedra up, follow the tetrahedra along the path defined by  $\alpha$  and glue consecutive faces.

We now have  $M[\alpha]$  decomposed into truncated tetrahedra. However, in the case where  $\alpha$  was on a torus boundary component, a spherical boundary component was created. So the vertex has to be glued back in to produce a triangulation for  $M[\alpha]$ .

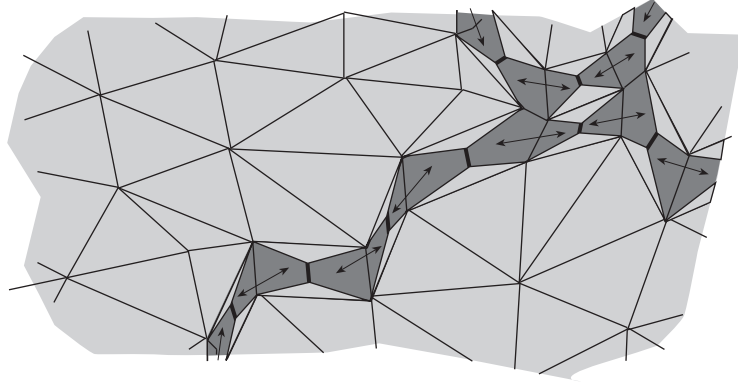


FIGURE 3.14. We proceed by sliding tetrahedra down the chasm. We fill the chasm by placing  $t(e)$  truncated tetrahedra down the gap at each pair of unidentified quadrilaterals  $(Q, Q')_e$ . Gluing consecutive faces as shown here produces the 2-handle.

### 3.3. Two simple examples

This chapter concludes by using Theorem 3.1 and the previously described algorithm to rigorously study two examples. Both the examples can be triangulated with two regular truncated hyperbolic tetrahedra with dihedral angles  $\frac{\pi}{6}$ . They are amongst the eight lowest volume hyperbolic 3-manifolds with geodesic boundary as described by Fujii in [25].

Both the examples that follow required the enumeration of simple closed geodesics on geodesic boundary surfaces. This is discussed in more detail in Section 3.3.3.

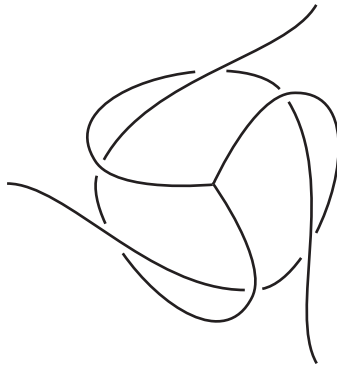


FIGURE 3.15. The knotted-Y  $\mathcal{G}_1$ . The complement of this graph in  $\mathbb{R}^3$  is a hyperbolic 3-manifold with geodesic boundary.

**3.3.1. Example one.** The first manifold  $\mathcal{M}_1$  is the complement of the knotted-Y or “tripos graph”  $\mathcal{G}_1$  illustrated in Figure 3.15 ([62]). The symmetry group  $G_1$  of  $\mathcal{M}_1$  is generated by two rotations  $\sigma_1$  and  $\sigma_2$  with  $G_1 = \langle \sigma_1, \sigma_2 | \sigma_1^3 = \sigma_2^2 = 1 \rangle$ .

Since an isometry of a hyperbolic 3-manifold with geodesic boundary is determined by its action on the boundary,  $\sigma_1$  and  $\sigma_2$  can be represented by the permutations on the dual 1-skeleton  $D$  (Figure 3.17) of  $\partial\mathcal{M}_1$  with

$$\sigma_1 = \begin{pmatrix} 1 & 2 & 3 & 4 & 5 & 6 & 7 & 8 & 9 & 10 & 11 & 12 \\ 2 & 3 & 1 & 10 & 11 & 12 & 4 & 5 & 6 & 7 & 8 & 9 \end{pmatrix}$$

and

$$\sigma_2 = \begin{pmatrix} 1 & 2 & 3 & 4 & 5 & 6 & 7 & 8 & 9 & 10 & 11 & 12 \\ 12 & 6 & 9 & 4 & 5 & 2 & 10 & 11 & 3 & 7 & 8 & 1 \end{pmatrix}.$$

A computer program implementing the handle attaching algorithm has been used to compile a list of all exceptional geodesics of length  $\leq c(S_2) \approx 16.192407$ . Refer to Table 3.1. The program found *no* exceptional separating curves and so according to Corollary 3.2 there are a finite number of exceptional curves on  $\partial\mathcal{M}_1$ . Unfortunately, because the program found separating curves with length less than  $c(S_2)$  we can not conclude that Table 3.1 is a complete list of exceptional curves.

Curve $\alpha$	length( $\alpha$ )	JSJ decomposition
(0,0,0,0,0,0,0,0,1,1,0)	1.66289	solid torus
(0,1,1,0,1,1,0,0,0,1,0,1)	4.24315	$\mathbb{T}(2, 7)$
(0,1,1,0,1,1,0,0,0,0,1,1)	4.41349	$\mathbb{T}(2, 3), \mathbb{T}(2, 4)$
(0,1,1,1,0,1,0,0,0,1,0,1)	4.41349	$\mathbb{T}(2, 6)$
(0,1,1,0,1,1,0,0,0,2,1,1)	5.25744	$\mathbb{T}(3, 5)$
(0,1,1,0,1,1,0,0,0,3,2,1)	6.77248	$\mathbb{T}(2, 3), \mathbb{T}(2, 4)$
(0,1,1,1,2,1,0,0,0,1,2,1)	6.90358	$\mathbb{T}(2, 4), \mathbb{T}(3, 3)$
(0,2,2,1,1,0,1,1,2,0,2,2)	8.8026	$\mathbb{T}(2, 3), \mathbb{T}(3, 3), m004$

TABLE 3.1. The list of exceptional curves on  $\partial\mathcal{M}_1$  (up to symmetry) of length  $\leq c(S_2)$ .

The proof of Corollary 3.2 indicates how Table 3.1 could be extended to a complete list of exceptional curves. For each separating curve  $\alpha$  with length  $\leq c(S_2)$  we can find (using SnapPea) the finite set of degenerating curves on  $\partial M[\alpha]$ . Each of these degenerating curves on  $\partial M[\alpha]$  corresponds to a degenerating curve on  $\partial M$  coplanar to  $\alpha$ .

The notation used to describe the curves is explained in Figures 3.16 and 3.17. By perturbing any curve  $\alpha \subset \partial M$  so it lies within an  $\epsilon$ -neighbourhood of  $D$ ,  $\alpha$  can be assigned a vector  $(a_1, a_2, \dots, a_{12}) \in \mathbb{Z}^{12}$ , where  $a_i$  denotes the number of arcs of  $\alpha$  running parallel to the  $i$ -th edge of  $D$ .

The last column in the table describes the JSJ decomposition of  $\mathcal{M}_1[\alpha]$  ([37],[38]) obtained by using **SnapPea** to cut  $\mathcal{M}_1[\alpha]$  open along essential tori or Klein bottles. The manifold  $\mathcal{M}_1[(0, 1, 1, 1, 0, 1, 0, 0, 0, 1, 0, 1)]$  is the only manifold on the list which contains an essential Klein bottle.  $\mathbb{T}(p, q)$  denotes the complement of the  $(p, q)$  torus link and *m004* the complement of the figure eight knot. The two manifolds  $\mathcal{M}_1[(0, 1, 1, 0, 1, 1, 0, 0, 0, 0, 1, 1)]$  and  $\mathcal{M}_1[(0, 1, 1, 0, 1, 1, 0, 0, 0, 3, 2, 1)]$  can be distinguished by the homology of their 3-fold covers.

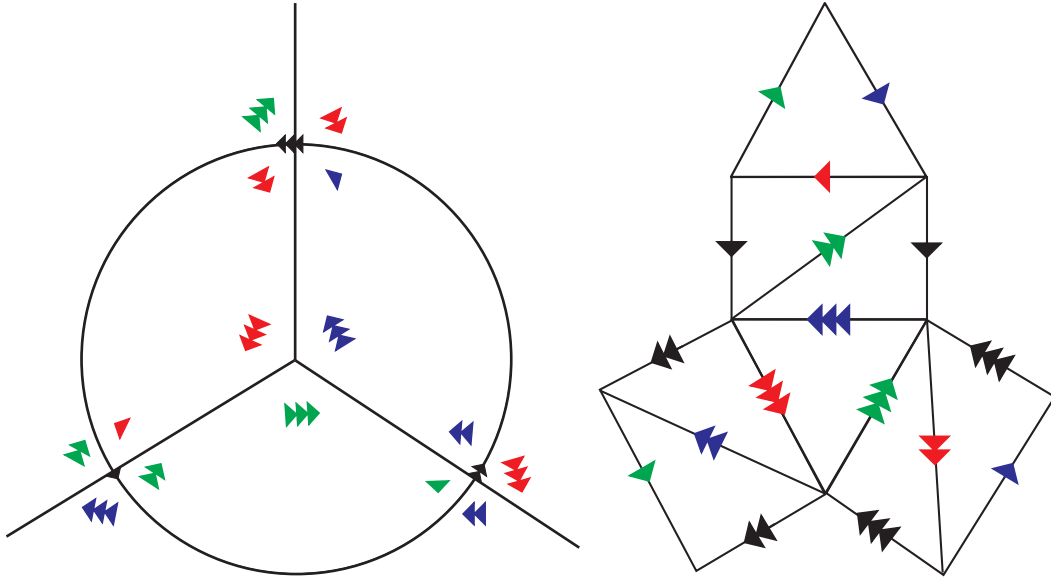


FIGURE 3.16. The gluing pattern for  $\mathcal{M}_1$  and the induced triangulation on the genus 2 boundary surface.

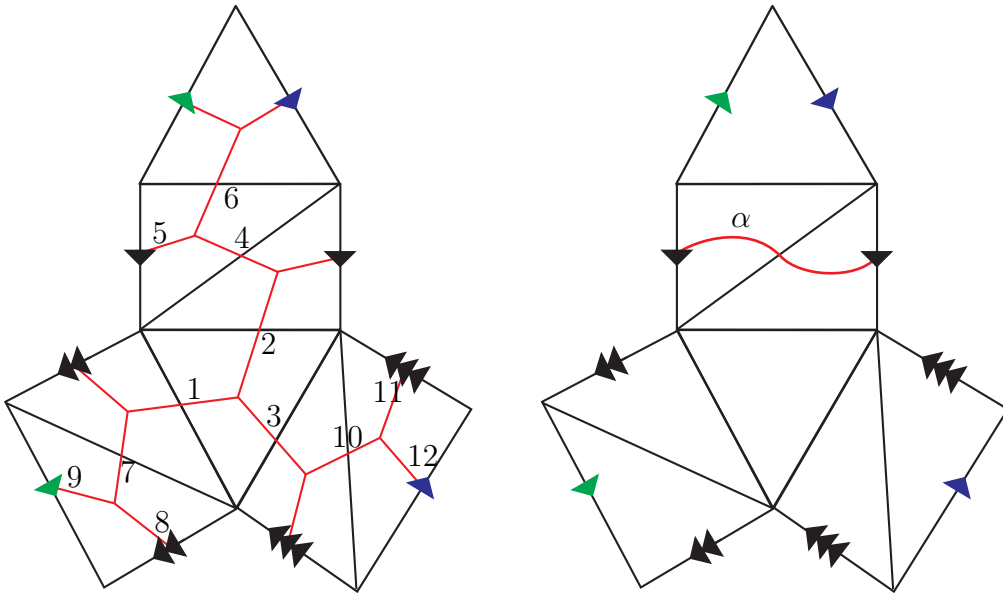


FIGURE 3.17. The curve  $\alpha = (0, 0, 0, 1, 1, 0, 0, 0, 0, 0, 0, 0)$  is one of the three short meridian curves on the boundary.

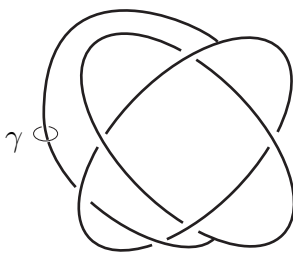


FIGURE 3.18.  $\mathcal{M}_2$  is the complement of  $\mathcal{G}_2$  in  $\mathbb{S}^3$ . Like  $\mathcal{M}_1$ ,  $\mathcal{M}_2$  is a hyperbolic 3-manifold with geodesic boundary.

**3.3.2. Example two.** The second example  $\mathcal{M}_2$  is the complement of the graph  $\mathcal{G}_2$  (illustrated in Figure 3.18) in  $\mathbb{S}^3$ . The geodesic meridian  $\gamma$  has approximate length 3.01274 on  $\partial\mathcal{M}_2$ . The manifold  $\mathcal{M}_2[\gamma]$  is the complement of the  $(2, 4)$  torus link, so it is clear that  $\gamma$  is an exceptional curve which separates  $\partial\mathcal{M}_2$  into two punctured tori  $P_1$  and  $P_2$ . Consequentially, any curve  $\alpha \subset \partial\mathcal{M}_2$  that can be homotoped so that it is contained in either of the  $P_i$  is also exceptional. Hence  $\mathcal{M}_2$  has an infinite number of exceptional curves. The symmetry group  $G_2$  of  $\mathcal{M}_2$  is generated by a rotation of order two,  $\sigma$ , which can be represented by the following permutation on the dual 1-skeleton (Figure 3.20) of  $\partial\mathcal{M}_2$ :

$$\sigma = \begin{pmatrix} 1 & 2 & 3 & 4 & 5 & 6 & 7 & 8 & 9 & 10 & 11 & 12 \\ 1 & 10 & 4 & 3 & 5 & 7 & 6 & 11 & 12 & 2 & 8 & 9 \end{pmatrix}$$

Table 3.2 lists all the exceptional geodesics of length  $\leq c(S_2)$  and whose intersection with  $\gamma$  is essential. The notation used is described in Figures 3.19 and 3.20.

Curve $\alpha$	length( $\alpha$ )	JSJ decomposition
(0,0,0,1,2,1,2,1,1,1,0,1)	6.12168	$\mathbb{T}(2, 3), \mathbb{T}(3, 3), X$
(0,1,1,1,2,1,1,1,0,1,1,0)	6.90358	$\mathbb{T}(2, 3), \mathbb{T}(3, 3), X$
(2,1,1,1,0,1,1,0,1,1,0,1)	6.90358	$m203$
(1,1,0,0,1,1,1,0,1,1,2,1)	7.27655	$\mathbb{T}(2, 4), m009$
(0,1,1,1,2,1,1,0,1,1,0,1)	7.82248	$m295$
(1,1,0,0,1,1,1,1,2,1,1,2)	8.59074	$\mathbb{T}(2, 3), m129$
(2,0,2,2,0,2,2,1,1,0,1,1)	8.8026	$\mathbb{T}(2, 3), T(3, 3), m004$
(2,0,2,1,0,1,2,1,1,1,2,3)	9.7475	$\mathbb{T}(2, 4), m015$
(0,1,1,3,2,1,1,1,0,3,2,1)	9.80376	$\mathbb{T}(2, 4), m032$
(0,1,1,2,2,2,1,2,1,2,1,1)	9.97732	$\mathbb{T}(2, 3), m203$
(2,1,1,1,0,1,1,2,3,1,2,3)	11.4963	$s776$

TABLE 3.2. The list of exceptional curves on  $\partial\mathcal{M}_2$  (up to symmetry) of length  $\leq c(S_2)$  and whose intersection with  $\gamma$  is essential.

$\mathcal{M}_2[(0, 0, 0, 1, 2, 1, 2, 1, 1, 1, 0, 1)]$  and  $\mathcal{M}_2[(0, 1, 1, 1, 2, 1, 1, 1, 0, 1, 1, 0)]$  are distinguished by the homology of their 2-fold covers. The only manifolds on the list that contain essential Klein bottles are  $\mathcal{M}_2[(2, 1, 1, 1, 0, 1, 1, 0, 1, 1, 0, 1)]$  and  $\mathcal{M}_2[(0, 1, 1, 1, 2, 1, 1, 0, 1, 1, 0, 1)]$ . The manifold  $X$  can be obtained by taking a solid torus, drilling out two longitudinal fibers and then performing  $(1, 3)$  and  $(-1, 3)$  Dehn surgery. The remaining JSJ pieces which are not torus links refer to the SnapPea cusped census.

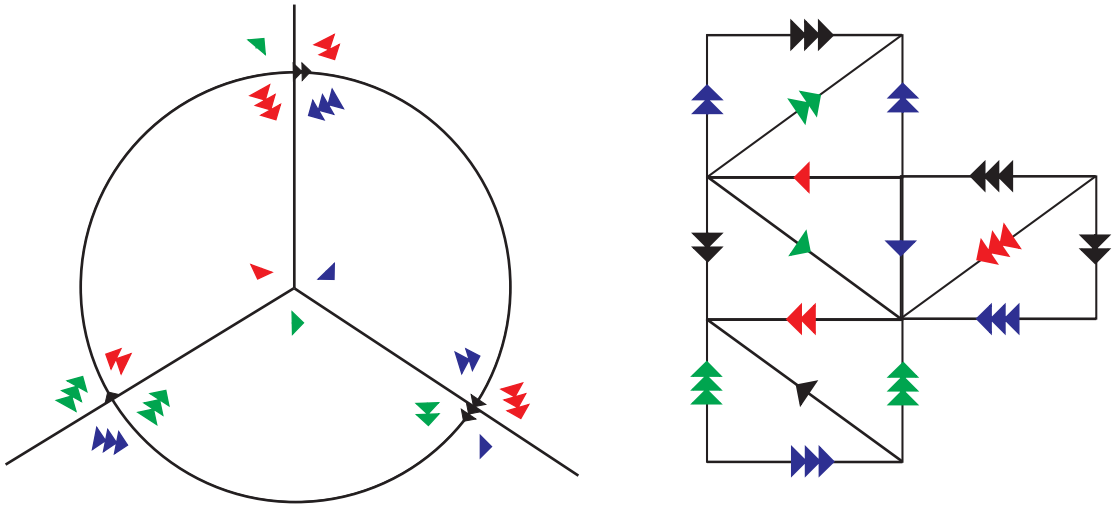


FIGURE 3.19. The gluing pattern for  $\mathcal{M}_2$  and the induced triangulation on the genus 2 boundary surface.

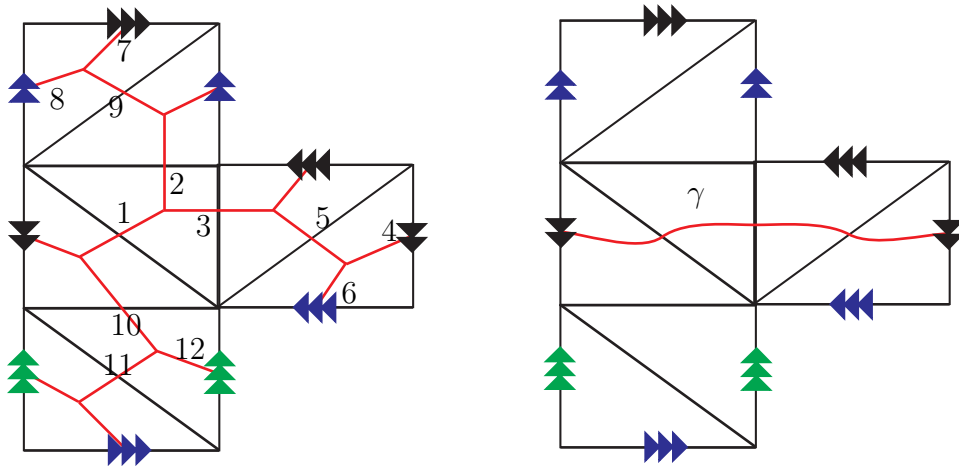


FIGURE 3.20. With the above labelling on the dual 1-skeleton, the curve  $\gamma$  is denoted by  $(1, 0, 1, 1, 1, 1, 0, 0, 0, 0, 0, 0)$ . Any simple closed curve on the boundary that can be homotoped so that it avoids  $\gamma$  is also exceptional since it lies on a punctured torus with boundary  $\gamma$ .

**3.3.3. Geodesic enumeration.** In this section we examine how the simple closed geodesics were enumerated on the boundary of  $\mathcal{M}_1$  and  $\mathcal{M}_2$ . As already mentioned, both these manifolds can be triangulated with two truncated tetrahedra with dihedral angles  $\frac{\pi}{6}$ . This induces a triangulation by eight regular hyperbolic triangles on each of their genus two boundary surfaces. Due to the similarities in these triangulations it is enough to examine the enumeration process on the boundary of  $\mathcal{M}_1$ .

Let  $S$  denote the genus two boundary of  $\mathcal{M}_1$ . Then by lifting the triangulation of  $S$  to its universal cover  $\tilde{S}$  we can produce a tiling of  $\mathbb{H}^2$  by regular hyperbolic triangles with angles  $\frac{\pi}{6}$ . The dual 1-skeleton  $D$  of  $S$  also lifts to  $\mathbb{H}^2$  giving an infinite trivalent graph  $\tilde{D}$  with vertices at the centres of the triangles in the tessellation. Let  $\Delta_c$  be one of the eight triangles on  $S$ , with centre  $c$ . Fix some lift  $\tilde{c}$  of  $c$  in  $\mathbb{H}^2$ .

The following lemma says that if we want to find all closed geodesics of length at most  $c(S_2)$  that pass through  $\Delta_c$ , it is enough to find all the lifts of  $c$  within a certain radius  $r$  of  $\tilde{c}$ .

**Lemma 3.4.** *For any geodesic  $\gamma$  passing through  $\Delta_c$  there exists a unique deck transformation  $d_\gamma$  of  $\tilde{S}$  associated with  $\gamma$ . Under the action of  $d_\gamma$  the point  $\tilde{c}$  is sent to some new vertex  $d_\gamma\tilde{c}$  of  $\tilde{D}$ . If  $\gamma$  is a geodesic of length at most  $l$  then the distance between  $\tilde{c}$  and  $d_\gamma\tilde{c}$  is at most*

$$r = 2\text{ArcCosh}\left(\frac{1 + \sqrt{3}}{3 - \sqrt{3}}\right) + l.$$

PROOF. Let  $\Delta_{\tilde{c}}$  be the triangle in  $\mathbb{H}^2$  containing  $\tilde{c}$  and let  $\Delta_{d_\gamma\tilde{c}}$  be the triangle containing  $d_\gamma\tilde{c}$ . Then since  $\gamma$  passes through  $\Delta_c$  we can lift it to an infinite geodesic  $\tilde{\gamma}$  that passes through  $\Delta_{\tilde{c}}$  and  $\Delta_{d_\gamma\tilde{c}}$ . (See Figure 3.21.) Let  $\rho$  denote the unique

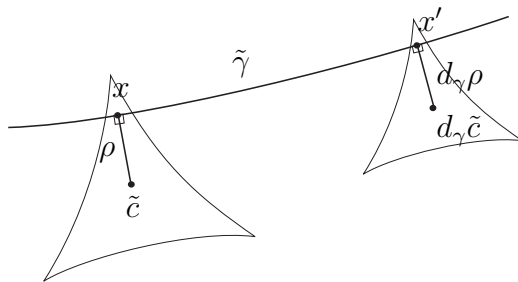


FIGURE 3.21. The set up in  $\mathbb{H}^2$ .

geodesic passing through  $\tilde{c}$  perpendicular to  $\tilde{\gamma}$ . Then by applying  $d_\gamma$  to  $\rho$  we can produce a geodesic segment passing through  $d_\gamma\tilde{c}$  perpendicular to  $\tilde{\gamma}$ . Let  $x$  and  $x'$  denote the points where  $\rho$  and  $d_\gamma\rho$  meet  $\tilde{\gamma}$ .

Now  $\text{length}(\rho) = \text{length}(d_\gamma \rho) \leq m$ , where  $m$  is the radius of the circle that inscribes a regular hyperbolic triangle with angles  $\frac{\pi}{6}$ . Applying the hyperbolic cosine law to the triangle in Figure 3.22,

$$m = \text{ArcCosh} \left( \frac{\cos \frac{2\pi}{3} \cos \frac{\pi}{12} + \cos \frac{\pi}{12}}{\sin \frac{2\pi}{3} \sin \frac{\pi}{12}} \right) = \text{ArcCosh} \left( \frac{1 + \sqrt{3}}{3 - \sqrt{3}} \right).$$

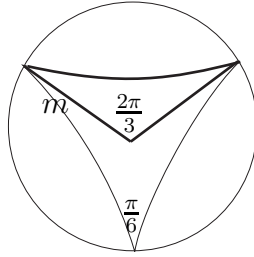


FIGURE 3.22. Calculating  $m$ .

Since the distance between  $x$  and  $x'$  is less than  $l$  we can conclude that the distance between  $\tilde{c}$  and  $d_\gamma \tilde{c}$  is at most  $2m + l$   $\square$

Let  $e_1$ ,  $e_2$  and  $e_3$  be the three edges of  $\tilde{D}$  incident to  $\tilde{c}$ . Then any piecewise geodesic curve in  $\tilde{D}$  starting at  $\tilde{c}$  and ending at a vertex of  $\tilde{D}$  can be represented by a pair  $(e_i, w)$ , where  $w$  is a (possibly empty) word consisting of  $L$ 's and  $R$ 's. The reader should interpret a  $L$  as meaning 'left' and a  $R$  as meaning 'right' e.g.: the pair  $(e_1, L)$  describes the piecewise geodesic path that starts at  $\tilde{c}$  follows  $e_1$  to the next vertex; then turns left and stops at the next vertex. Figure 3.23 illustrates the path  $(e_1, LRR)$ . Let  $v(e_i, w)$  denote the vertex at the end of the path  $(e_i, w)$ .

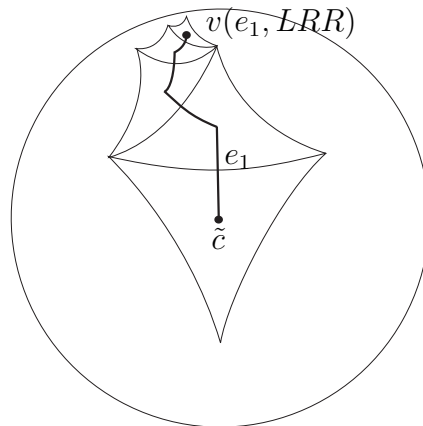


FIGURE 3.23. The piecewise geodesic path  $(e_i, LRR)$  in the Poincaré disc model of  $\mathbb{H}^2$ .

The following lemma says that in searching for lifts of  $c$  we need only follow paths in  $\tilde{D}$  that move away from  $\tilde{c}$ :

**Lemma 3.5.** *Let  $x$  be a vertex of  $\tilde{D}$  with  $x \neq \tilde{c}$ . Then there exists a piecewise geodesic path  $(e_i, w)$  where  $w = a_1 a_2 \cdots a_n$  is a word made up from  $L$ 's and  $R$ 's such that  $x = v(e_i, a_1 a_2 \cdots a_n)$  with the property that*

$$\text{dist}(\tilde{c}, p_{m-1}) < \text{dist}(\tilde{c}, p_m)$$

for  $1 \leq m \leq n$ , where  $p_m = v(e_i, a_1 a_2 \cdots a_m)$ .

**PROOF.** We first claim that one of the vertices of  $\tilde{D}$  neighbouring  $x$  will be closer to  $\tilde{c}$  than  $x$ . The result then follows immediately since we can construct the sequence of points  $p_m$  in reverse by starting at  $x$  and moving towards  $\tilde{c}$ .

Recall that the vertices of  $\tilde{D}$  are the centres of regular hyperbolic triangles in a tessellation. So we know the edges leaving  $x$  are equally spaced with angles of  $\frac{2\pi}{3}$  between them. (See Figure 3.24.)

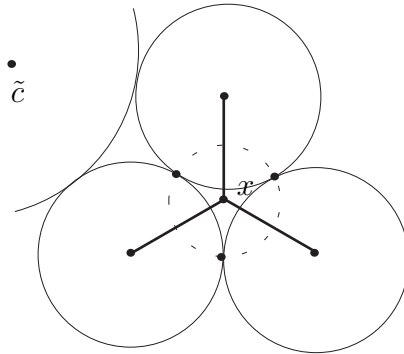


FIGURE 3.24. Expanding balls around the neighbours of  $x$ . The point  $x$  is at the centre of the Poincaré disc model.

Expand three balls  $B_1, B_2, B_3$  of equal radius around each of the vertices neighbouring  $x$  until they bump. These bumping points lie on the boundary of a ball  $B_x$  centered at  $x$ . If we expand a ball centered at  $\tilde{c}$  it is clear it will bump with one of the  $B_i$  ( $i = 1, 2, 3$ ) before  $B_x$ . Our claim immediately follows.  $\square$

Combining Lemmas 3.4 and 3.5 we can now describe an algorithm for enumerating all simple closed geodesic on  $S$  passing through  $\Delta_c$  with length at most  $c(S_2)$ .

We start with the three piecewise geodesic paths

$$\mathcal{L}_0 = \{(e_1, \cdot), (e_2, \cdot), (e_3, \cdot)\},$$

and extend them. We define  $\mathcal{L}_n$  recursively, for  $n \geq 0$  as follows. For each  $(e_i, w) \in \mathcal{L}_n$  consider the extensions  $(e_i, wL)$  and  $(e_i, wR)$ . If

- (1)  $\text{dist}(v(e_i, w), \tilde{c}) < \text{dist}(v(e_i, wL), \tilde{c}) \leq r$ ; and
- (2)  $(e_i, wL)$  projects to a simple normal curve on  $S$  (this may require a slight perturbation of the curve);

then add  $(e_i, wL)$  to  $\mathcal{L}_{n+1}$ . We check condition (2) by tracing the curve out in the surface  $S$  as well as the universal cover. This also allows us to check if the curve can close up on  $S$ . If  $(e_i, wL)$  does close up on  $S$  we add it to our list of simple closed geodesics. We then perform the same checks on  $(e_i, wR)$ .

We repeat the process on  $\mathcal{L}_{n+1}$ . This process will terminate because there are only finitely many vertices of  $\tilde{D}$  within distance  $r$  of  $\tilde{c}$  and at each stage the endpoints of the paths in  $\mathcal{L}_n$  are moving further away from  $\tilde{c}$ . So eventually the list  $\mathcal{L}_n$  will be empty. The output will contain the complete list of geodesics of length at most  $c(S_2)$ , which pass through  $\Delta_c$ . Since we trace out each of the curves in the surface we will also have a normal curve representation for each of the geodesics.

To get the complete list of simple closed geodesics on  $S$  with length at most  $c(S_2)$  we need to repeat the procedure for each of the eight triangles of  $S$ . To limit the amount of repetition, each time we rerun the process we need only collect the curves that do not pass through a ‘base’ triangle we have already used.

**Technical remark:** When we are extending our curves above, there may be more than one way to represent the curve on  $S$  as a normal curve. We need to keep track of all simple normal curve representations to ensure we get the complete list of curves that close up on  $S$ .

Table 3.1 only lists the exceptional geodesics on  $S$  up to symmetries of  $\mathcal{M}_1$ . Repetition was removed in two stages:

- (1) Geodesics with matching normal curve representations were rejected.
- (2) Geodesics whose normal curve representations were equivalent under symmetry were rejected. This is easy to detect as the symmetries of  $\mathcal{M}_1$  just permute normal curve representations.

The lengths of geodesics and JSJ decompositions in Table 3.1 distinguish between the remainder of the geodesics. Table 3.2 was produced in precisely the same way, except 3 duplicate geodesics were removed by hand by explicitly tracing them out on  $S$ .

### 3.4. Remarks on implementation

Ultimately we would like to use the algorithm in Section 3.2 to study how the geometry of the manifold  $M[\alpha]$  depends on the choice of the curve  $\alpha$ . Unfortunately, this algorithm is yet to be implemented in complete generality. The biggest obstacle seems to be arriving at a practical method of representing simple closed curves on boundary surfaces.

The Dehn-Thurston coordinates ([50]) seem to present the most effective method of parametrizing simple closed curves on boundary surfaces. This parametrization has the advantage that any family of disjoint simple closed curves can be represented. So by gluing on multiple 2-handles we could attach entire handlebodies to the boundary.



## CHAPTER 4

### Applications

Much of the theory discussed in this thesis has been implemented in `Orb`. The final chapter displays some applications of this computer program. It is hoped that it proves to be as useful in studying 3-orbifolds as `SnapPea` and `Geo` have been in studying 3-manifolds.

The section that follows examines how `Orb` can be used in the field of spatial graph enumeration. Until now the difficulty has not been the construction of these graphs, but in determining if two graphs are distinct up to ambient isotopy. By treating a spatial graph as the singular set of an orbifold a list of geometric invariants can be associated to any given graph, which can be used to overcome this obstacle.

The chapter concludes by compiling tables of low volume hyperbolic 3-orbifolds obtained by prescribing cone angles along the edges of spatial graphs in  $\mathbb{S}^3$ .

#### 4.1. Knotted $\theta$ -curves

In 1989 Litherland wrote a letter to colleagues ([43]) containing what he hoped was a complete list of all prime  $\theta$ -curves with up to seven crossings. A  $\theta$ -curve is a spatial graph in  $\mathbb{S}^3$  consisting of two vertices and three edges, where each edge joins the two vertices.

A graph is *n-composite* if there exists a 2-sphere meeting the graph in at most  $n$  places dividing it into non-trivial pieces. A graph is *prime* if it is not 3-composite. (See Figure 4.1).

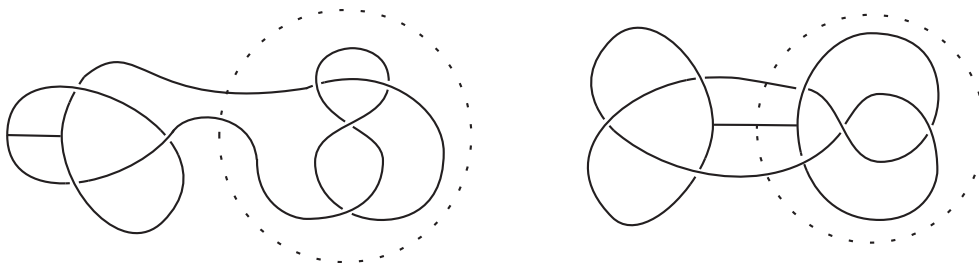


FIGURE 4.1. Two composite graphs.

Moriuchi ([47]) has verified Litherland's list of 90  $\theta$ -curves by using a method of Conway ([14]). While Litherland employed the Alexander polynomial, Moriuchi

used the Yamada polynomial to distinguish between the  $\theta$ -curves. Although these polynomial invariants are easy to define they are both computationally expensive and, in practice, difficult to implement.

More recently, Chiodo, Heard, Hodgson, Saunderson and Sheridan ([15]) have extended Moriuchi's work to enumerate *all* prime spatial graphs with two and four trivalent vertices and up to seven crossings. Rather than using polynomial invariants, graphs were distinguished completely using hyperbolic invariants of 3-orbifolds associated with each spatial graph. This method is illustrated in more detail using Litherland's table.

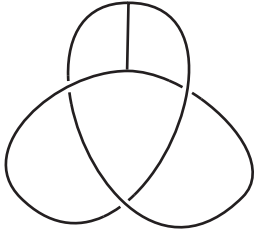
Each  $\theta$ -curve  $\Gamma$  in Litherland's table is depicted along with:

- (1) its symmetry group and reversibility (indicated by an 'r' or a 'n');
- (2) its three constituent knots, obtained by considering any two edges of  $\Gamma$  as a knot;
- (3) the hyperbolic volume of the associated pared manifold  $M_\Gamma = (\mathbb{S}^3, \Gamma)$  where the labels on the edges of  $\Gamma$  are taken to be  $\infty$ .

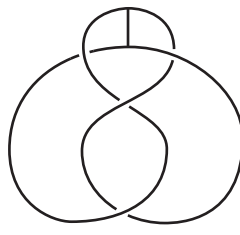
A *symmetry* of an embedded graph in  $\mathbb{S}^3$  gives a homeomorphism of  $\mathbb{S}^3$  that takes the graph to itself. A  $\theta$ -curve  $\Gamma$  is *reversible* if it has a symmetry which fixes its edges but reverses their orientations. Litherland was unable to determine the reversibility of 32 of the  $\theta$ -curves; but this has been resolved by using the canonical cell decompositions of the  $M_\Gamma$  to compute symmetry groups. The volumes of the  $M_\Gamma$  are enough to completely distinguish between graphs in the table.

Symmetry groups of the graphs were found by computing the symmetry groups of the pared manifolds. Any homeomorphism of  $M_\Gamma$  gives a homeomorphism of the complement of  $\Gamma$  sending meridians to meridians. These symmetries can be extended to  $\mathbb{S}^3$  and hence the graph  $\Gamma$ . So the symmetry group of  $M_\Gamma$  is isomorphic to the symmetry group of  $\Gamma$ .

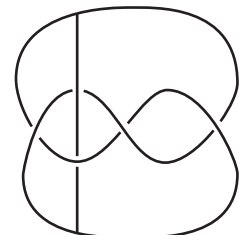
Hyperbolic structures were also used to show that all of Litherland's  $\theta$ -curves are prime. Since  $M_\Gamma$  is hyperbolic for each  $\Gamma$  we can conclude that no  $\theta$ -curve on Litherland's list is 2-composite. If there was a 2-composite graph  $\Gamma$  then the associated  $M_\Gamma$  would contain an essential annulus, which contradicts its hyperbolicity. It was also shown that for each  $\theta$ -curve  $\Gamma$  the orbifold  $Q = (\mathbb{S}^3, \Gamma)$  is hyperbolic, where  $\Gamma$  is labelled 3. This shows that no  $\theta$ -curve is 3-composite; otherwise the associated  $Q$  would contain an essential Euclidean  $\mathbb{S}^2(3, 3, 3)$  suborbifold.



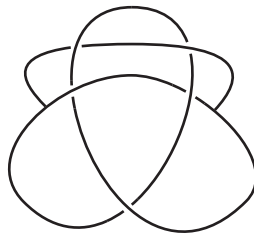
**3<sub>1</sub>**:  $D_2$  r  
 $3_1$   $0_1$   $0_1$   
 5.333489566898



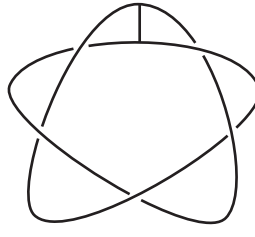
**4<sub>1</sub>**:  $D_2$  r  
 $4_1$   $0_1$   $0_1$   
 7.706911802810



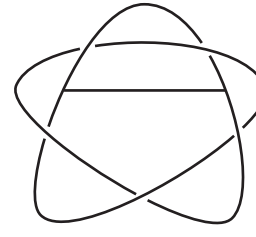
**5<sub>1</sub>**:  $D_3$  n  
 $0_1$   $0_1$   $0_1$   
 10.396867320885



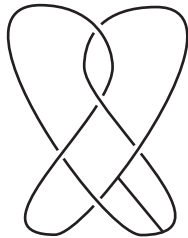
**5<sub>2</sub>**:  $D_2$  r  
 $3_1$   $0_1$   $0_1$   
 8.929317823097



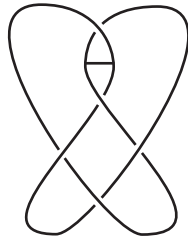
**5<sub>3</sub>**:  $D_2$  r  
 $5_1$   $0_1$   $0_1$   
 6.551743287888



**5<sub>4</sub>**:  $C_2$  r  
 $5_1$   $3_1$   $0_1$   
 8.355502146380



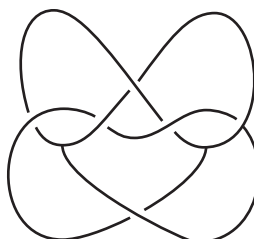
**5<sub>5</sub>**:  $D_2$  r  
 $5_2$   $0_1$   $0_1$   
 8.967360848788



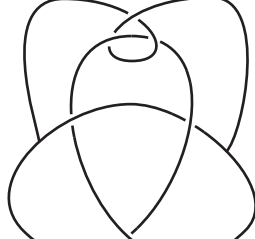
**5<sub>6</sub>**:  $D_2$  r  
 $5_2$   $0_1$   $0_1$   
 8.793345603865



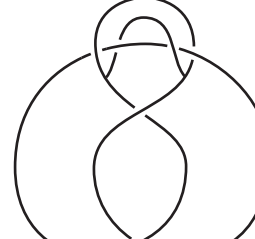
**5<sub>7</sub>**:  $C_2$  r  
 $5_2$   $3_1$   $0_1$   
 9.966511883698



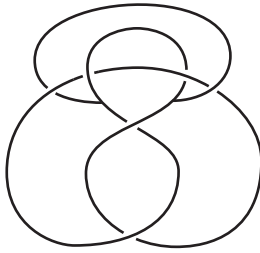
**6<sub>1</sub>**:  $C_2$  n  
 $0_1$   $0_1$   $0_1$   
 11.868927767799



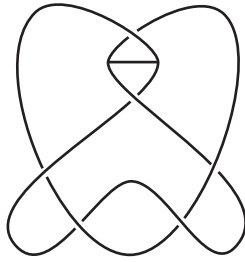
**6<sub>2</sub>**:  $C_2$  r  
 $3_1$   $0_1$   $0_1$   
 12.541436480028



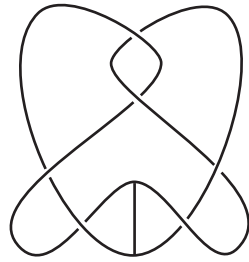
**6<sub>3</sub>**:  $C_2$  r  
 $4_1$   $3_1$   $0_1$   
 12.011086682981



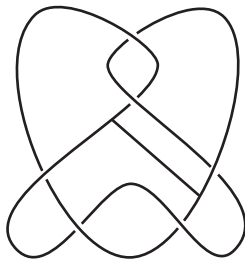
**6<sub>4</sub>**:  $C_2$  r  
 $4_1$   $3_1$   $0_1$   
 10.556866255202



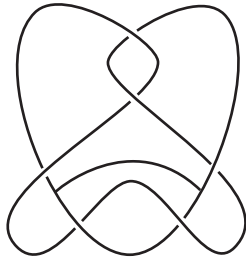
**6<sub>5</sub>**:  $D_2$  r  
 $6_1$   $0_1$   $0_1$   
 9.312341316558



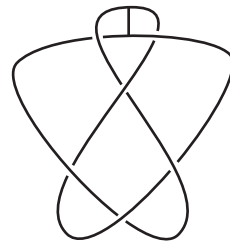
**6<sub>6</sub>**:  $D_2$  r  
 $6_1$   $0_1$   $0_1$   
 9.665346419357



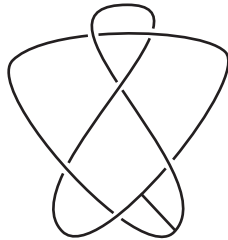
**6<sub>7</sub>**:  $C_2$  n  
 $6_1$   $0_1$   $0_1$   
 11.082166624374



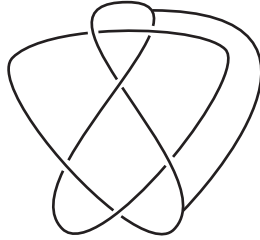
**6<sub>8</sub>**:  $C_2$  r  
 $6_1$   $4_1$   $0_1$   
 11.284602977439



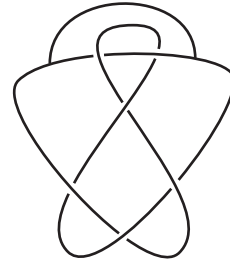
**6<sub>9</sub>**:  $D_2$  r  
 $6_2$   $0_1$   $0_1$   
 10.562806312097



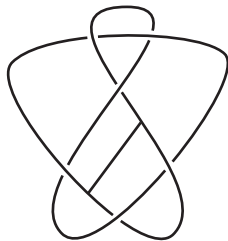
**6<sub>10</sub>**:  $D_2$  r  
 $6_2$   $0_1$   $0_1$   
 10.740257667713



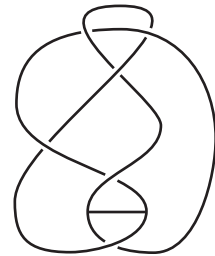
**6<sub>11</sub>**:  $C_1$  n  
 $6_2$   $0_1$   $0_1$   
 12.642324892012



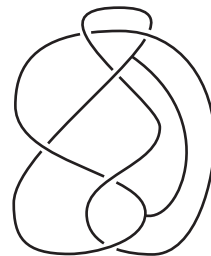
**6<sub>12</sub>**:  $C_2$  r  
 $6_2$   $3_1$   $0_1$   
 11.294969135799



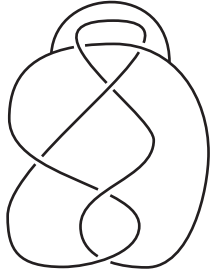
**6<sub>13</sub>**:  $C_2$  r  
 $6_2$   $4_1$   $0_1$   
 12.005951173197



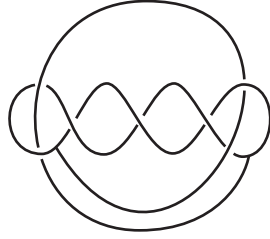
**6<sub>14</sub>**:  $D_2$  r  
 $6_3$   $0_1$   $0_1$   
 11.762234287078



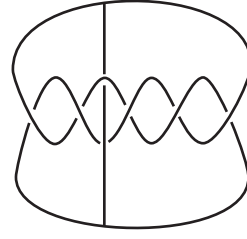
**6<sub>15</sub>**:  $C_1$  n  
 $6_3$   $0_1$   $0_1$   
 13.318458109849



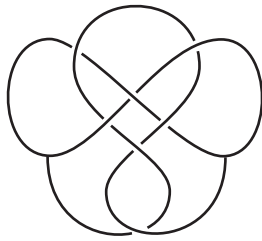
**6<sub>16</sub>**:  $C_2$  r  
 $6_3$   $3_1$   $0_1$   
 12.276562777744



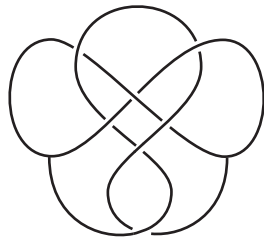
**7<sub>1</sub>**:  $C_2$  n  
 $0_1$   $0_1$   $0_1$   
 13.573971061801



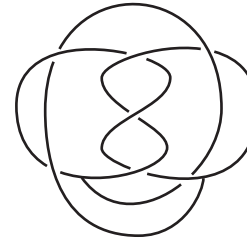
**7<sub>2</sub>**:  $C_2$  n  
 $0_1$   $0_1$   $0_1$   
 14.489285702422



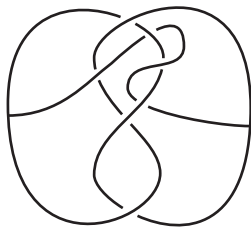
**7<sub>3</sub>**:  $C_2$  n  
 $0_1$   $0_1$   $0_1$   
 14.815103651458



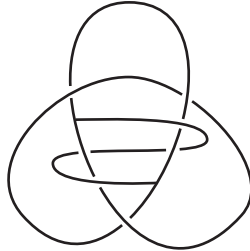
**7<sub>4</sub>**:  $C_2$  n  
 $0_1$   $0_1$   $0_1$   
 15.423672859318



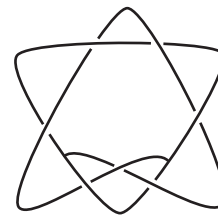
**7<sub>5</sub>**:  $C_2$  n  
 $3_1$   $0_1$   $0_1$   
 12.597206646484



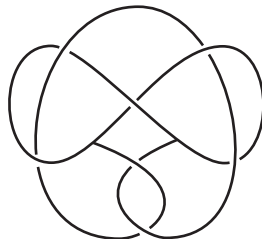
**7<sub>6</sub>**:  $C_2$  r  
 $3_1$   $0_1$   $0_1$   
 13.245997432362



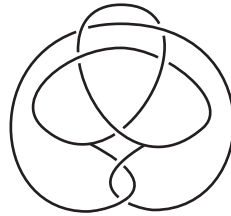
**7<sub>7</sub>**:  $C_2$  n  
 $3_1$   $0_1$   $0_1$   
 12.947638671000



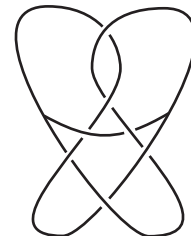
**7<sub>8</sub>**:  $C_2$  r  
 $3_1$   $3_1$   $0_1$   
 10.439255155210



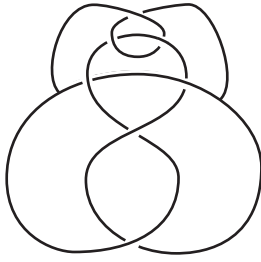
**7<sub>9</sub>**:  $C_2$  n  
 $3_1$   $3_1$   $0_1$   
 14.490908501382



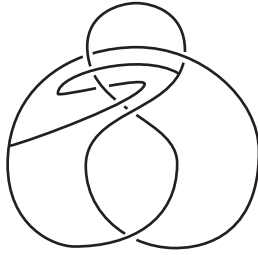
**7<sub>10</sub>**:  $C_2$  r  
 $3_1$   $3_1$   $0_1$   
 14.468602083546



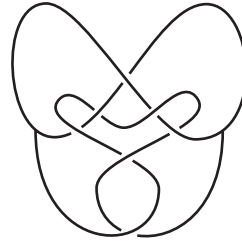
**7<sub>11</sub>**:  $C_2$  n  
 $4_1$   $0_1$   $0_1$   
 12.904404738301



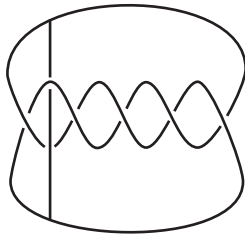
**7<sub>12</sub>**:  $C_2$  r  
 $4_1$   $0_1$   $0_1$   
 15.357601981467



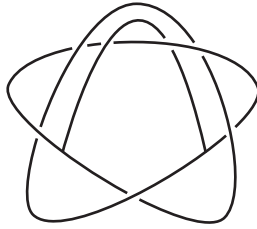
**7<sub>13</sub>**:  $C_1$  n  
 $4_1$   $0_1$   $0_1$   
 13.701755893889



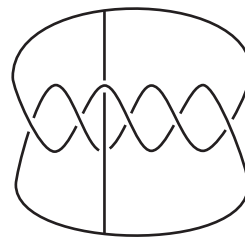
**7<sub>14</sub>**:  $C_2$  n  
 $4_1$   $4_1$   $0_1$   
 14.616810435892



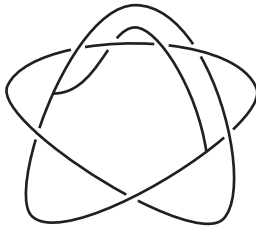
**7<sub>15</sub>**:  $C_2$  n  
 $5_1$   $0_1$   $0_1$   
 12.214804374290



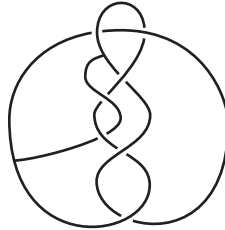
**7<sub>16</sub>**:  $C_2$  r  
 $5_1$   $0_1$   $0_1$   
 10.947325448997



**7<sub>17</sub>**:  $D_2$  r  
 $5_1$   $0_1$   $0_1$   
 13.492084244588



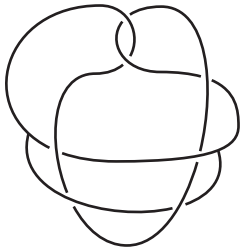
**7<sub>18</sub>**:  $C_1$  n  
 $5_1$   $5_2$   $0_1$   
 12.216314783920



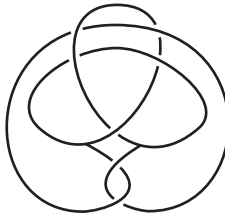
**7<sub>19</sub>**:  $C_1$  n  
 $5_2$   $0_1$   $0_1$   
 14.551772135375



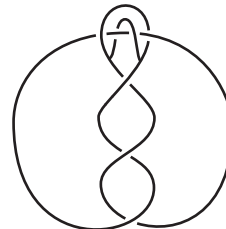
**7<sub>20</sub>**:  $C_2$  n  
 $5_2$   $0_1$   $0_1$   
 11.393881778213



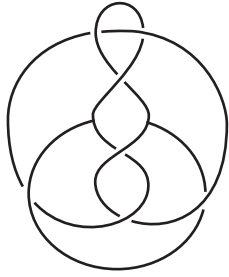
**7<sub>21</sub>**:  $C_2$  r  
 $5_2$   $0_1$   $0_1$   
 13.209738771206



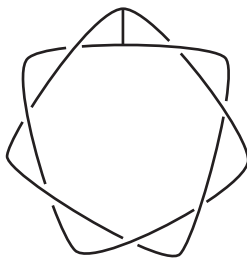
**7<sub>22</sub>**:  $C_2$  r  
 $5_2$   $3_1$   $0_1$   
 13.443117140749



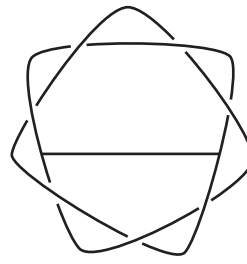
**7<sub>23</sub>**:  $C_2$  r  
 $5_2$   $4_1$   $0_1$   
 13.439519474221



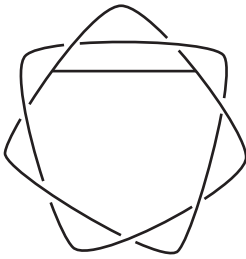
**724:**  $C_2$  r  
 $5_2$   $4_1$   $0_1$   
 12.732652137455



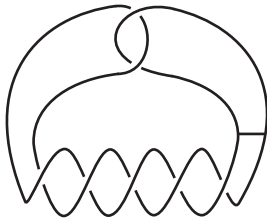
**725:**  $D_2$  r  
 $7_1$   $0_1$   $0_1$   
 6.927377112306



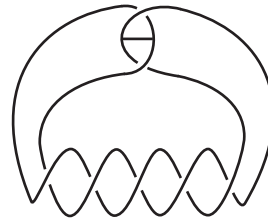
**726:**  $C_2$  r  
 $7_1$   $3_1$   $0_1$   
 10.225901957780



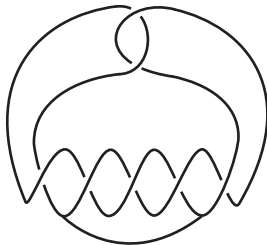
**727:**  $C_2$  r  
 $7_1$   $5_1$   $0_1$   
 9.272866191653



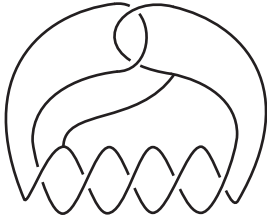
**728:**  $D_2$  r  
 $7_2$   $0_1$   $0_1$   
 10.070078535424



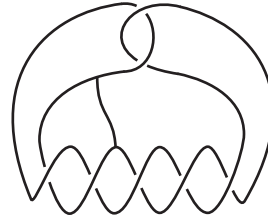
**729:**  $D_2$  r  
 $7_2$   $0_1$   $0_1$   
 9.585859493954



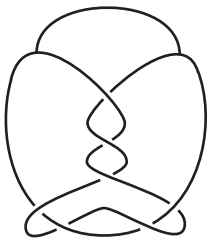
**730:**  $C_2$  n  
 $7_2$   $0_1$   $0_1$   
 12.490066019901



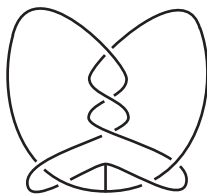
**731:**  $C_2$  r  
 $7_2$   $3_1$   $0_1$   
 11.679957517516



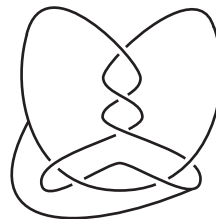
**732:**  $C_2$  r  
 $7_2$   $5_2$   $0_1$   
 12.074061339622



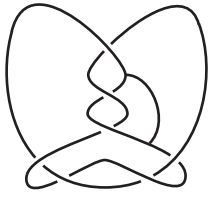
**733:**  $D_2$  r  
 $7_3$   $0_1$   $0_1$   
 10.847925015932



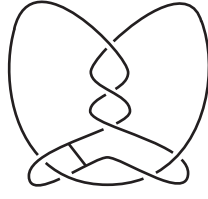
**734:**  $D_2$  r  
 $7_3$   $0_1$   $0_1$   
 11.079643110813



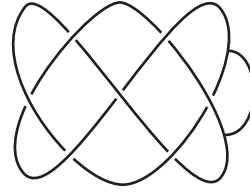
**735:**  $C_2$  r  
 $7_3$   $3_1$   $0_1$   
 12.370018761958



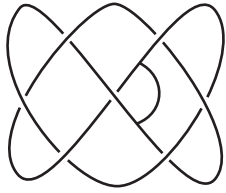
**736:**  $C_2$  r  
 $7_3$   $5_1$   $0_1$   
 11.817414810890



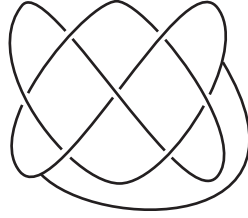
**737:**  $C_2$  r  
 $7_3$   $5_2$   $0_1$   
 12.624442757289



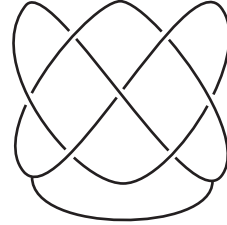
**738:**  $D_2$  r  
 $7_4$   $0_1$   $0_1$   
 11.571896813191



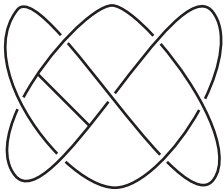
**739:**  $D_2$  r  
 $7_4$   $0_1$   $0_1$   
 12.479708871748



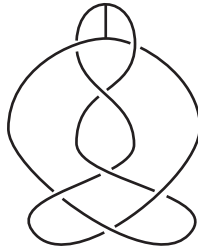
**740:**  $C_2$  r  
 $7_4$   $3_1$   $0_1$   
 14.398985619298



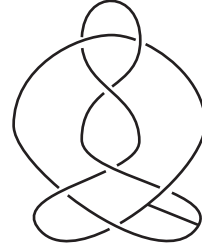
**741:**  $C_2$  r  
 $7_4$   $3_1$   $0_1$   
 14.114056597217



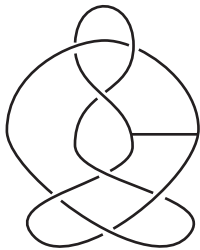
**742:**  $C_2$  r  
 $7_4$   $5_2$   $0_1$   
 12.962466708422



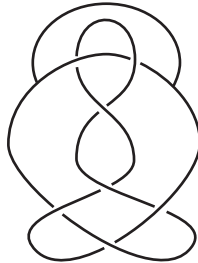
**743:**  $D_2$  r  
 $7_5$   $0_1$   $0_1$   
 12.551759219670



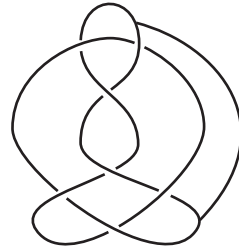
**744:**  $D_2$  r  
 $7_5$   $0_1$   $0_1$   
 12.721765197316



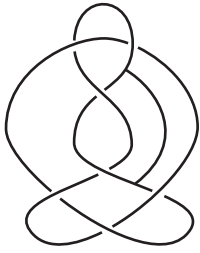
**745:**  $C_2$  r  
 $7_5$   $3_1$   $0_1$   
 13.550005663255



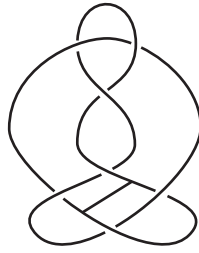
**746:**  $C_2$  r  
 $7_5$   $3_1$   $0_1$   
 13.027986690924



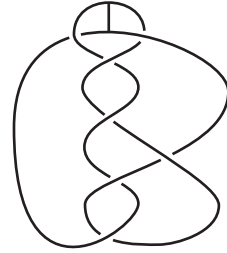
**747:**  $C_1$  n  
 $7_5$   $3_1$   $0_1$   
 14.546958401303



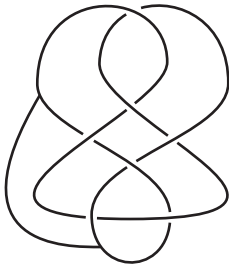
**748:**  $C_1$  n  
 $7_5$   $5_1$   $0_1$   
 14.217006654939



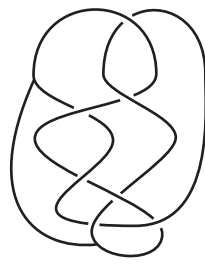
**749:**  $C_2$  r  
 $7_5$   $5_2$   $0_1$   
 13.810713428216



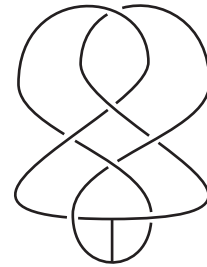
**750:**  $D_2$  r  
 $7_6$   $0_1$   $0_1$   
 13.206174565976



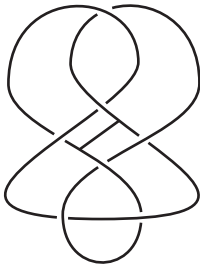
**751:**  $C_1$  n  
 $7_6$   $0_1$   $0_1$   
 15.301776517492



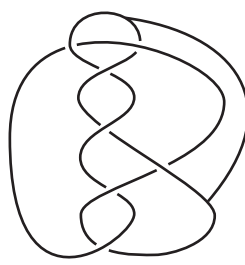
**752:**  $C_1$  n  
 $7_6$   $0_1$   $0_1$   
 15.408564394952



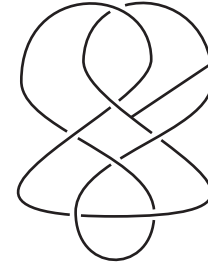
**753:**  $D_2$  r  
 $7_6$   $0_1$   $0_1$   
 13.250639587594



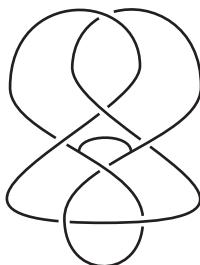
**754:**  $C_2$  n  
 $7_6$   $0_1$   $0_1$   
 14.490092485423



**755:**  $C_1$  n  
 $7_6$   $3_1$   $0_1$   
 14.873424607035



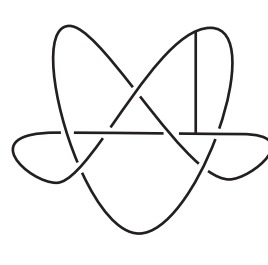
**756:**  $C_2$  r  
 $7_6$   $3_1$   $0_1$   
 13.640388911026



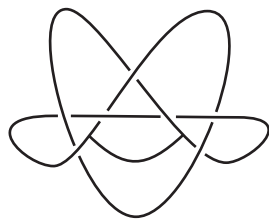
**757:**  $C_2$  r  
 $7_6$   $4_1$   $0_1$   
 13.955866986152



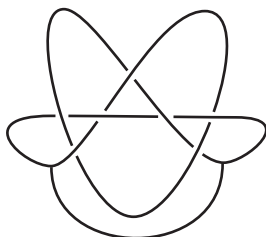
**758:**  $C_1$  n  
 $7_6$   $5_2$   $0_1$   
 14.967937204950



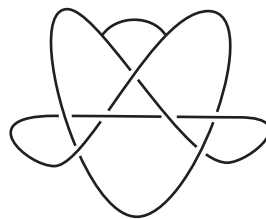
**759:**  $D_2$  r  
 $7_7$   $0_1$   $0_1$   
 13.775530476259



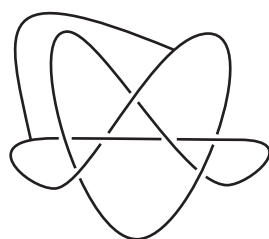
**760:**  $C_2$  r  
 $7_7$   $0_1$   $0_1$   
 15.727779400243



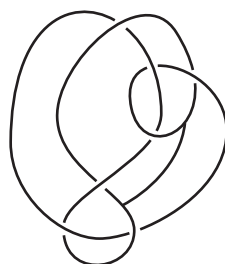
**761:**  $C_2$  r  
 $7_7$   $0_1$   $0_1$   
 16.056229296107



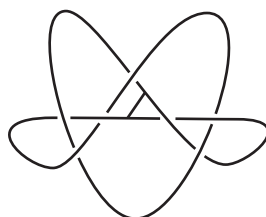
**762:**  $D_2$  r  
 $7_7$   $0_1$   $0_1$   
 14.323760017556



**763:**  $C_1$  n  
 $7_7$   $0_1$   $0_1$   
 15.606332837243



**764:**  $C_2$  r  
 $7_7$   $3_1$   $0_1$   
 15.569549316021



**765:**  $C_2$  r  
 $7_7$   $4_1$   $0_1$   
 14.390331965426

**4.2. Low volume hyperbolic 3-orbifolds**

Like the volumes of hyperbolic 3-manifolds, the volumes of hyperbolic 3-orbifolds form a well-ordered nondiscrete subset of  $\mathbb{R}$  of order type  $\omega^\omega$ , and each volume is realized by only finitely many orbifolds (Dunbar, Meyerhoff [18]).

The smallest known orientable hyperbolic 3-orbifold  $\mathcal{Q}_1$  has approximate volume 0.039050285615 (see Figure 4.2). Chinburg and Friedman ([13]) have shown that  $\mathcal{Q}_1$  is the smallest arithmetic orientable hyperbolic 3-orbifold. Gehring, Marshall and Martin have recently announced a proof that  $\mathcal{Q}_1$  is the smallest orientable hyperbolic 3-orbifold, but details have yet to be written down. (See also [26].) Meyerhoff ([45]) has proven that smallest cusped orientable hyperbolic 3-orbifold is a tetrahedral orbifold with approximate volume 0.084578467201.

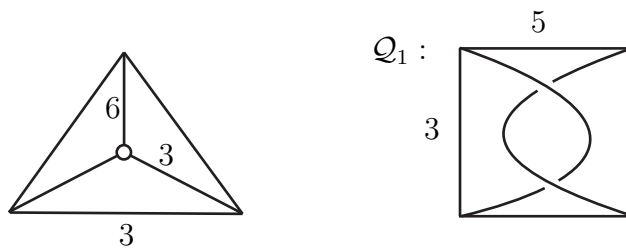


FIGURE 4.2. The smallest cusped orientable hyperbolic 3-orbifold and the smallest known orientable hyperbolic 3-orbifold  $\mathcal{Q}_1$  have the above singular sets and underlying space  $\mathbb{S}^3$ . All edges are labelled 2 unless otherwise indicated.

The three smallest orientable hyperbolic 3-orbifolds with nonrigid cusps were found by Adams (see [1] and refer to Figure 4.3). The smallest of these ( $\mathcal{A}_1$  below) has approximate volume 0.305321865 and consequently is the smallest limit volume.

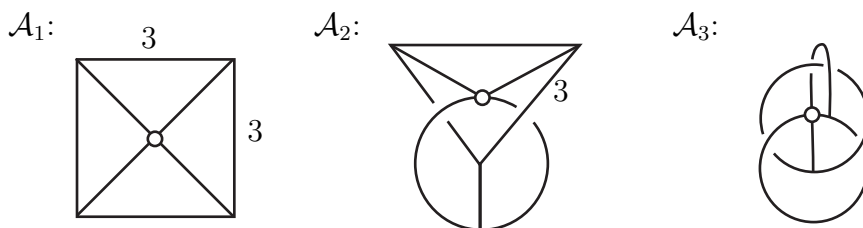


FIGURE 4.3. The three smallest orientable hyperbolic 3-orbifolds with nonrigid cusps have the above singular sets and underlying space  $\mathbb{S}^3$ . Found by Adams, their volumes are approximately 0.305322, 0.444457 and 0.457982. All edges are labelled 2 unless otherwise indicated.

SnapPea has given some insight into this set of volumes by allowing the computation of volumes of hyperbolic 3-orbifolds with links as the singular loci. However,

`SnapPea` cannot directly handle orbifolds with more complicated singular sets. Until now volumes have generally been computed by using `SnapPea` to study suitable orbifold covers (e.g. Vesin, Mednykh, Zimmerman, [68], Zimmerman [73]). `Orb` is designed to overcome this shortfall and should prove invaluable in the future study of hyperbolic 3-orbifolds.

To illustrate this, we conclude with a brief survey of the 3-orbifolds with underlying space  $\mathbb{S}^3$  and whose singular set is a connected, prime, two or four vertex trivalent spatial graph whose projection has up to seven crossings.

The graphs were enumerated by a process based on the method of Conway. First *basic prime polyhedra* with vertices of degree 3 and 4 were enumerated using the computer program `plantri` by McKay and Brinkmann ([11]). Vertices of degree 4 were then replaced by *algebraic tangles* ([14]) to produce projections of knotted graphs. The notation used to describe a basic prime polyhedron  $P$  is  $N_4^n$  where  $N$  is the number of degree 4 vertices and  $n$  is the number of degree 3 vertices in  $P$ .

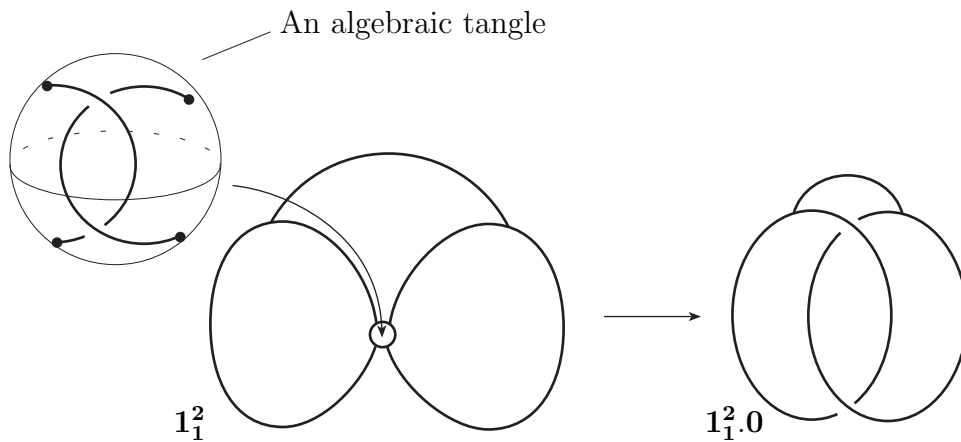


FIGURE 4.4. First we enumerate basic prime polyhedra with vertices of degree 3 and 4. Then we replace vertices of degree 4 by algebraic tangles to produce a knotted graph. The polyhedron information is encoded into the names of the projections of each graph. In this example an algebraic tangle is inserted into polyhedron  $1_1^2$  producing the projection  $1_1^2.0$ .

Repeated projections are removed using an idea from `plantri` to give a canonical description of each projection (up to homeomorphism of  $\mathbb{S}^2$ ). Finally, `Orb` was used to compute hyperbolic invariants such as the volumes of associated orbifolds and Kojima's canonical decomposition. These invariants showed that the remaining knotted graphs are distinct. The full details of how the graphs were enumerated will appear in [15] which is currently in preparation.

The orbifolds in Table 4.1 were produced by considering all *connected* two vertex graphs in [15] as the singular set of orbifolds with underlying space  $\mathbb{S}^3$ . The edge

labels on the graphs were varied from 2 to 6 and all orbifolds with volume less than 0.5 were noted. The singular sets of the orbifolds are illustrated in Table 4.2 where the colourings match the labelling in Table 4.1.

The orbifolds in Table 4.3 were produced by considering the first 21 connected, prime, four vertex graphs in [15] as singular sets. The edge labels on the graphs were varied from 2 to 6 and all orbifolds with volume less than 0.2 were noted. The singular sets of the orbifolds are illustrated in Table 4.4 where the colourings match the labelling in Table 4.3.

There are several orbifolds worth noting:

- $6_5^2.7(2, 2, 2)$  is the smallest known 3-orbifold with the entire singular set labelled 2.
- $1_1^4.1(3, 5, 2, 2, 2, 2)$  is the smallest known hyperbolic 3-orbifold;
- $0_1^4.1(2, 2, 6, 3, 2, 3)$  is the smallest volume cusped hyperbolic 3-orbifold ([45]).

The first fourteen orbifolds in Table 4.3 agree with those listed in a paper by Zimmerman ([73]) but this is the first time their volumes have been computed to such accuracy. From this point on, new low volume orbifolds begin to emerge.

**Question:** In practice, ‘bad’ triangulations seem to be the greatest obstruction to finding a hyperbolic structure and at times some retriangulation is necessary. Is there an efficient way to search for ‘nice’ triangulations?

### 4.3. Future applications

There are many avenues for continuing the research produced in this thesis. An obvious useful addition to the algorithm outlined in Chapter 2 would be Dehn filling. Dehn filling would enable the study of orbifolds with underlying spaces other than  $\mathbb{S}^3$ . The 2-handle addition algorithm in Chapter 3 could be implemented, but ultimately a method for continuously deforming hyperbolic structures like that present in `SnapPea` is more desirable. Orbifold Dehn filling also presents an extremely effective method for deforming hyperbolic structures.

In the short term, more time needs to be spent analyzing the orbifolds in the previous section. The fact that we can now find hyperbolic structures on these objects is really just the beginning. This presents us with access to new information like Dirichlet domains, symmetry groups and length spectra. Matrix generators can be calculated and fed into the computer program `Snap` [27] by Goodman to find exact representations and arithmetic invariants. All this should assist us greatly in developing our understanding of hyperbolic 3-orbifolds.

$\Gamma$		Volume	$\Gamma$		Volume
$6_5^2.7$	2 2 2	0.117838420347	$1_1^2.1$	3 2 4	0.274956314143
$1_1^2.1$	4 2 3	0.132387219941	$1_1^2.0$	4 2 3	0.305321864725
$1_1^2.20$	2 3 2	0.132387219941	$1_1^2.25$	2 2 3	0.327122942964†
$1_1^2.70$	2 3 2	0.157117893796	$1_1^2.3$	3 2 3	0.338313868803
$1_1^2.10$	2 3 2	0.157117893796†	$1_1^2.1$	5 2 3	0.362887228283
$6_5^2.6$	2 2 2	0.157963654832	$6_5^2.4$	2 2 2	0.406613506058
$1_1^2.4$	3 2 3	0.205686016390†	$4_1^2.111$	2 2 2	0.439281507297†
$7_5^2.1$	2 2 2	0.235676840694	$1_1^2.19$	3 2 3	0.446892793603†
$5_1^2.5$	2 2 2	0.245342207223†	$5_1^2.8$	2 2 2	0.456086080550†
$5_1^2.44$	2 2 2	0.253735401602	$1_1^2.3$	2 4 2	0.457982797088
$1_1^2.8$	2 4 2	0.253735401602	$7_8^2.1$	2 2 3	0.461756942682
$1_1^2.8$	3 3 2	0.254944838148	$1_1^2.8$	2 5 2	0.468603427380
$1_1^2.1$	2 3 3	0.264774439883	$1_1^2.4$	4 2 3	0.492361631010†

† Solution found contained negatively oriented tetrahedra.

TABLE 4.1. The orbifolds of the type  $Q = (\mathbb{S}^3, \Gamma)$  found with  $\text{vol}(Q) < 0.5$ , where  $\Gamma$  is a connected, prime, trivalent two vertex graph with at most 7 crossings.

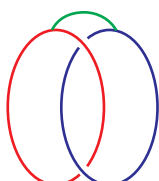
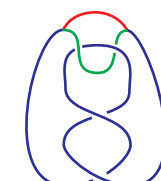
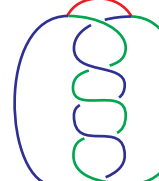
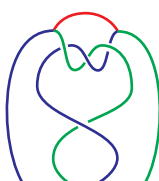
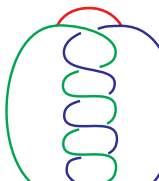
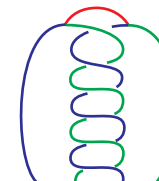
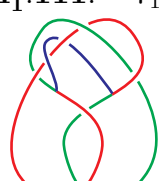
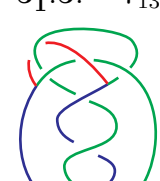
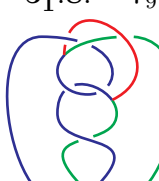
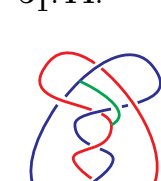
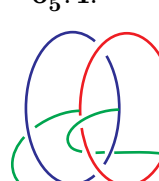
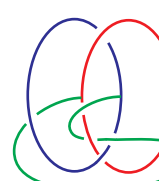
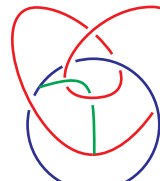
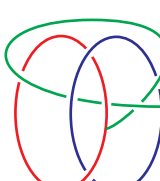
$1_1^2.0:$ —	$1_1^2.1:$ $3_1$	$1_1^2.3:$ —	$1_1^2.4:$ $4_1$	$1_1^2.8:$ $5_3$
				
3.663862	5.333490	6.138139	7.706912	6.551743
$1_1^2.10:$ $5_6$	$1_1^2.19:$ $5_7$	$1_1^2.20:$ —	$1_1^2.25:$ $6_5$	$1_1^2.70:$ $7_{25}$
				
8.793346	9.966512	6.784756	9.312341	6.927377
$4_1^2.111:$ $7_{19}$	$5_1^2.5:$ $7_{13}$	$5_1^2.8:$ $7_9$	$5_1^2.44:$ —	$6_5^2.4:$ —
				
14.551772	13.701756	14.490909	12.496170	13.505377
$6_5^2.6:$ —	$6_5^2.7:$ —	$7_8^2.1:$ —	$7_8^2.1:$ —	
				
12.279280	11.603186	10.658691	8.140719	

TABLE 4.2. Some simple, prime, trivalent two vertex graphs whose projection contains at most 7 crossings. Hyperbolic volumes of the associated pared manifolds are listed along with Litherland's notation where relevant.

$\Gamma$		Volume	$\Gamma$		Volume
$1_1^4.1$	3 5 2 2 2 2	0.039050285615	$1_1^4.2$	2 2 3 3 2 2	0.132387219941
$1_1^4.4$	3 2 2 2 2 3	0.040890367870†	$1_1^4.2$	2 2 2 2 4 3	0.137478157071
$1_1^4.3$	3 3 2 2 2 2	0.052654551610	$0_1^4.1$	5 3 2 3 2 2	0.143540253357
$3_2^4.5$	2 3 2 2 2 2	0.065965277526	$1_1^4.6$	2 2 2 3 2 3	0.149237805232
$1_1^4.2$	2 4 2 2 3 2	0.066193609970	$1_1^4.5$	3 3 2 2 2 2	0.150362044240
$0_1^4.1$	2 4 2 3 5 2	0.071770126678	$0_1^4.1$	4 4 2 2 3 2	0.152660932362
$0_1^4.1$	2 3 5 2 3 2	0.078100571230	$1_1^4.4$	3 2 2 2 2 4	0.165428734328†
$4_2^4.2$	2 2 3 2 2 2	0.078558946898	$1_1^4.1$	3 2 2 2 2 6	0.169156934401
$1_1^4.1$	3 2 2 2 3 3	0.081780735741	$0_1^4.1$	3 2 2 3 3 3	0.169156934401
$0_1^4.1$	2 2 6 3 2 3	0.084578467201	$0_1^4.1$	4 3 2 2 3 3	0.171540364016
$1_1^4.1$	2 3 3 2 2 4	0.085770182008	$1_1^4.7$	3 2 2 2 2 3	0.180420812849
$1_1^4.1$	2 2 2 5 2 3	0.093325539506	$1_1^4.2$	2 5 2 3 2 2	0.181443614141
$3_2^4.6$	3 2 3 2 2 2	0.102843008195	$0_1^4.1$	5 2 3 2 2 5	0.186651079013
$1_1^4.2$	2 3 3 2 2 3	0.105309103221	$1_1^4.84$	2 3 2 2 3 2	0.192773545469
$2_1^4.9$	4 2 2 2 2 2	0.126867700801	$2_1^4.37$	3 2 2 2 2 2	0.196397367245
$2_1^4.9$	3 2 2 2 2 3	0.127472419074	$3_2^4.5$	2 2 2 2 4 2	0.198580829912†

† Solution found contained negatively oriented tetrahedra.

TABLE 4.3. The orbifolds of the type  $Q = (\mathbb{S}^3, \Gamma)$  found with  $\text{vol}(Q) < 0.2$ , where  $\Gamma$  is a connected, prime, trivalent four vertex graph with at most 7 crossings.

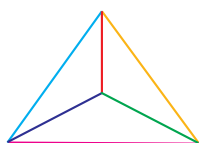
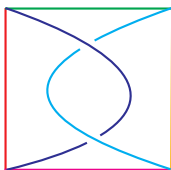
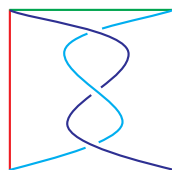
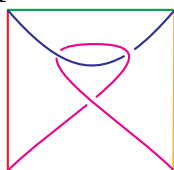
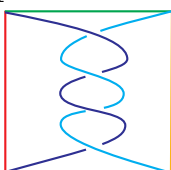
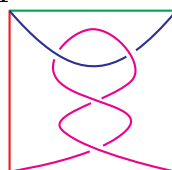
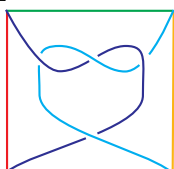
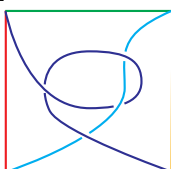
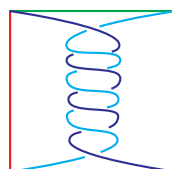
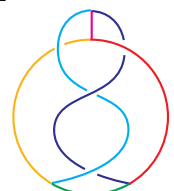
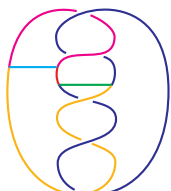
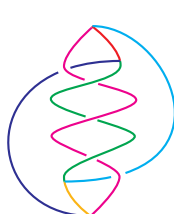
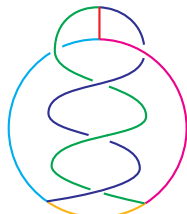
$0_1^4.1$ : 7.327725 $1_1^4.1$ : 10.149416 $1_1^4.2$ : 11.751836 $1_1^4.3$ : 12.844853 $1_1^4.4$ : 12.709173 $1_1^4.5$ : 14.603061 $1_1^4.6$ : 14.135593 $1_1^4.7$ : 15.088873 $1_1^4.84$ : 13.905701 $2_1^4.9$ : 13.939686 $2_1^4.37$ : 15.204650 $3_2^4.5$ : 14.262930 $3_2^4.6$ : 13.294406 $4_2^4.2$ : 15.189754

TABLE 4.4. Some simple, prime, trivalent four vertex graphs whose projection contains at most 7 crossings. The hyperbolic volumes of the associated pared manifolds are also listed.



## Bibliography

- [1] C. Adams, *Limit volumes of hyperbolic 3-orbifolds*, J. Differential Geom. 34 (1991), no. 1, 115–141.
- [2] C. Adams, M. Hildebrand, J. Weeks, *Hyperbolic invariants of knots and links*. Trans. Amer. Math. Soc. 326 (1991), no. 1, 1–56.
- [3] I. Agol, *Bounds on exceptional Dehn filling*, Geom. Topol. 4 (2000), 431–449.
- [4] A. Basmajian, *Tubular neighbourhoods of totally geodesic hypersurfaces in hyperbolic manifolds*, Invent. Math. 117 (1994) 207–225.
- [5] R. Benedetti, C. Petronio, “Lectures in Hyperbolic Geometry”, Universitext, Springer-Verlag Berlin, 1992.
- [6] S. Bleiler, C. Hodgson, *Spherical space forms and Dehn filling*, Topology 35 (1996), 809–833.
- [7] M. Boileau, J. Porti, *Geometrization of 3-orbifolds of cyclic type*, Appendix A by Michael Heusener and Porti. Astérisque No. 272, (2001).
- [8] M. Boileau, S. Maillot, J. Porti, *Three-dimensional orbifolds and their geometric structures*, Panoramas et Synthèses [Panoramas and Syntheses], 15. Société Mathématique de France, Paris, 2003.
- [9] F. Bonahon, L. Siebenmann, *The characteristic toric splitting of irreducible compact three-orbifolds*, Math. Ann. 278 (1987), 441–479.
- [10] F. Bonahon, L. Siebenmann, *The classification of Seifert fibered three-manifolds*, Low Dimensional Topology (R. Fenn, ed.), London Math. Soc. Lecture Notes Ser., vol. 95, Cambridge Univ. Press, Cambridge, 1985, pp. 19–85.
- [11] G. Brinkmann, B. McKay, **plantri**, a computer program for generating planar graphs. Available at <http://cs.anu.edu.au/~bdm/plantri/>.
- [12] A. Casson, **Geo**, the computer program. Available at <http://computop.org>.
- [13] T. Chinburg, E. Friedman, *The smallest arithmetic hyperbolic three-orbifold*, Invent. Math. 86 (1986), no. 3, 507–527.
- [14] J. Conway, *An enumeration of knots and links, and some of their algebraic properties*, in: Computational Problems in Abstract Algebra (Proc. Conf., Oxford, 1967), 329–358, Pergamon, Oxford, 1970.
- [15] M. Chiodo, D. Heard, C. Hodgson, J. Saunderson, N. Sheridan, *Enumeration of knotted graphs using hyperbolic invariants*, in preparation.
- [16] D. Cooper, C. Hodgson, S. Kerckhoff, *Three dimensional Orbifolds and Cone Manifolds*, Mathematical Society of Japan Memoirs 5 (2000).
- [17] H. Coxeter, “Non-Euclidean Geometry”, 6th ed. Washington, DC: Math. Assoc. Amer., 1988.
- [18] W. Dunbar, G. Meyerhoff, *Volumes of hyperbolic 3-orbifolds*, Indiana Univ. Math. J. 43 (1994), no. 2, 611–637.
- [19] D. Epstein, R. Penner, *Euclidean decompositions of noncompact hyperbolic manifolds*, J. Differential Geom. 27 (1988) 67–80.

- [20] E. Flapan, *When topology meets chemistry*, Cambridge University Press, Cambridge, 2000.
- [21] R. Frigerio, B. Martelli, C. Petronio, *ographs*, a computer program for computing structures on hyperbolic 3-manifolds with geodesic boundary, available from <http://www.dm.unipi.it/pages/petronio/public.html/progs.html>.
- [22] R. Frigerio, B. Martelli, C. Petronio, *Small hyperbolic 3-manifolds with geodesic boundary*, Experiment. Math. 13 (2004), no. 2, 171–184.
- [23] R. Frigerio, C. Petronio, *Construction and recognition of hyperbolic 3-manifolds with geodesic boundary*, Trans. Amer. Math. Soc., 356 (2004), 3243–3282.
- [24] M. Fujii, *Hyperbolic 3-manifolds with totally geodesic boundary*, Osaka J. Math. 27 (1990), 539–553.
- [25] M. Fujii, *Hyperbolic 3-manifolds with totally geodesic boundary which are decomposed into hyperbolic truncated tetrahedra*, Tokyo J. Math. 13 (1990), 353–373.
- [26] F. Gehring, G. Martin, *On the minimal volume hyperbolic 3-orbifold*, Mathematical Research Letters 1, 107–114 (1994).
- [27] O. Goodman, C. Hodgson, W. Neumann, *Snap*, a program for exact arithmetic on hyperbolic 3-manifolds, available from <http://www.ms.unimelb.edu.au/~snap/>
- [28] M. Gromov, W. Thurston, *Pinching constants for hyperbolic manifolds*, Invent. Math., 89 (1987), 1–12.
- [29] I. Gradshteyn, I. Ryzhik, *Tables of Integrals, Series, and Products*, 6th ed. San Diego, CA: Academic Press, p. 1062, 2000.
- [30] D. Heard, *Hyperbolic Three-Orbifolds*, Honours project, The University of Melbourne, 2001.
- [31] M. Hildebrand, J. Weeks, *A computer generated census of cusped hyperbolic 3-manifolds*, Computers and mathematics (Cambridge, MA, 1989), 53–59, Springer, New York, 1989.
- [32] C. Hodgson, S. Kerckhoff, *Universal bounds for hyperbolic Dehn surgery*, Annals of Mathematics, 162 (2005), 1–55.
- [33] C. Hodgson, J. Weeks, *Symmetries, isometries and length spectra of closed hyperbolic three-manifolds*, Experiment. Math. 3 (1994), 261–274.
- [34] C. Hodgson, R. Meyerhoff, J. Weeks, *Surgeries on the Whitehead link yield geometrically similar manifolds*, in B. Apanasov, W. Neumann, A. Reid, L. Siebenmann (eds), *Topology 90, Proc. Research Semester in Low Dimensional Topology at Ohio State University*, de Gruyter Verlag, Berlin, 1992, pp. 195–206.
- [35] J. Hoste, M. Thistlethwaite and J. Weeks, *The first 1,701,936 knots*. Math. Intelligencer 20 (1998), no. 4, 33–48.
- [36] M. Kapovich, *Hyperbolic manifolds and discrete groups*, Progress in Mathematics, 183. Birkhuser Boston, Inc., Boston, MA, 2001.
- [37] W. Jaco, P. Shalen, *Seifert fibred spaces in 3-manifolds*, Memoirs Amer. Math. Soc., No. 220, Amer. Math. Soc., Providence, 1979.
- [38] K. Johannson, *Homotopy equivalences of 3-manifolds with boundaries*, Lecture Notes in Mathematics, Vol 761, Springer-Verlag, New York, Berlin, Heidelberg, 1979.
- [39] S. Kojima, *Polyhedral decomposition of hyperbolic manifolds with boundary*, Proc. Work. Pure Math. 10 (1990), 37–57.
- [40] S. Kojima, *Polyhedral decomposition of hyperbolic 3-manifold with with totally geodesic boundary*, In: “Aspects of low-dimensional manifolds, Kinokuniya, Tokyo”, Adv. Stud. Pure Math. 20 (1992), 93–112.
- [41] M. Lackenby, *Attaching handlebodies to 3-manifolds*, Geom. Topol. 6 (2002), 889–904.

- [42] M. Lackenby, *Word hyperbolic Dehn surgery*, Invent. Math. 140 (2000), 243–282.
- [43] R. Litherland, *A table of all prime theta-curves in  $\mathbb{S}^3$  up to 7 crossings*, a letter, 1989.
- [44] T. Marshall, G. Martin, *Packing strips in the hyperbolic plane*, Proceedings of the Edinburgh Mathematical Society (2), 46(1), 67-73, 2003.
- [45] R. Meyerhoff, *The cusped hyperbolic 3-orbifold of minimum volume*, Bull. Amer. Math. Soc. (N.S.) 13 (1985), no. 2, 154–156.
- [46] J. Morgan, *On Thurston’s uniformization theorem for three-dimensional manifolds*, The Smith conjecture (New York, 1979), 37–125, Pure Appl. Math., 112, Academic Press, Orlando, FL, 1984.
- [47] H. Moriuchi, *An enumeration of theta-curves with up to seven crossings*, p171–185 in: Proceeding of the East Asian School of Knots, Links, and Related topics, 2004, Seoul, Korea. (<http://knot.kaist.ac.kr/2004/proceedings/MORIUCHI.pdf>)
- [48] G. Mostow, *Strong rigidity of locally symmetric spaces. Annals of Mathematics Studies*, No. 78. Princeton University Press, Princeton, N.J.; University of Tokyo Press, Tokyo, 1973. v+195 pp.
- [49] J. Murakami, A. Ushijima, *A volume formula for hyperbolic tetrahedra in terms of edge lengths*, preprint (<http://arxiv.org/abs/math/0402087>).
- [50] R. Penner, *The action of the Mapping Class Group on the Curves in a Surface*, Enseign. Math. (2) 30 (1984), no. 1-2, 39–55.
- [51] C. Petronio, J. Weeks, *Partially flat ideal triangulations of cusped hyperbolic 3-manifolds*, Osaka J. Math. 37 (2000), 453-466.
- [52] G. Prasad, *Strong rigidity of  $Q$ -rank 1 lattices*, Invent. Math. 21 (1997), 255-286.
- [53] V. Prasolov, *Problems and Theorems in Linear Algebra*, Translations of Mathematical Monographs, Volume 134, American Mathematical Society (1994).
- [54] J. Ratcliffe, *Foundations of Hyperbolic Manifolds*, Springer-Verlag, 1994.
- [55] M. Sakuma, J. Weeks, *The Generalized Tilt Formula*, Geometriae Dedicata, 55 (1993), 115-123.
- [56] P. Scott, *The geometries of 3-manifolds*, Bull. London Math. Soc. 15 (1983), 401-487.
- [57] R. Henry, J. Weeks, *Symmetry groups of hyperbolic knots and links*, J. Knot Theory Ramifications 1 (1992), no. 2, 185–201
- [58] M. Scharlemann, Y. Wu, *Hyperbolic manifolds and degenerating handle additions*, J. Austral. Math. Soc. Ser. A 55 (1993), 72–89.
- [59] J. Simon, *A topological approach to the stereochemistry of nonrigid molecules*, Graph theory and topology in chemistry (Athens, Ga., 1987), 43–75, Stud. Phys. Theoret. Chem., **51**, Elsevier, Amsterdam, 1987.
- [60] M. Thistlethwaite, The computer program *Knotscape*, available at <http://www.math.utk.edu/~morwen/knightscape.html>
- [61] W. Thurston, *The Geometry and Topology of Three-Manifolds*, Princeton Univ. Math. Dept. (1978). These are available at <http://msri.org/publications/books/gt3m/>.
- [62] W. Thurston, *Three-dimensional Geometry and Topology, Volume 1*, Princeton Univ. Press, 1997.
- [63] W. Thurston, *Three-dimensional manifolds, Kleinian groups and hyperbolic geometry*, Bull. Amer. Math. Soc. (N.S.) 6 (1982), 357-381.
- [64] W. Thurston, *Hyperbolic Structures on 3-manifold I: Deformation of Acylindrical Manifolds*, Annals of Mathematics, 2nd Ser., Vol. 124, No. 2, pp. 203-246, 1986.

- [65] G. Tóth, *Regular Figures*, Pergamon Press, Oxford, 1964.
- [66] A. Ushijima, *A volume formula for generalized hyperbolic tetrahedra*, preprint (ArXiv:math.GT/0309216).
- [67] A. Ushijima, *The Tilt Formula for Generalized Simplices in Hyperbolic Space*, Discrete and Computational Geometry, Springer-Verlag New York, Volume 28, Number 1, pp. 19-27, 2002.
- [68] A. Vesin, A. Mednykh, B. Zimmermann, *Surgeries on small volume hyperbolic 3-orbifolds*, Siberian Mathematical Journal, 42 (2001), No. 2, 271-281.
- [69] J. Weeks, *SnapPea*, a computer program for computing hyperbolic structures on 3-manifolds, available at <http://geometrygames.org/>.
- [70] J. Weeks, *Convex hulls and isometries of cusped hyperbolic 3-manifolds*, Topology Appl., 52 (1993), 127-149.
- [71] J. Weeks, *Hyperbolic Structures on Three-Manifolds*, PhD thesis, Princeton University, 1985.
- [72] J. Weeks, *Computation of Hyperbolic Structures in Knot Theory*, to appear in *Handbook of Knot Theory*, preprint (ArXiv:math.GT/0309407.)
- [73] B. Zimmerman, *On hyperbolic 3-orbifolds of small volume and small Heegaard genus*, Rend. Istit. Mat. Univ. Trieste 32 (2001), suppl. 2, 149–161 (2002).

## APPENDIX A

### Triangulating orbifolds of type $Q = (\mathbb{S}^3, \Gamma)$

This appendix describes how the algorithm `SnapPea` employs to triangulate link complements in  $\mathbb{S}^3$  can be extended to triangulate orbifolds of the type  $Q = (\mathbb{S}^3, \Gamma)$ . For more details see [72] which has an extensive discussion of `SnapPea`'s algorithm. This extension was initially conceived in [30]. Towards the end of the appendix we explain how this algorithm can be modified to triangulate graph complements in  $\mathbb{S}^3$ .

Let  $\Gamma$  be a graph in  $\mathbb{S}^3$  with vertices of degree 3 and edges labelled by integers  $\geq 2$ . The triangulation for  $Q = (\mathbb{S}^3, \Gamma)$  will have:

- (1)  $\Sigma(Q)$  contained in the 1-skeleton; and
- (2) one vertex for each vertex of  $\Gamma$ .

Vertices of  $T$  can be finite, ideal and hyperinfinite.

**Technical remark:** To triangulate an orbifold with singular loops we will introduce a finite vertex along each of the loops. This is the only time we will allow degree 2 vertices.

To ensure the algorithm functions as we would expect in all cases we ask that the projection of  $\Gamma$  is connected. Of course, if this is not the case we can easily rectify the problem by performing Reidemeister II moves as necessary. The algorithm is best understood using truncated tetrahedra, so we slice off a neighbourhood of each of the vertices of  $\Gamma$ .

There is one additional requirement asked of the projection of  $\Gamma$ : No edge of  $\Sigma(Q)$  may pass through a crossing. This requirement can be met by shrinking any offending edges of  $\Sigma(Q)$  down until they avoid all crossings. (See Figure A.1.)

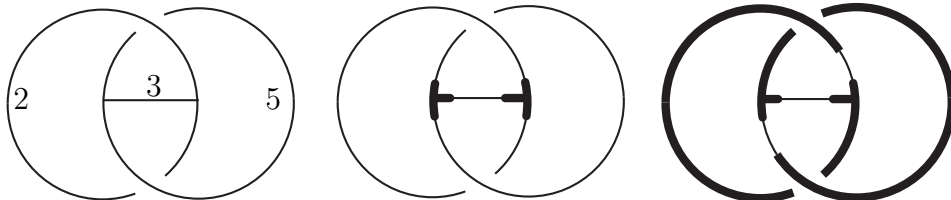


FIGURE A.1. Truncating the vertices and then shrinking edges of  $\Sigma(Q)$ .

The graph  $\Gamma$  is then placed near the equatorial 2-sphere in  $\mathbb{S}^3$  where it will act as a scaffolding as the triangulation for  $Q$  is built around it. To make this easy,

finite vertices are placed at the north and south pole of  $\mathbb{S}^3$ . Weeks has developed a method for removing unnecessary vertices so these can be removed easily after triangulation is complete. Since truncated tetrahedra will be used, neighbourhoods of these vertices are removed and  $\Gamma$  is now positioned in  $\mathbb{S}^2 \times I$ . (See Figure A.2.)

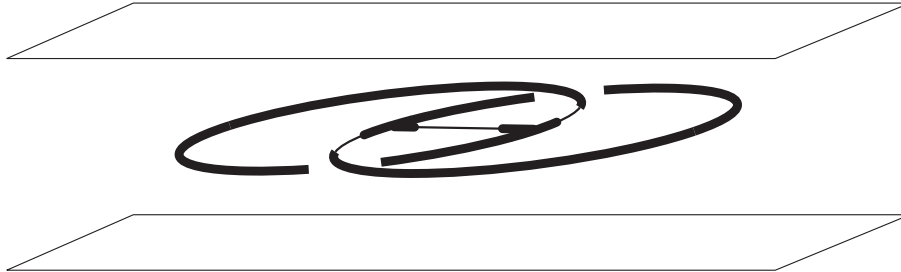


FIGURE A.2.  $\Gamma$  is in  $\mathbb{S}^3$  which looks like  $\mathbb{S}^2 \times I$  since neighbourhoods of the north and south poles have been removed.

It is now necessary to make a series of cuts straight down through  $\mathbb{S}^2 \times I$ . After all the cuts are made,  $\mathbb{S}^2 \times I$  will be broken into pieces around the thickened  $\Gamma$ . There are four type of incisions (refer to Figure A.3):

- (1) Between every pair of neighbouring crossings of  $\Gamma$  make an incision that separates them;
- (2) For every crossing next to an edge of  $\Sigma(Q)$  make an incision that separates them;
- (3) At every vertex of  $\Gamma$  make an incision that separates neighbouring edges;
- (4) Make one long incision all the way along  $\Gamma$ .

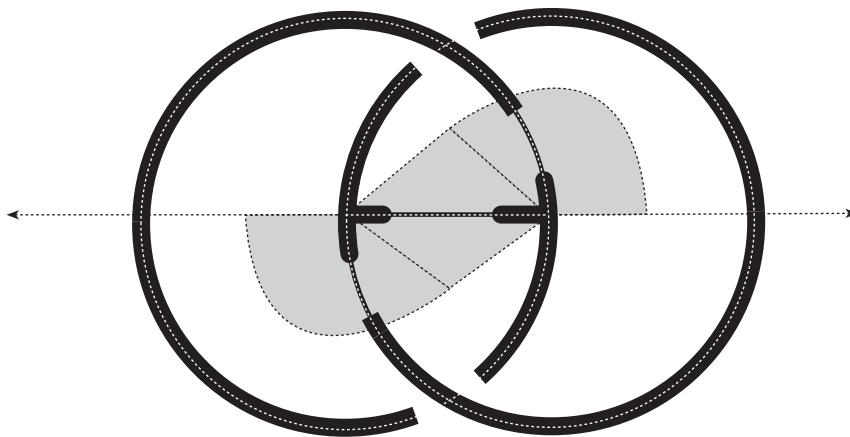


FIGURE A.3. Cutting up  $\mathbb{S}^2 \times I$ . The dotted lines represent our incisions. The shaded area indicates the four pieces of type (1). Each of these four pieces is topologically a truncated tetrahedron. The remaining area is filled by eight pieces of type (2).

After all the incisions are made there are two types of pieces:

- (1) Those that are incident to an edge of  $\Sigma(Q)$ , which have a labelling induced on their edges;
- (2) Those that are incident to a crossing.

For every edge in  $\Sigma(Q)$  there are two pieces of type (1); topologically these are truncated tetrahedra. For every crossing in the projection of  $\Gamma$  there are four pieces of type (2). (Figure A.4.)

The type (2) pieces have four truncated vertices, two of which border a neighbourhood of the vertices of  $\Gamma$  and two of which border the upper and lower surfaces of  $\mathbb{S}^2 \times I$ , along with six ordinary faces, four of which are combinatorial hexagons and two of which are combinatorial squares. By collapsing each combinatorial square to a vertical edge each of these pieces becomes a truncated tetrahedron.

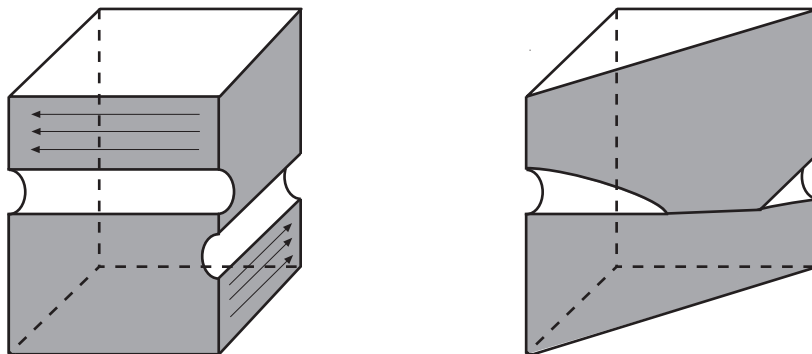


FIGURE A.4. One of the second types of pieces. After collapsing the combinatorial squares it is topologically a tetrahedron.

This completes the algorithm. As in *SnapPea*, the vertices at the north and south poles can be removed and the triangulation can be simplified. Refer to [72] for more details.

We now examine how this algorithm can be modified to triangulate graph complements in  $\mathbb{S}^3$ . We begin with the projection of a graph  $\Gamma$  in  $\mathbb{S}^3$ . The triangulation will have one vertex for each component of  $\Gamma$ . Removing a neighbourhood of these vertices produces the required triangulation.

As before, the projection of  $\Gamma$  must be connected. In addition we ask that every longitudinal curve on  $\Gamma$  must pass through a crossing on both an over and an under strand. These conditions can be met by performing Reidemeister II and III moves.

We use truncated tetrahedra to visualize the algorithm, so slice off a neighbourhood  $N(\Gamma)$  of  $\Gamma$  and position it on the equatorial 2-sphere. Truncate finite vertices at the north and south poles leaving our thickened  $\Gamma$  in  $\mathbb{S}^2 \times I$ .

We now make a series of cuts straight down through  $\mathbb{S}^2 \times I$ . After all the cuts are made,  $\mathbb{S}^2 \times I$  will be broken into pieces around the thickened  $\Gamma$ . This time there are three types of incisions (refer to Figure A.5):

- (1) Between every pair of neighbouring crossings of  $\Gamma$  make an incision that separates them;
- (2) At every vertex of  $\Gamma$  make an incision that separates neighbouring edges;
- (3) Make one long incision all the way along  $\Gamma$ .

What results is a decomposition of  $(\mathbb{S}^2 \times I) - N(\Gamma)$  with four pieces around each crossing in the projection of  $\Gamma$ . It turns out each of these pieces is equivalent to the polyhedron pictured in Figure A.4 and so by collapsing all bigons to vertical edges we produce a triangulation of  $(\mathbb{S}^2 \times I) - N(\Gamma)$  by truncated tetrahedra. We then replace the north and south poles to complete the algorithm.

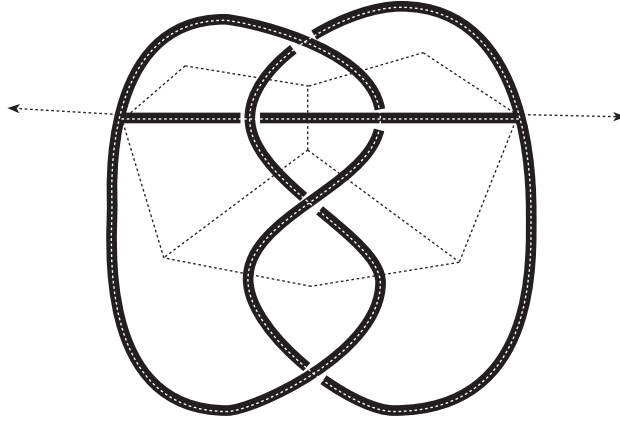


FIGURE A.5. Cutting up  $\mathbb{S}^2 \times I$ . The dotted lines represent our incisions. All the pieces produced are equivalent to those pictured in Figure A.4.

**Technical remark:** Ensuring that every longitudinal curve on  $\Gamma$  must pass through a crossing on both an over and an under strand guarantees that our decomposition of  $(\mathbb{S}^2 \times I) - N(\Gamma)$  does not contain a circular chain of bigons. So when we collapse the bigons to vertical edges the topology is unchanged.